Strongly fluorescent spiro-type tetracoordinate complexes of dibenzo[*b*,*e*][1,4]thiaborinine dioxide with functionalized 2-(benzo[*d*]heterazol-2-yl)phenolate ligands displaying TADF

Mateusz Urban,[a] Karolina Wrochna,[a] Paulina H. Marek-Urban,[a] Dawid R. Natkowski,[a] Krzysztof Woźniak,[b] Piotr Pander,*[c,d] Andrew P. Monkman,[e] Krzysztof Durka,*[a] Sergiusz Luliński*[a]

[a] *Faculty of Chemistry, Warsaw University of Technology, Noakowskiego 3, 00-664 Warsaw, Poland.*

[b]*Department of Chemistry, University of Warsaw, Pasteura 1, 02-093 Warsaw, Poland.*

[c]*Faculty of Chemistry, Silesian University of Technology, Strzody 9, 44-100 Gliwice, Poland*

[d]*Centre for Organic and Nanohybrid Electronics, Silesian University of Technology, Konarskiego 22B, 44-100 Gliwice, Poland*

[e]*Department of Physics, Durham University, Stockton Road, Durham, DH1 3LE, UK*

Table of contents

1. Crystal structure analysis

Table S1.1. Selected bond length (*d*), valence angles (α) and torsion angles (τ) in complexes **7d** (two molecules in the asymmetric part of the unit cell abbreviated as **7d_A** and **7d_B**), **8a**, **8b** and **8d**.

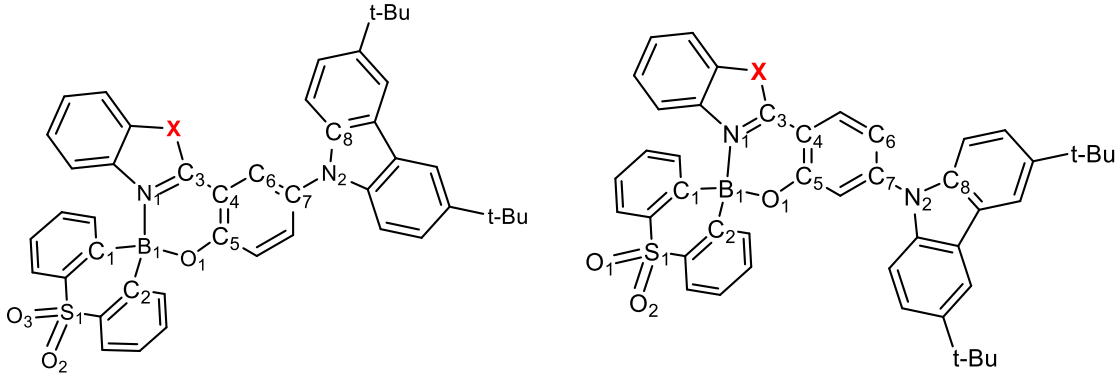

	7d_A	**7d_B**	**8a**	**8b**	**8d**
$d_{B1–N1}$ / Å	1.60(1)	1.59(1)	1.591(3)	1.624(5)	1.581(2)
$d_{B1–O1}$ / Å	1.49(1)	1.50(1)	1.505(3)	1.494(5)	1.503(2)
$d_{B1–C1}$ / Å	1.60(2)	1.66(1)	1.620(4)	1.612(8)	1.613(2)
$d_{B1–C2}$ / Å	1.63(2)	1.58(2)	1.608(4)	1.618(6)	1.615(2)
$d_{S1–O1}$ / Å	1.451(8)	1.432(8)	1.441(2)	1.443(3)	1.441(1)
$d_{S1–O2}$ / Å	1.440(7)	1.434(8)	1.443(2)	1.444(3)	1.443(2)
$d_{N1–C3}$ / Å	1.34(1)	1.35(1)	1.316(3)	1.332(5)	1.338(2)
$d_{N2–C7}$ / Å	1.41(1)	1.41(1)	1.403(3)	1.419(4)	1.411(3)
$\alpha_{N1-B1-O1}$ / °	104.7(8)	105.0(8)	105.6(2)	105.9(3)	105.5(1)
$\alpha_{C1-B1-C2}$ / °	117.5(5)	115.3(9)	112.5(2)	115.5(4)	115.7(1)
$\alpha_{O1-S1-O2}$ / °	115.3(8)	116.4(5)	117.0(1)	116.3(2)	117.20(9)
$\gamma_{N1-C3-C4-C5}$ / °	10(1)	13(1)	4.6(3)	12.0(5)	12.9(2)
$\gamma_{C6-C7-N2-C8}$ / °	51(1)	53(1)	54.6(3)	49.5(5)	45.8(2)

Table S1.2. Geometry of intermolecular interactions in crystal structures **7d**, **8a**, **8b** and **8d**.

	Interaction	$d_{C\ldots O}$ / Å or $d_{C\ldots C}$ / Å	$d_{H\ldots O}$ / Å or $d_{H\ldots C}$ / Å	$\alpha_{C\text{-}H\ldots O}$ / Å or $\alpha_{C\text{-}H\ldots C}$ / Å	Symmetry
7d	C35-H35…O5$^{\#1}$	3.42(1)	2.496	164.5	1-x,-y,-z
	C36-H36…O6$^{\#1}$	3.18(2)	2.483	129.9	1-x,-y,-z
	C14-H14C…O3$^{\#2}$	3.52(1)	2.565	165.2	x,-1+y,z
	C88-H88…O2$^{\#3}$	3.18(1)	2.489	129.5	1-x,1-y,1-z
	C57-H57…O2$^{\#3}$	3.57(1)	2.623	173.5	1-x,1-y,1-z
	C18-H18C…C57	3.73(2)	2.84	148	x,y,z
	C18-H18C…C58	3.71(2)	2.84	151	x,y,z
	C39-H39…C60$^{\#4}$	3.65(1)	2.81	148.4	1-x,1-y,-z
	C39-H39…C61$^{\#4}$	3.73(2)	2.80	165.8	1-x,1-y,-z
	C74-H74…C31$^{\#4}$	3.55(1)	2.67	154.2	1-x,1-y,-z
	C67-H67A…C80$^{\#5}$	3.80(1)	2.827	172.7	2-x,-y,1-z
	C66-H66C…C42$^{\#3}$	3.51(1)	2.77	125.0	1-x,1-y,1-z
	C66-H66C…C43$^{\#3}$	3.52(1)	2.857	133.7	1-x,1-y,1-z

	C91-H91…C54$^{\#5}$	3.38(1)	2.958	108.6	2-x,-y,1-z
	C91-H91…C55$^{\#5}$	3.54(1)	2.894	126.0	2-x,-y,1-z
8a	C30-H30…O4$^{\#6}$	3.408(3)	2.630	139.3	x,y,-1+z
	C31-H31…O3$^{\#6}$	3.289(3)	2.452	146.8	x,y,-1+z
	C35-H35…O4$^{\#7}$	3.270(3)	2.511	136.9	x,y,-1+z
	C19-H19A…O3$^{\#3}$	3.475(3)	2.694	137.0	1-x,1-y,1-z
	C29-H29…C34$^{\#8}$	3.622(4)	2.813	143.5	-x,1-y,-z
	C23-H23…C8$^{\#3}$	3.750(3)	2.812	169.8	1-x,1-y,1-z
	C20-H20B…C21$^{\#9}$	3.399(4)	2.878	114.2	1-x,1/2+y,1/2-z
	C20-H20B…C53$^{\#9}$	3.595(4)	2.799	139.0	1-x,1/2+y,1/2-z
	C18-H18B…C38$^{\#9}$	3.630(4)	2.650	179.8	1-x,1/2+y,1/2-z
8b	C25-H25…O2$^{\#10}$	3.144(4)	2.434	131.3	x,1.5-y,1/2+z
	C45-H45…O3$^{\#11}$	3.552(5)	2.662	156.3	1-x,-1/2+y,1/2-z
	C19-H19C…C11$^{\#12}$	3.645(6)	2.716	127.4	x,1/2-y,-1/2+z
	C2-H2…C30$^{\#11}$	3.469(6)	2.810	158.2	1-x,-1/2+y,1/2-z
	C3-H3…C31$^{\#11}$	3.558(6)	2.870	130.2	1-x,-1/2+y,1/2-z
	C15-H15B…C2$^{\#8}$	3.559(6)	2.819	132.9	-x,1-y,-z
	C38-H38…C3$^{\#12}$	3.546(5)	2.658	155.8	x,1+y,z
8d	C10-H10…O3$^{\#13}$	3.443(2)	2.685	137.2	1/2-x,-1/2+y,1/2-z
	C15-H15…O1$^{\#14}$	3.521(3)	2.584	168.8	x,-y,1/2+z
	C45-H45B…O2$^{\#15}$	3.534(4)	2.701	143.1	1/2+x,-1/2+y,z
	C4-H4…C13$^{\#16}$	3.656(3)	2.830	146.0	1/2-x,1/2-y,1-z
	C4-H4…C18$^{\#16}$	3.734(3)	2.824	160.8	1/2-x,1/2-y,1-z
	C20-H20…C13$^{\#17}$	3.759(2)	2.834	164.7	1/2-x,-1/2-y,1-z
	C20-H20…C17$^{\#17}$	3.549(2)	2.889	127.5	1/2-x,-1/2-y,1-z
	C20-H20…C18$^{\#17}$	3.544(2)	2.661	154.9	1/2-x,-1/2-y,1-z
	C22-H22...C40$^{\#14}$	3.534(3)	2.928	170.1	x,-y,1/2+z
	C22-H22...C41$^{\#14}$	3.565(2)	2.724	148.0	x,-y,1/2+z
	C30-H30…C39$^{\#18}$	3.324(2)	2.544	139.4	1-x,-y,1-z
	C47-H47C…C6$^{\#15}$	3.702(4)	2.791	155.0	1/2+x,-1/2+y,z

Table S1.3. Selected crystal data, data collection and refinement parameters for **7d**, **8a**, **8b** and **8d**.

	7d	**8a**	**8b**	**8d**
Empirical formula	$C_{51}H_{44}BN_3O_3S$	$C_{44}H_{40}N_4O_4SB$	$C_{45}H_{39}N_2O_3BS_2$	$C_{51}H_{44}N_3O_3SB$
Formula weight	789.76	714.65	730.71	789.76
Temperature/K	100.01(10)	100.01(10)	100.00(10)	100.00(10)
Crystal system	triclinic	monoclinic	monoclinic	monoclinic
Space group	*P*-1	$P2_1/c$	$P2_1/c$	$C2/c$
a/Å	14.6893(17)	20.0869(5)	19.0158(15)	33.9982(14)
b/Å	17.0215(12)	15.9689(4)	12.9302(5)	13.0244(2)
c/Å	17.5516(11)	11.5988(2)	17.3986(12)	20.0796(5)
α/°	72.926(6)	90	90	90
β/°	89.280(7)	95.769(2)	114.241(9)	116.302(4)
γ/°	89.954(8)	90	90	90
Volume /$Å^3$	4194.7(6)	3701.65(15)	3900.7(5)	7970.9(5)
Z	4	4	4	8
ρ_{calc} /gcm^{-3}	1.251	1.282	1.244	1.316
μ/mm^{-1}	1.054	1.150	1.570	1.110
F(000)	1664.0	1504.0	1536.0	3328.0
Crystal size/mm^3	0.1321 × 0.1063 × 0.0755	0.078 × 0.071 × 0.01	0.121 × 0.085 × 0.02	0.167 × 0.151 × 0.084
Radiation	Cu Kα (λ = 1.54184)	Cu Kα (λ = 1.54184)	Cu Kα (λ = 1.54184)	Cu Kα (λ = 1.54184)
2Θ range for data collection/°	5.268 to 130.898	4.422 to 141.894	8.53 to 124.182	5.8 to 147.836
Index ranges	-17 ≤ h ≤ 13, -20 ≤ k ≤ 19, -20 ≤ l ≤ 20	-22 ≤ h ≤ 24, -18 ≤ k ≤ 19, -14 ≤ l ≤ 13	-21 ≤ h ≤ 20, -9 ≤ k ≤ 14, -9 ≤ l ≤ 19	-41 ≤ h ≤ 40, -14 ≤ k ≤ 16, -22 ≤ l ≤ 24
Reflections collected	21491	14828	12281	31156
Independent reflections	12681 [R_{int} = 0.0757, R_{sigma} = 0.1327]	6949 [R_{int} = 0.0372, R_{sigma} = 0.0513]	5994 [R_{int} = 0.0584, R_{sigma} = 0.0901]	7926 [R_{int} = 0.0271, R_{sigma} = 0.0204]
Data/restraints/parameters	12681/2/1074	6949/0/478	5994/0/478	7926/0/532
Goodness-of-fit on F^2	1.436	0.936	0.971	1.036
Final R indexes [I>=2σ (I)]	R_1 = 0.1661, wR_2 = 0.4312	R_1 = 0.0479, wR_2 = 0.1276	R_1 = 0.0584, wR_2 = 0.1382	R_1 = 0.0430, wR_2 = 0.1179
Final R indexes [all data]	R_1 = 0.2102, wR_2 = 0.4708	R_1 = 0.0780, wR_2 = 0.1491	R_1 = 0.0980, wR_2 = 0.1611	R_1 = 0.0490, wR_2 = 0.1234
Largest diff. peak/hole / e $Å^{-3}$	1.30/-0.58	0.30/-0.39	0.30/-0.56	0.61/-0.60

2. Steady state UV-Vis spectroscopy

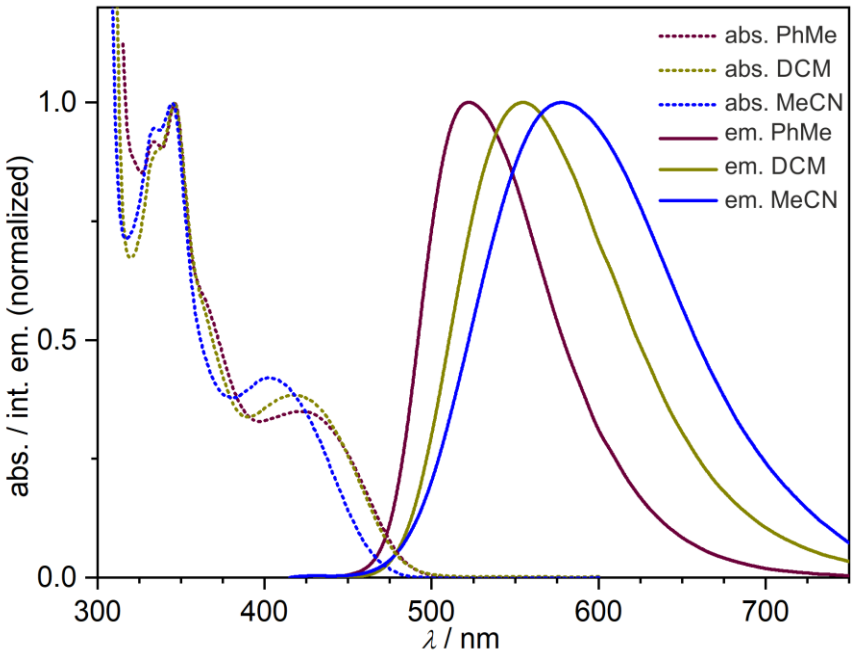

Figure S2.1. Steady state absorption and photoluminescence spectra of **7a** in dilute solution in solvents of various polarity indicated in figure legend.

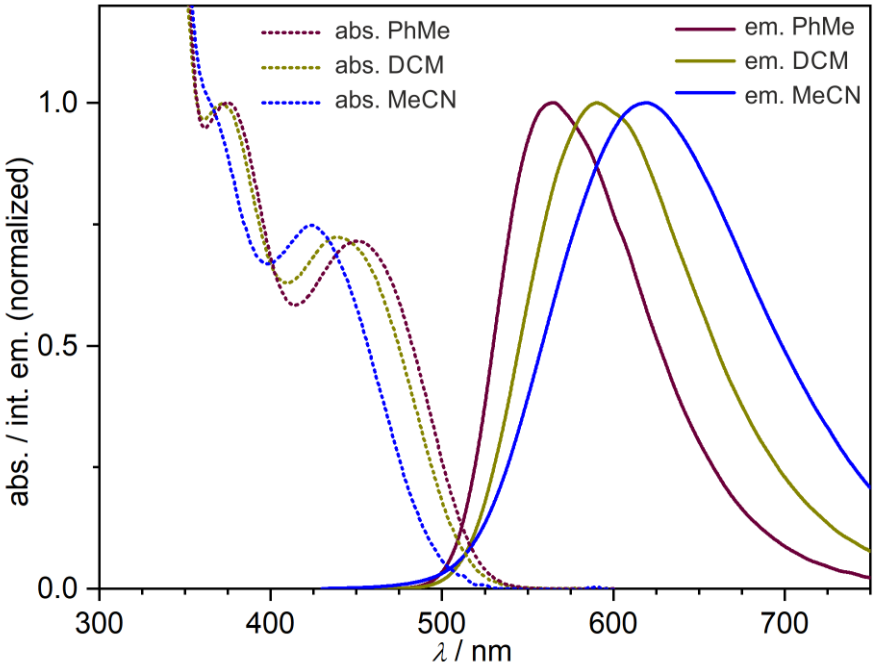

Figure S2.2. Steady state absorption and photoluminescence spectra of **7b** in dilute solution in solvents of various polarity indicated in figure legend.

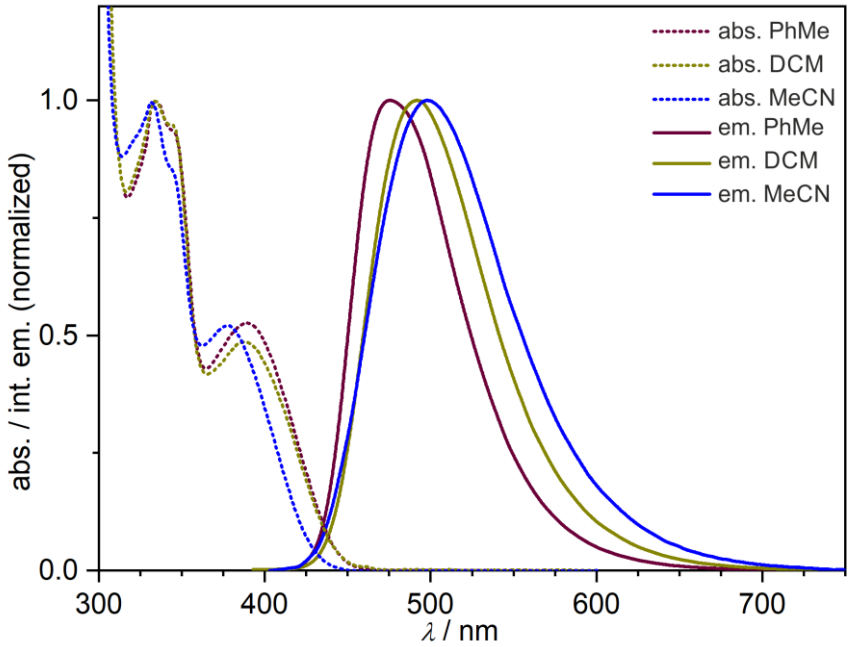

Figure S2.3. Steady state absorption and photoluminescence spectra of **7c** in dilute solution in solvents of various polarity indicated in figure legend.

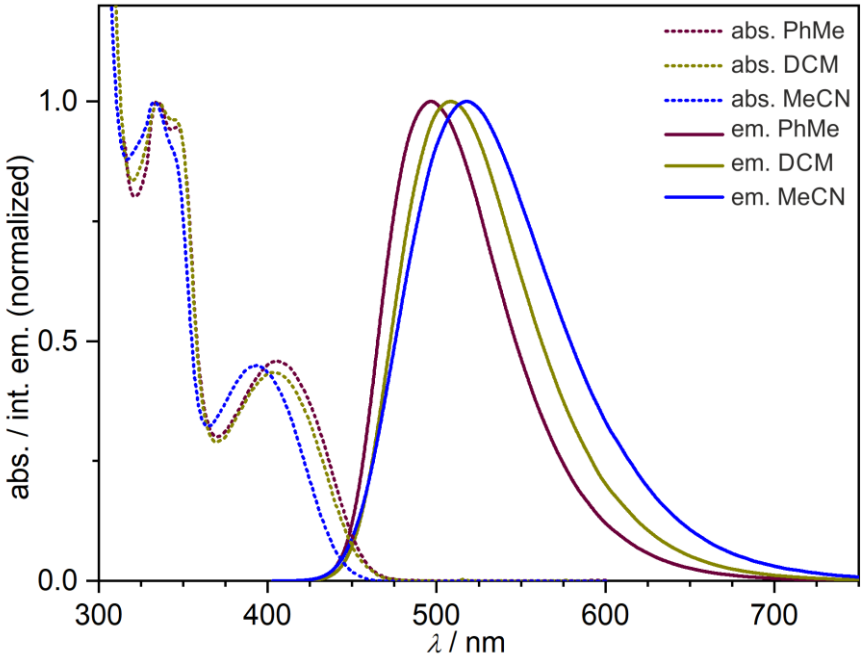

Figure S2.4. Steady state absorption and photoluminescence spectra of **7d** in dilute solution in solvents of various polarity indicated in figure legend.

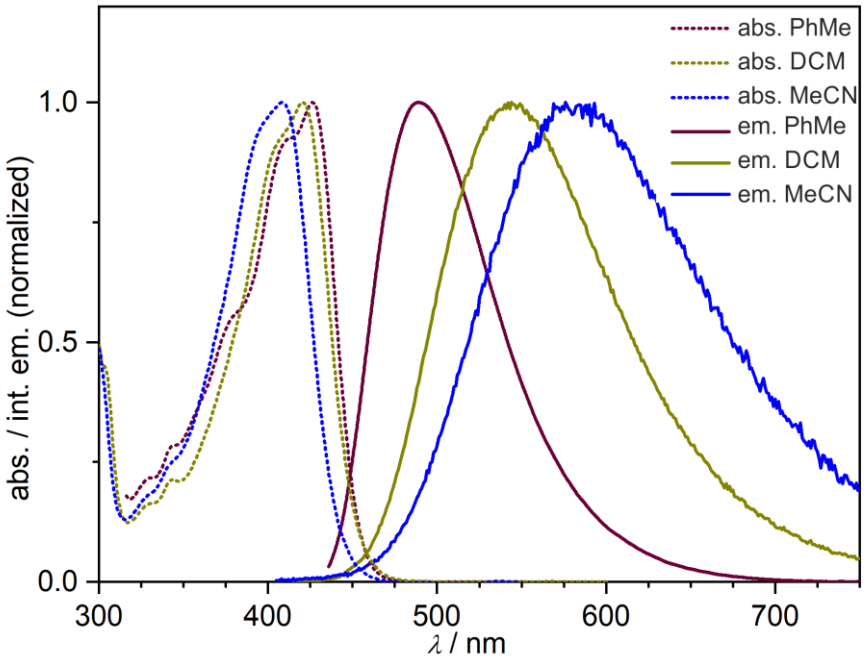

Figure S2.5. Steady state absorption and photoluminescence spectra of **8a** in dilute solution in solvents of various polarity indicated in figure legend.

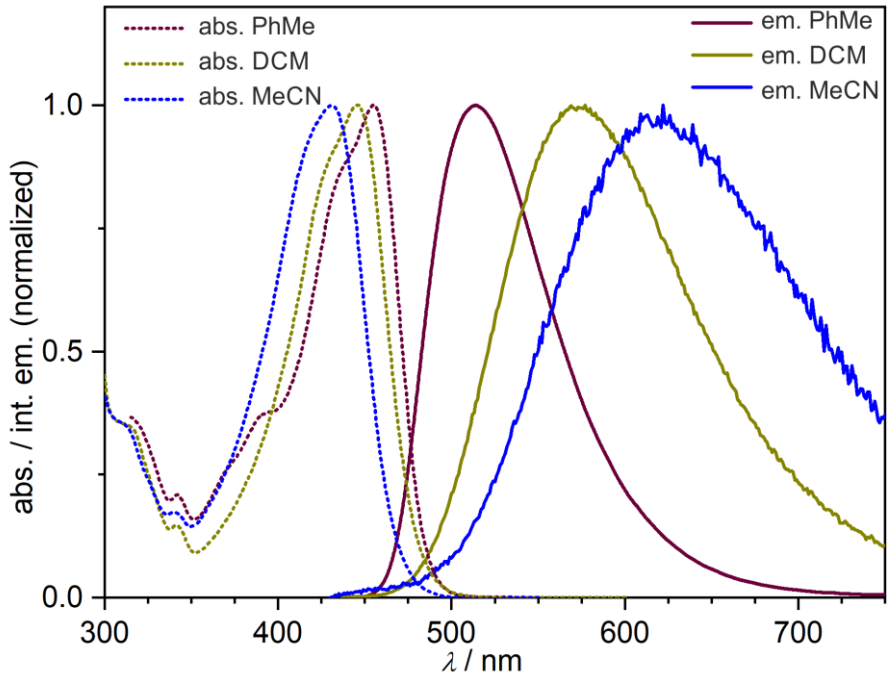

Figure S2.6. Steady state absorption and photoluminescence spectra of **8b** in dilute solution in solvents of various polarity indicated in figure legend.

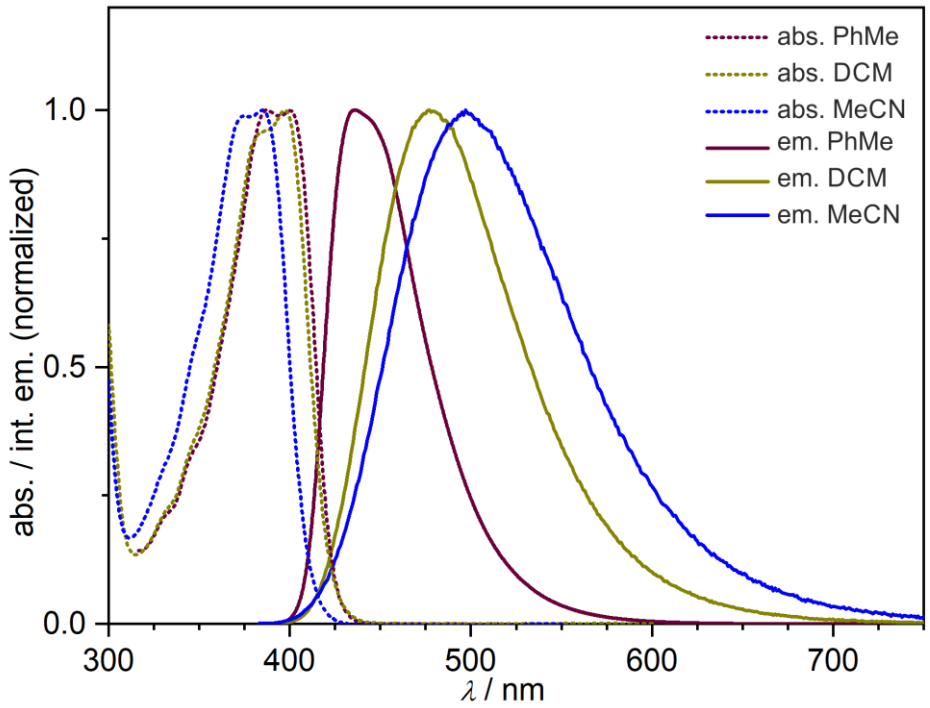

Figure S2.7. Steady state absorption and photoluminescence spectra of **8c** in dilute solution in solvents of various polarity indicated in figure legend.

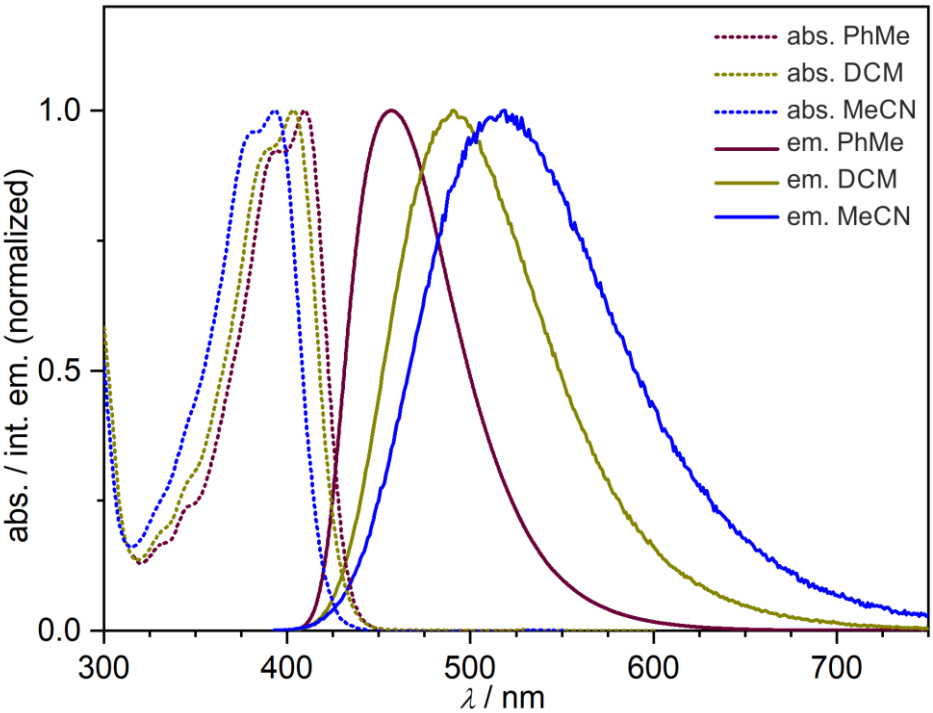

Figure S2.8. Steady state absorption and photoluminescence spectra of **8d** in dilute solution in solvents of various polarity indicated in figure legend.

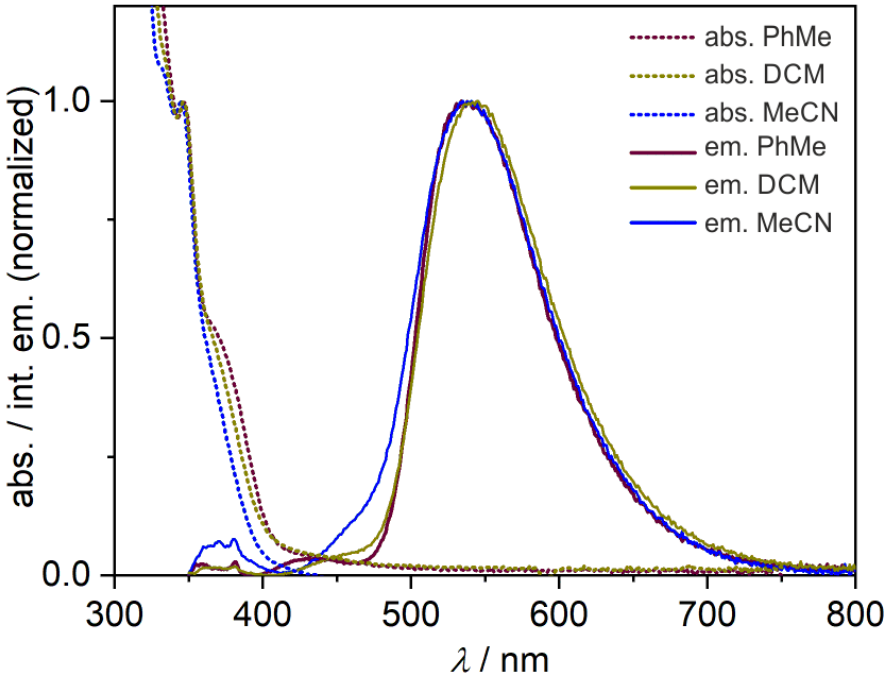

Figure S2.9. Steady state absorption and photoluminescence spectra of **9** in dilute solution in solvents of various polarity indicated in figure legend.

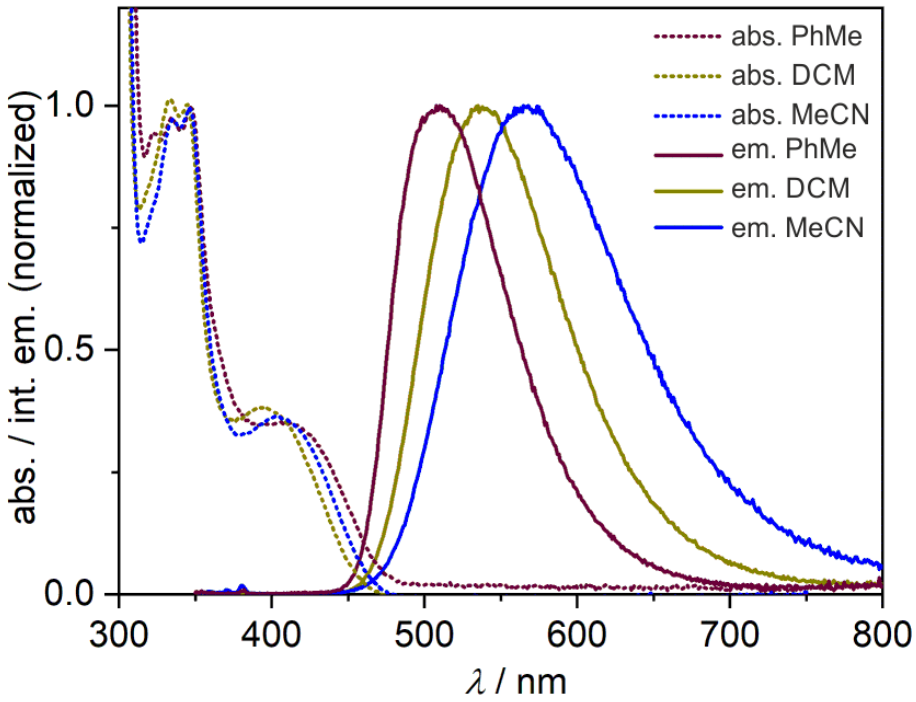

Figure S2.10. Steady state absorption and photoluminescence spectra of **10** in dilute solution in solvents of various polarity indicated in figure legend.

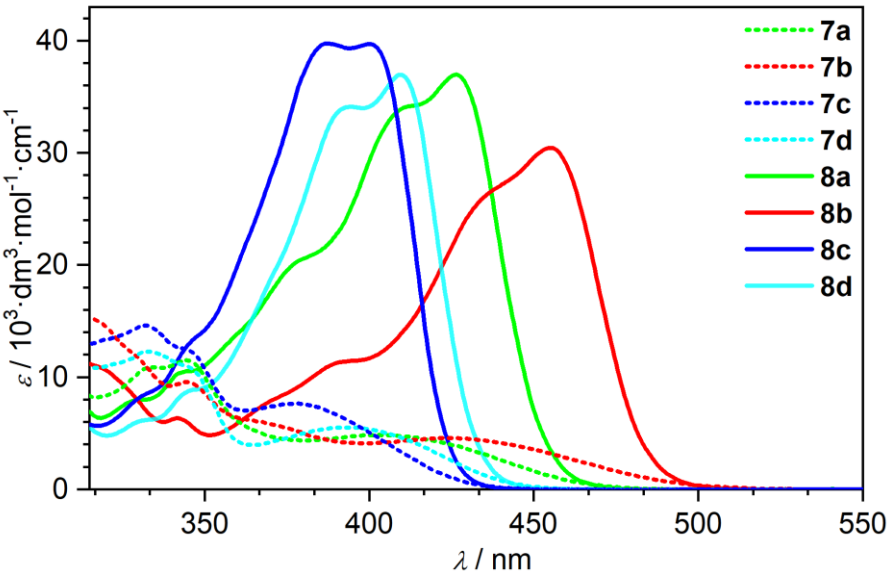

Figure S2.11. The UV-Vis absorption spectra (toluene) of **7a–7d**, **8a–8d** shown as molar absorptivity.

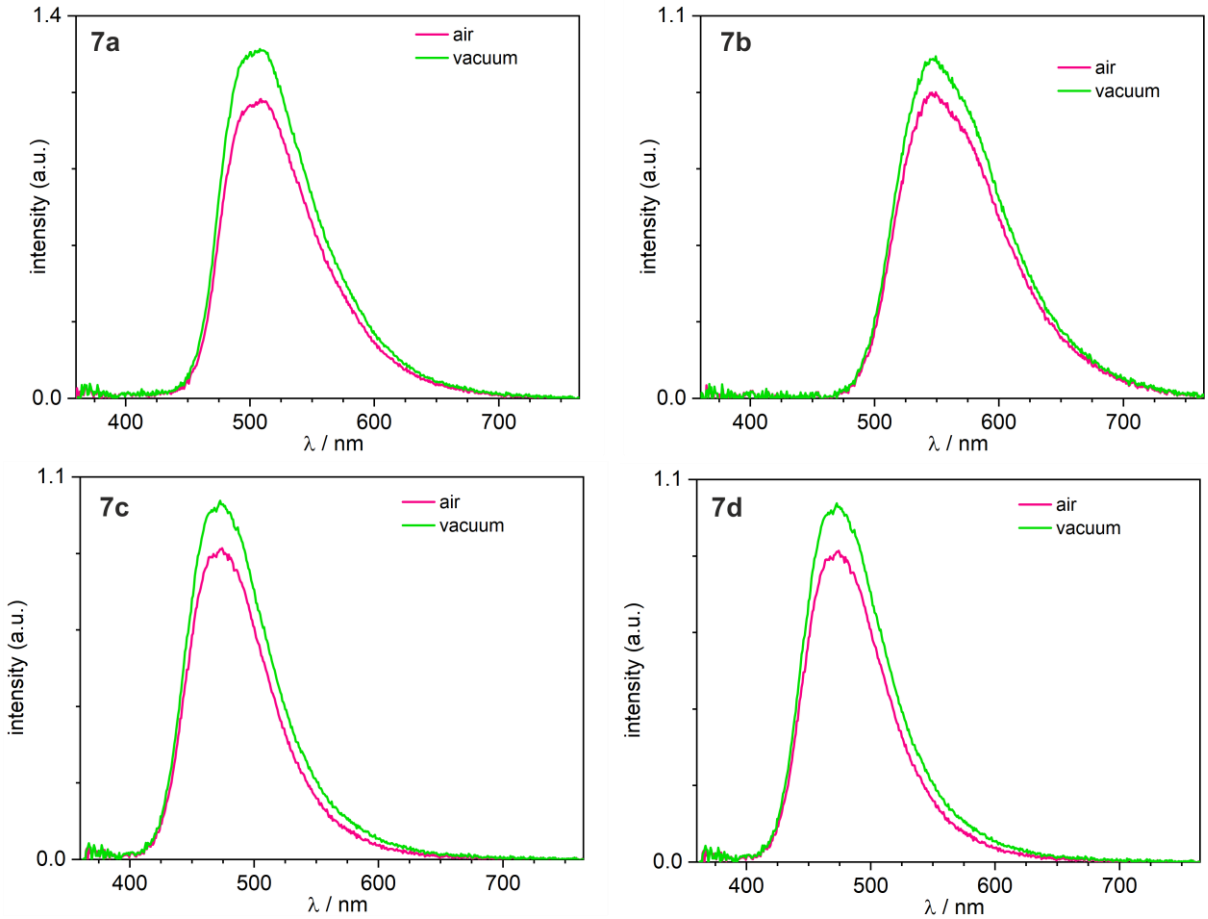

Figure S2.12. Emission spectra of **7a–7d** (1wt% in Zeonex) under air-equilibrated conditions and upon degassing.

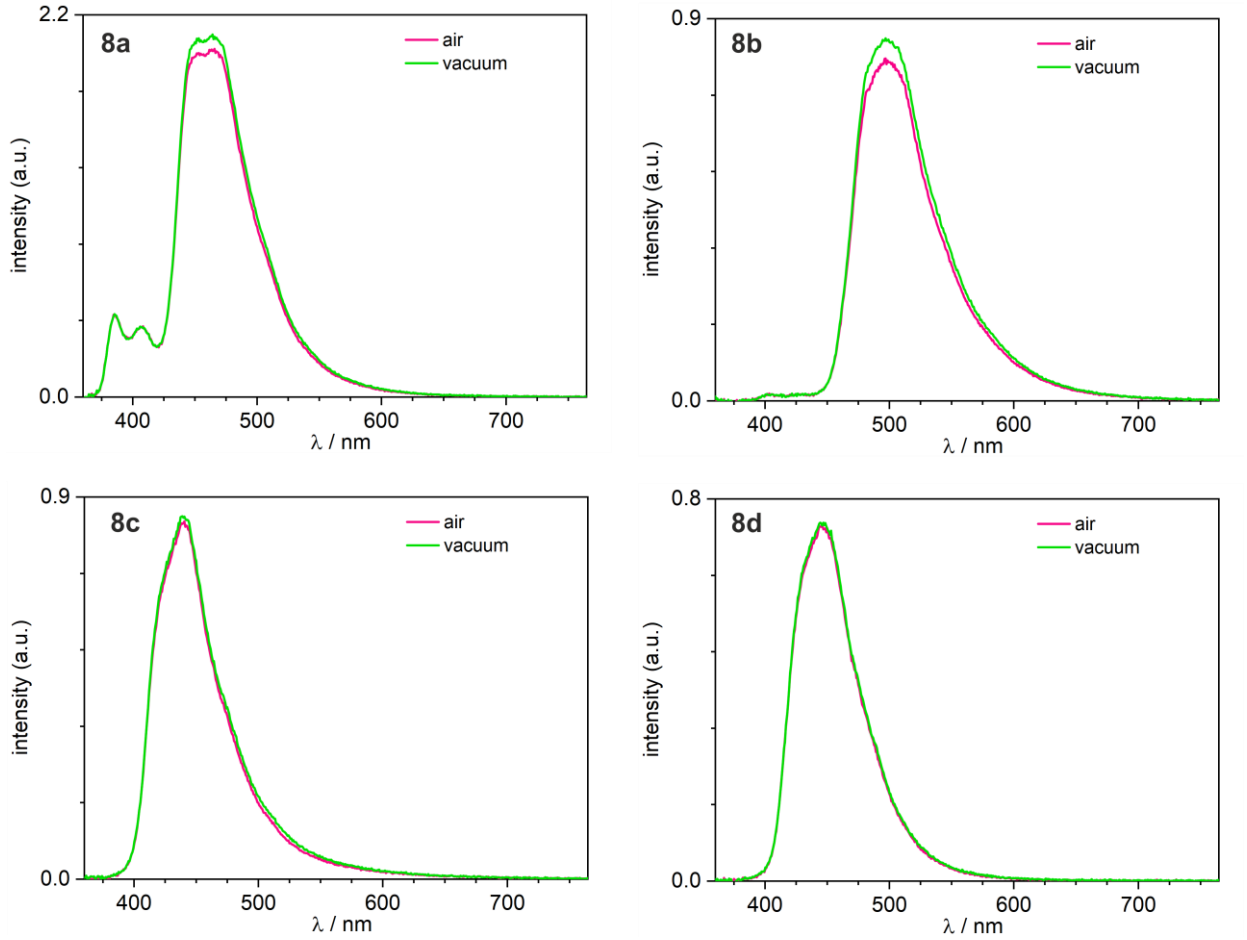

Figure S2.13. Emission spectra of **8a–8d** (1wt% in Zeonex) under air-equilibrated conditions and upon degassing.

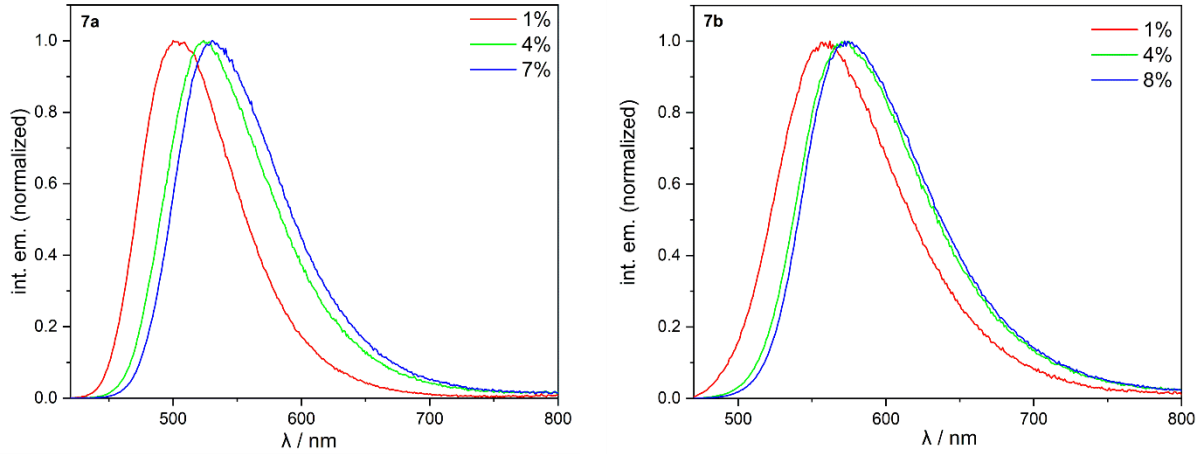

Figure S2.14. Emission spectra of **7a** and **7b** in thin films at varying concentrations (1–8wt%).

Table S2.1. The dependence of the emission wavelength and QY on doping concentration for thin films prepared through spin-coating technique.

	wt%	λ_{em} / nm	QY
7a	0.1	510	0.97
	1.0	511	0.98
	4.0	524	0.87
	7.0	531	0.86
7b	0.1	545	1.0
	1.0	560	0.82
	4.0	571	0.63
	8.0	575	0.61

Table S2.2. Summary of photoluminescence characteristics in toluene, calculated using the Strickler-Berg method,[1] according to the methodology described earlier.[2]

	k_{PF} / 10^7 s^{-1} [a]	τ_{0PF} / ns [b]	$f(S_1 \rightarrow S_0)$ [c]
7a	2.4	42.4	0.043
7b	2.4	41.8	0.051
7c	4.9	20.6	0.074
7d	4.4	22.8	0.072
8a	23.9	4.2	0.382
8b	18.4	5.4	0.326
8c	42.3	2.4	0.538
8d	33.5	3.0	0.469

[a] Prompt fluorescence radiative decay rate; [b] natural prompt fluorescence lifetime; [c]singlet oscillator strength.

3. Time-resolved spectroscopy

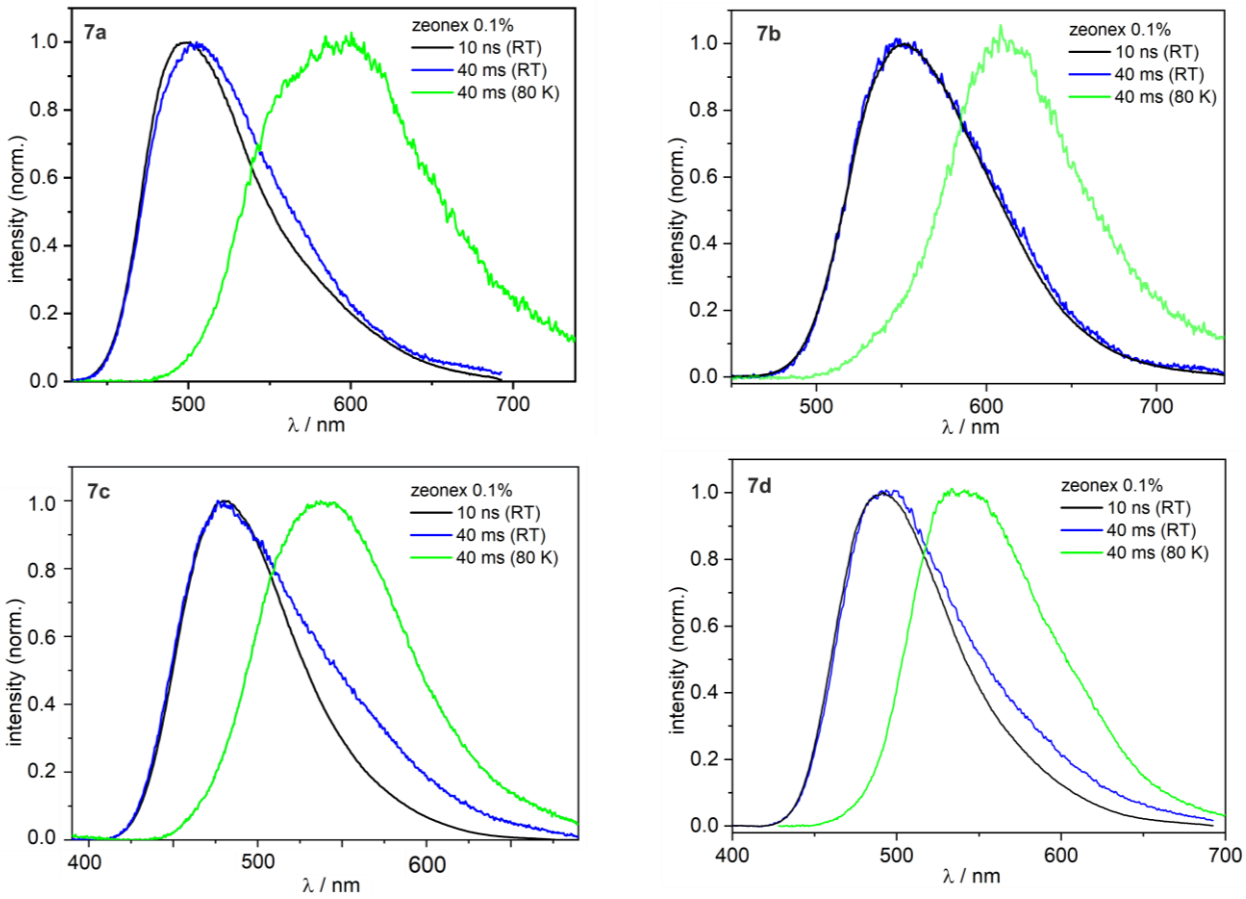

Figure S3.1 Time-resolved prompt, delayed fluorescence (RT) and phosphorescence spectra (80 K) of **7a–7d** in Zeonex films. Delay times are indicated in figure legend.

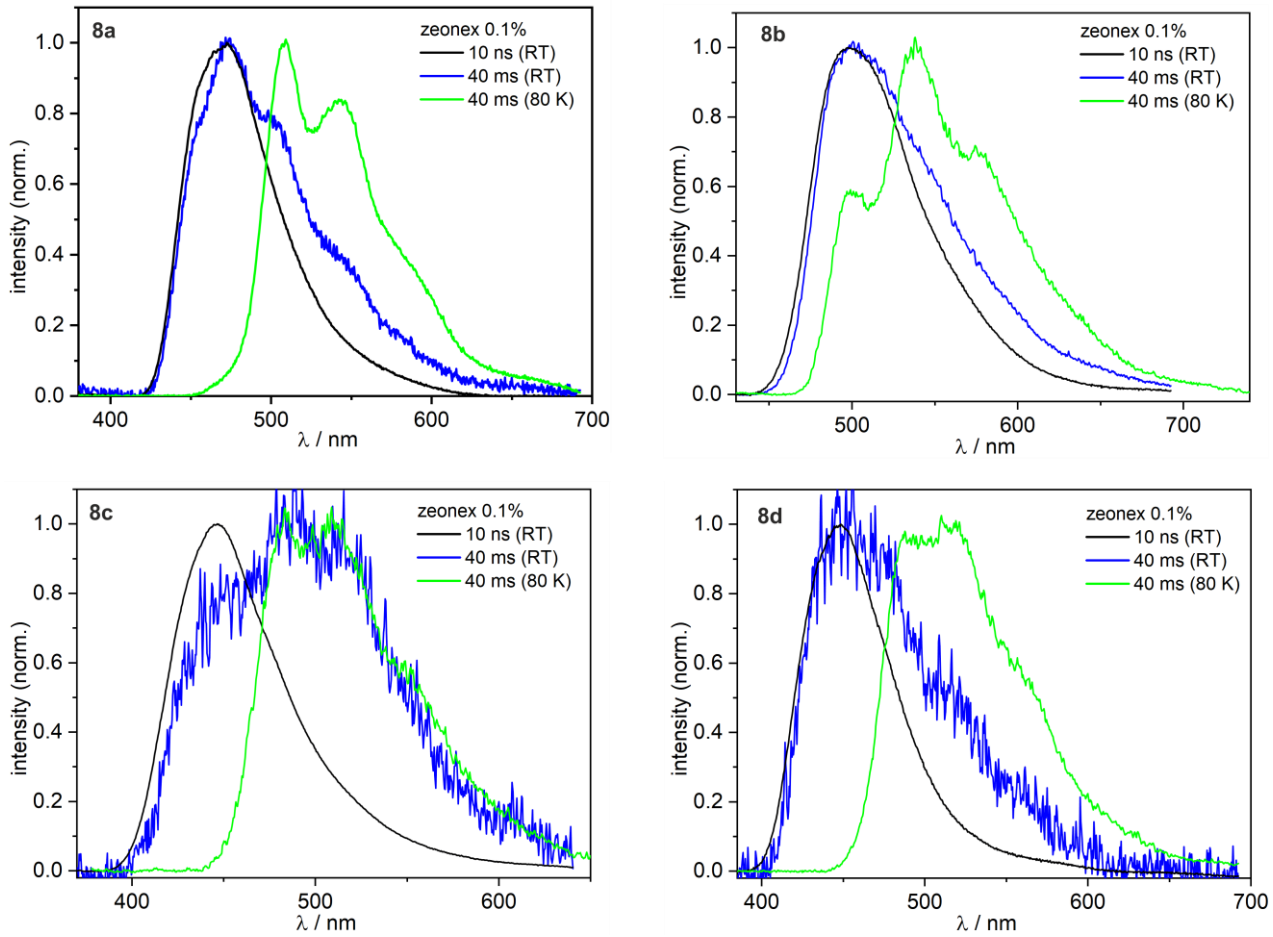

Figure S3.2. Time-resolved prompt, delayed fluorescence (RT) and phosphorescence spectra (80 K) of **8a–8d** in Zeonex films. Delay times are indicated in figure legend.

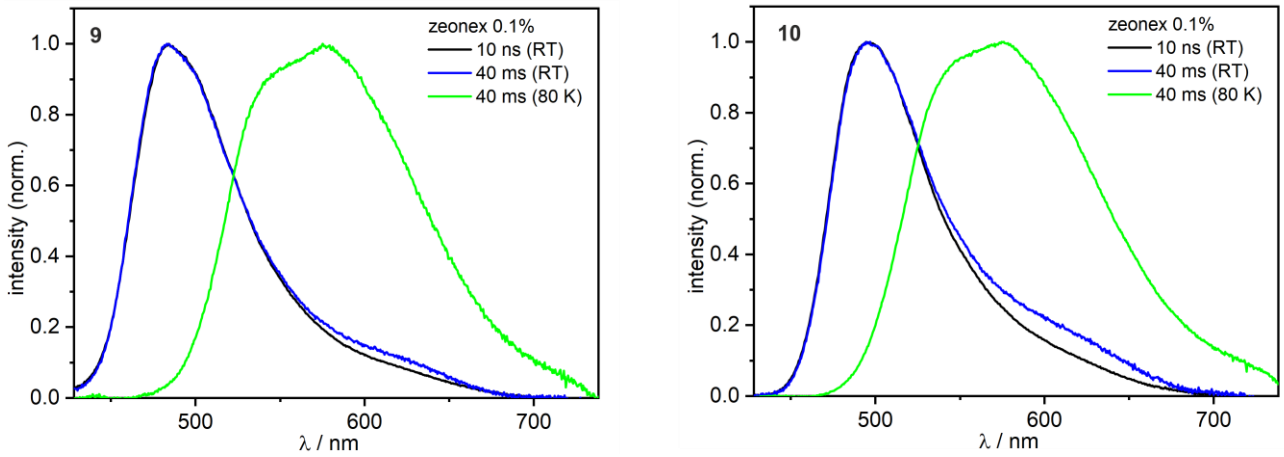

Figure S3.3. Time-resolved prompt, delayed fluorescence (RT) and phosphorescence spectra (80 K) of **9** and **10** in Zeonex films. Delay times are indicated in figure legend.

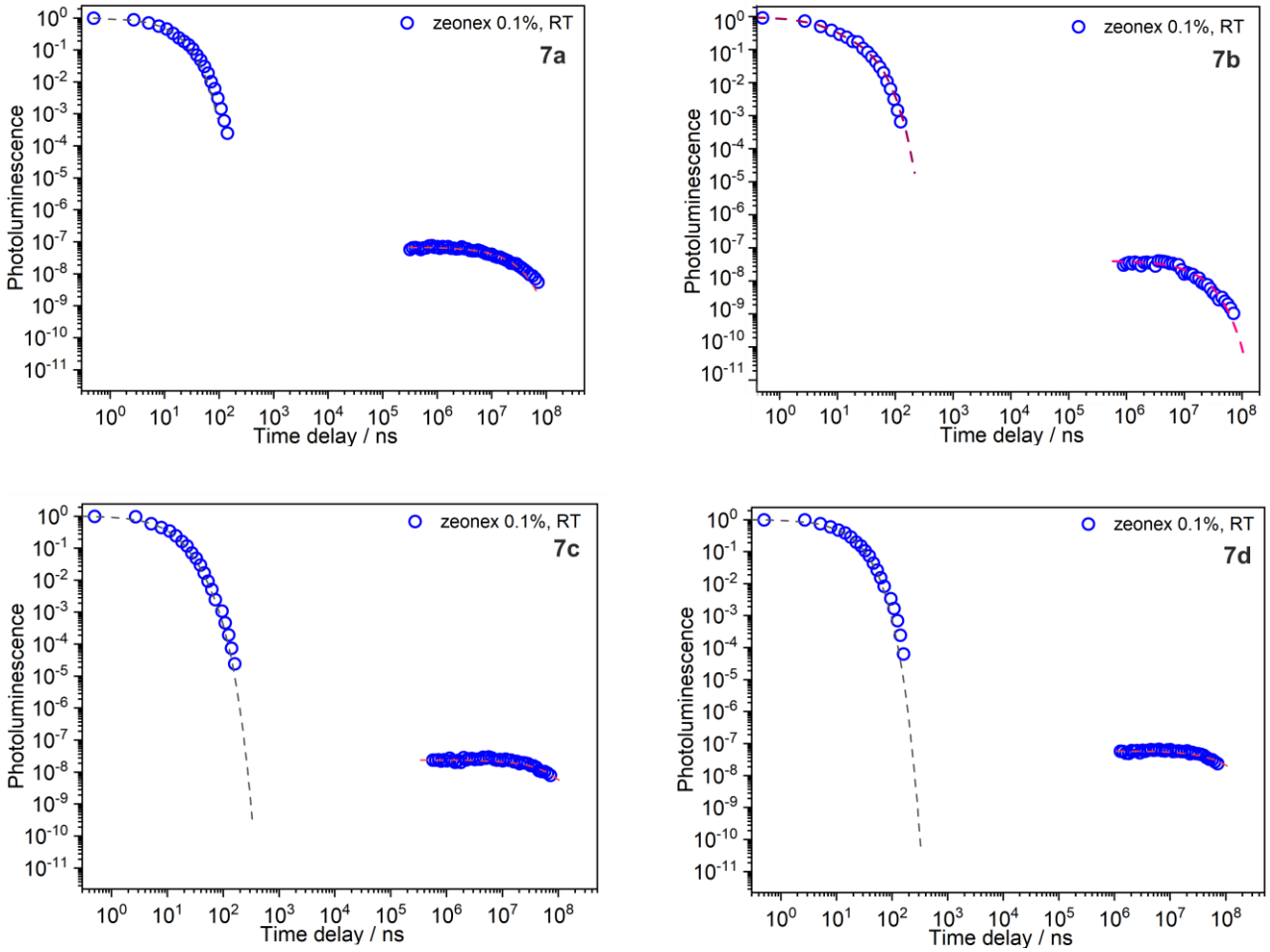

Figure S3.4. Photoluminescence decay traces for **7a–7d** in Zeonex films at room temperature.

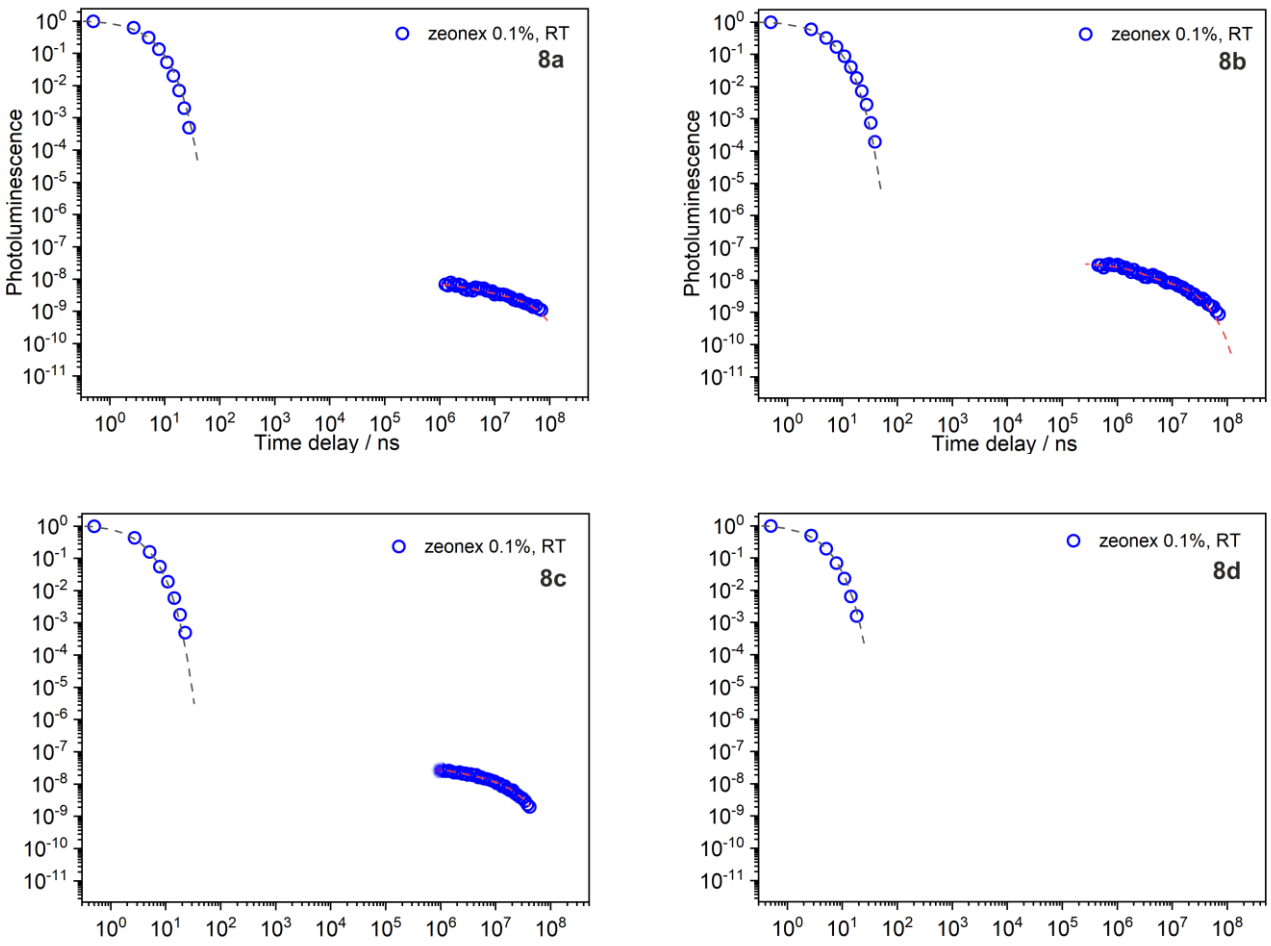

Figure S3.5. Photoluminescence decay traces for **8a–8d** in Zeonex films at room temperature.

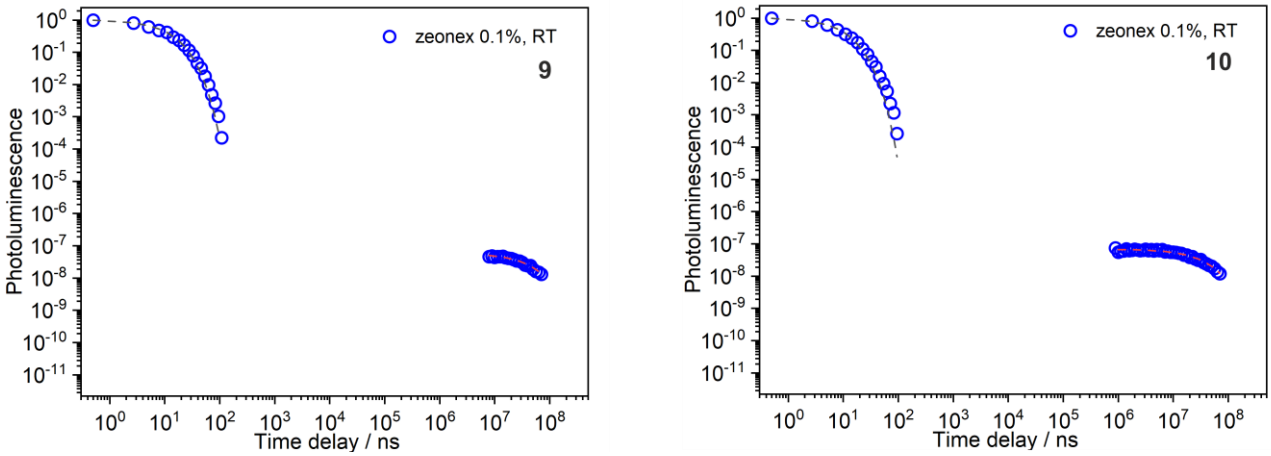

Figure S3.6. Photoluminescence decay traces for **9** and **10** in Zeonex films at room temperature.

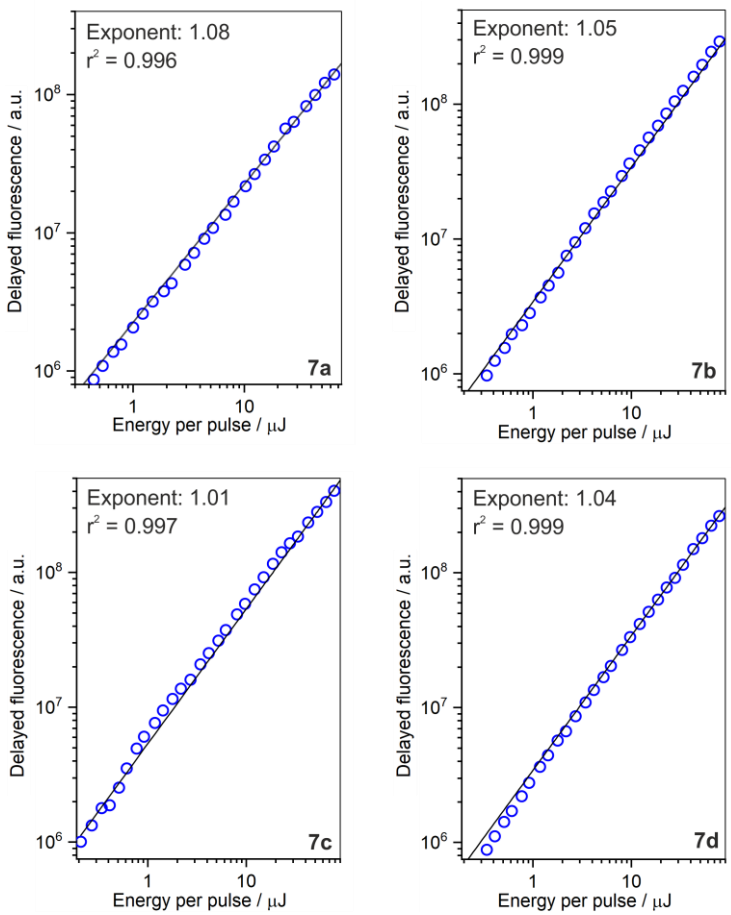

Figure S3.7. Relationship between the intensity of delayed fluorescence for **7a–7d** in 0.1wt% Zeonex films and excitation dose, presented in a logarithmic scale.

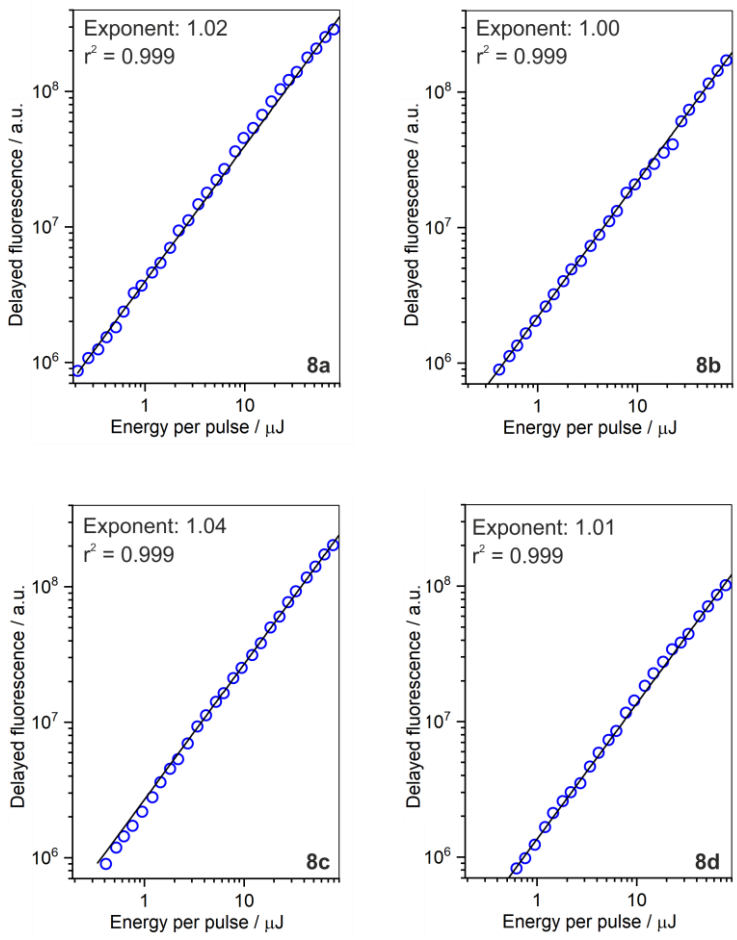

Figure S3.8. Relationship between the intensity of delayed fluorescence for **8a–8d** in 0.1wt% Zeonex films and excitation dose, presented in a logarithmic scale.

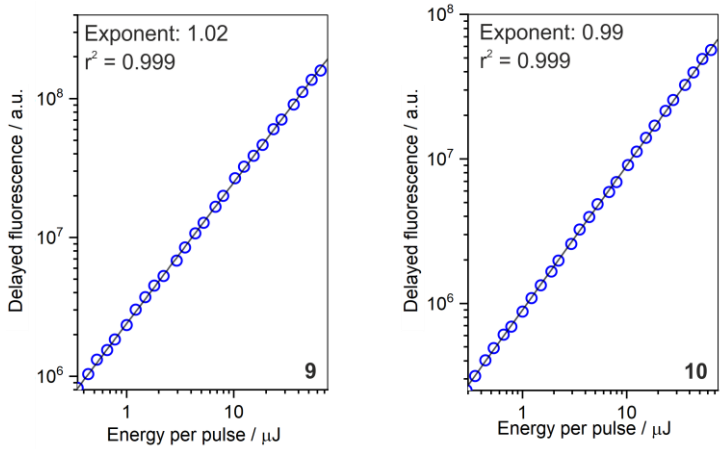

Figure S3.9. Relationship between the intensity of delayed fluorescence for **9** and **10** in 0.1% Zeonex films and excitation dose, presented in a logarithmic scale.

Table S3.1. Summary of rate constants calculated at RT for studied complexes in 0.1% solid film in Zeonex.

	k_{PF} / 10^7 s^{-1} [a]	k_{ISC} / 10^7 s^{-1} [b]	Φ_{rISC} [c]	k_{rISC} / s^{-1} [d]
7a	6.5	0.9	0.77	42.3
7b	5.6	0.4	1.00	76.4
7c	8.1	1.3	1.00	20.7
7d	5.1	2.1	0.90	16.4
8a	19.5	6.2	0.16	5.2
8b	15.0	9.3	0.17	11.4
8c	35.8	2.7	0.14	9.6
8d	33.1	5.4	-*	-*
9	4.7	5.2	0.40	13.1
10	6.3	1.7	0.92	21.6

[a]Prompt fluorescence radiative decay rate; [b]ISC rate; [c]rISC yield; rISC rate. The values were calculated assuming all non-radiative losses occur from the T_1 state and according to the methodology described elsewhere.[3] *k_{rISC} could not be estimated due to negligible DF intensity.

4. Electrochemical data

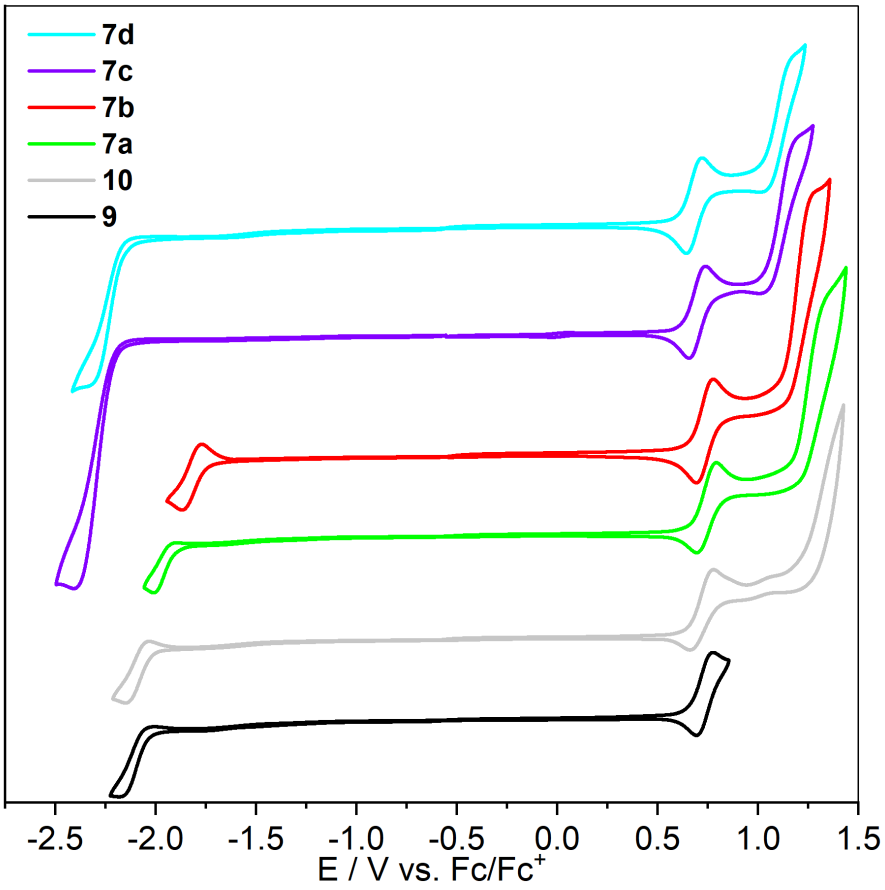

Figure S4.1. Overlay of CV for **7a–7d** and **9**, **10** in DCM.

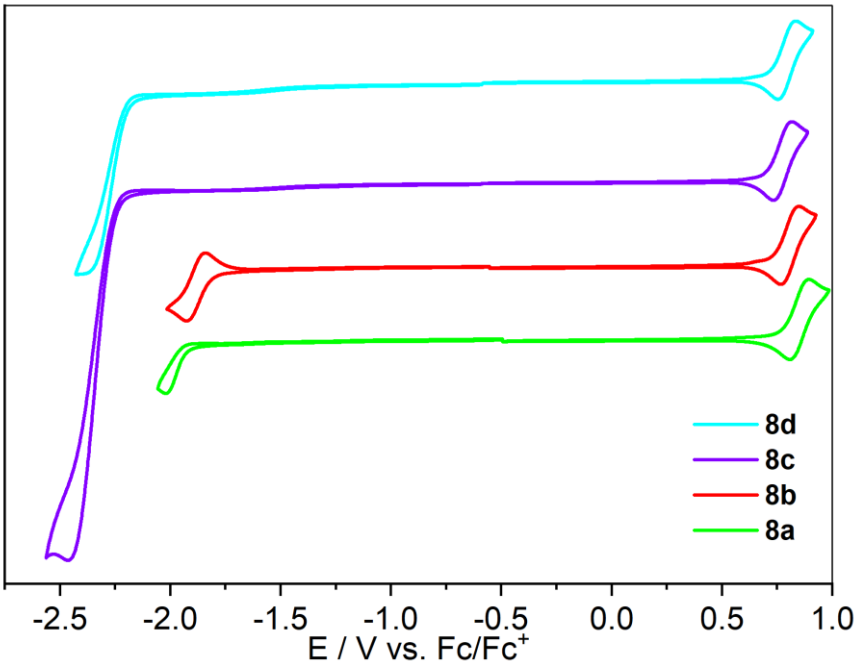

Figure S4.2. Overlay of CV for **8a–8d** in DCM.

5. Thermal properties.

Differential scanning calorimetric analysis was conducted using a Mettler-Toledo DSC1 experimental setup under dry nitrogen atmosphere. The calibration of the instrument was performed using the phase-transition temperature and phase-transition enthalpy of indium as a reference material. Samples were located in covered 40 μL aluminum pans with a lid hole to allow venting, whereas an empty pan was used as a reference. Heating was performed with a rate of 5 °C·min^{-1}. Thermogravimetric analyses were performed on a TGA/DSC1 (Mettler-Toledo) system under continuous flow of argon at the ramp rate of 10 K min^{-1} from 30 °C to 450 °C. The samples were prepared in covered ceramic crucibles. An empty crucible was used as a reference. α-Al_2O_3 was used for instrument calibration.

Table S5.1. Summary of DSC and TGA analysis for studied complexes. Melting temperatures were determined from the onset temperatures.

	7a	**7b**	**7c**	**7d**
m.p. (DSC) / °C	366	342	364	415
mass loss / %	>350	>350	170–300 °C (10.1%)	200–300 °C (3.6%)
	8a	**8b**	**8c**	**8d**
m.p. (DSC) / °C	390	> 420	> 420	399
mass loss / %	200–300 °C (4.5%)	150–230 °C (3.7%)	>450	110–170 °C (5.5%) 220–350 °C (9.8%)

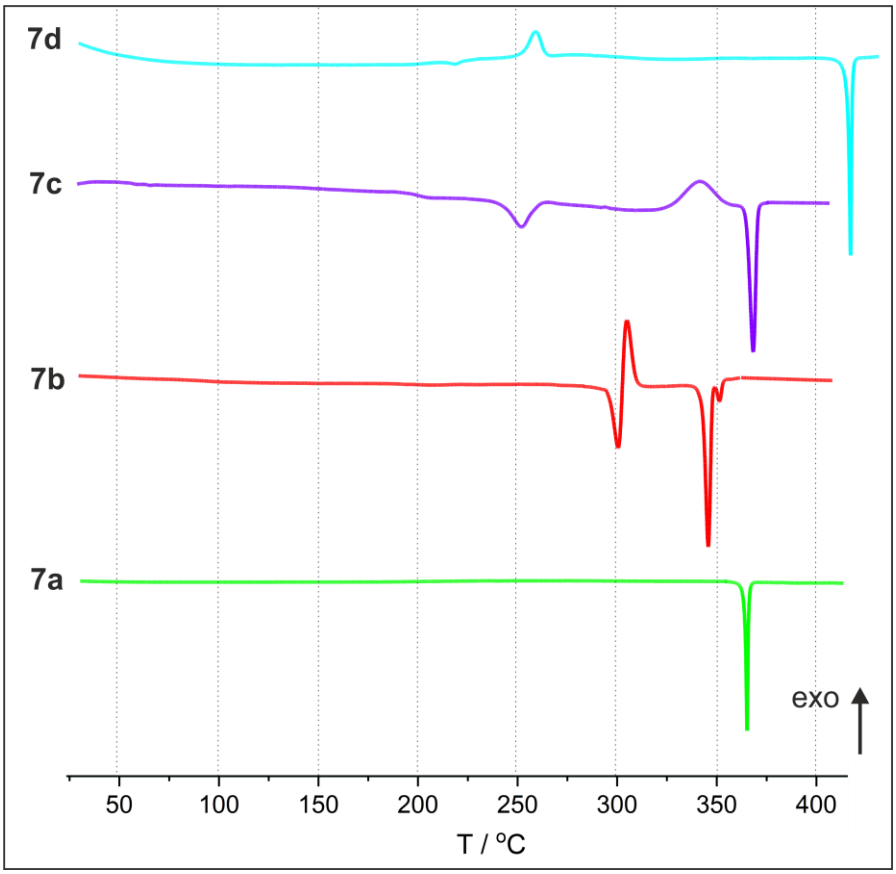

Figure S5.1. DSC curves of **7a–7d**.

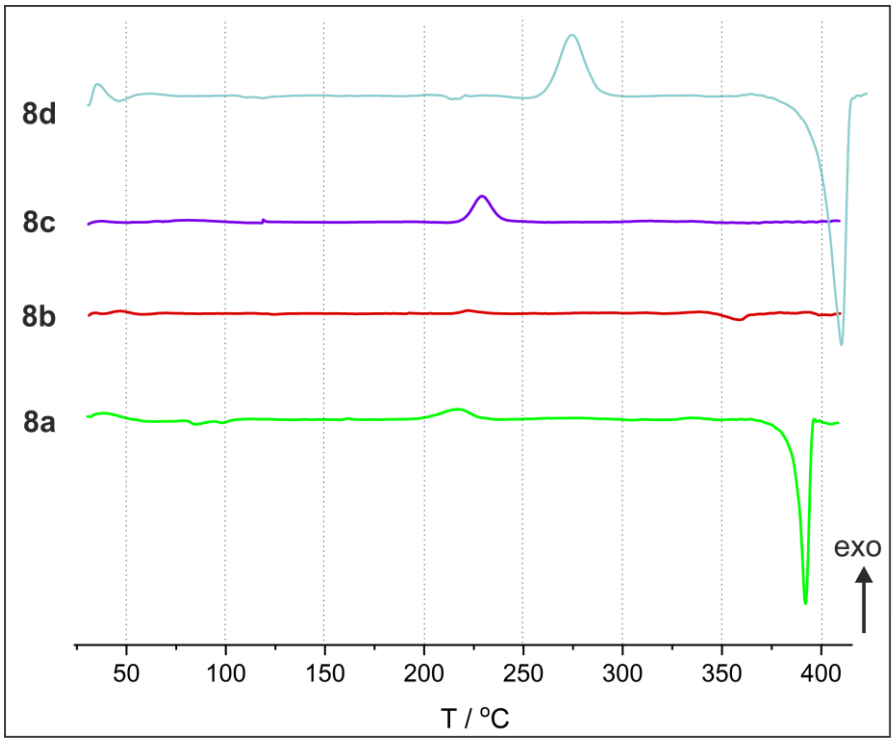

Figure S5.2. DSC curves of **8a–8d**.

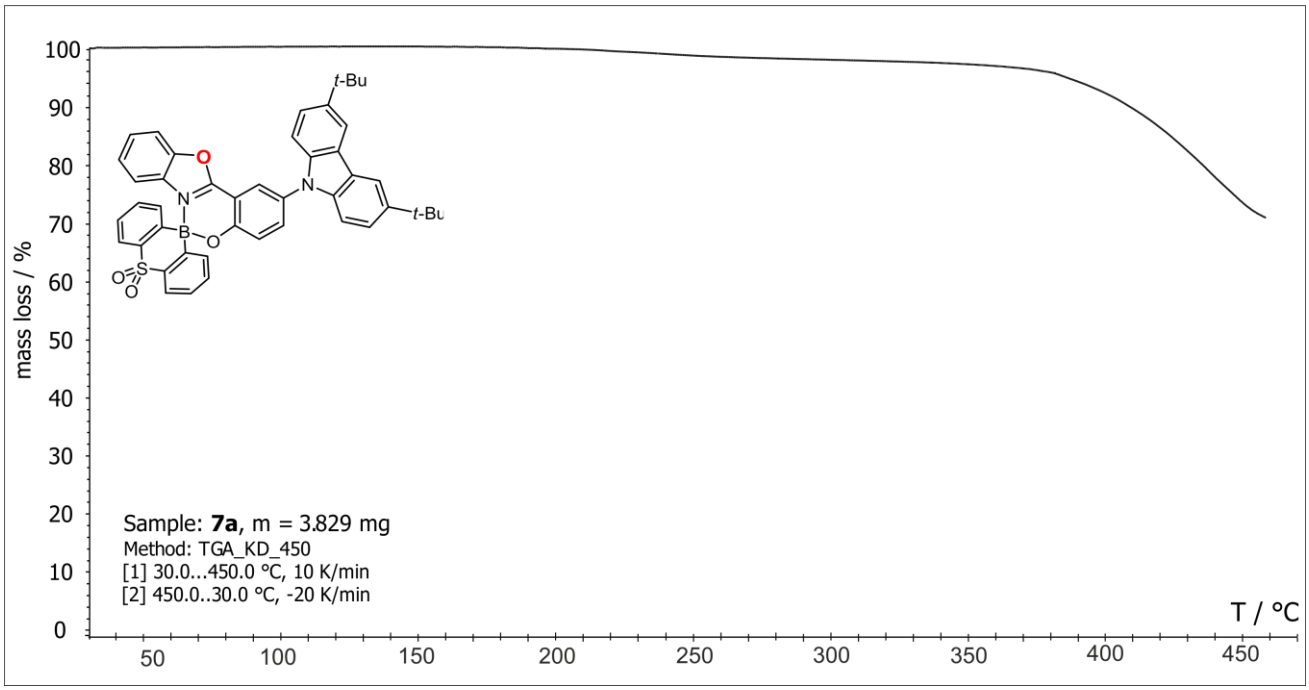

Figure S5.3. TGA curves of **7a**.

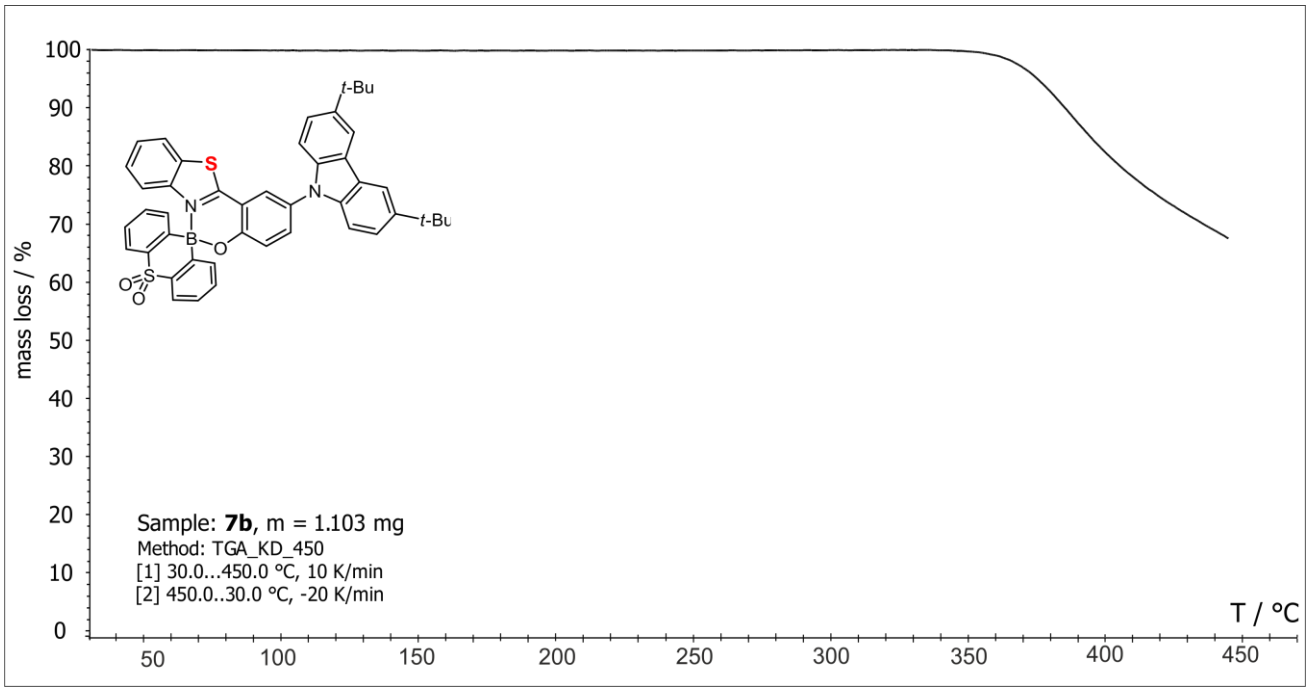

Figure S5.4. TGA curves of **7b**.

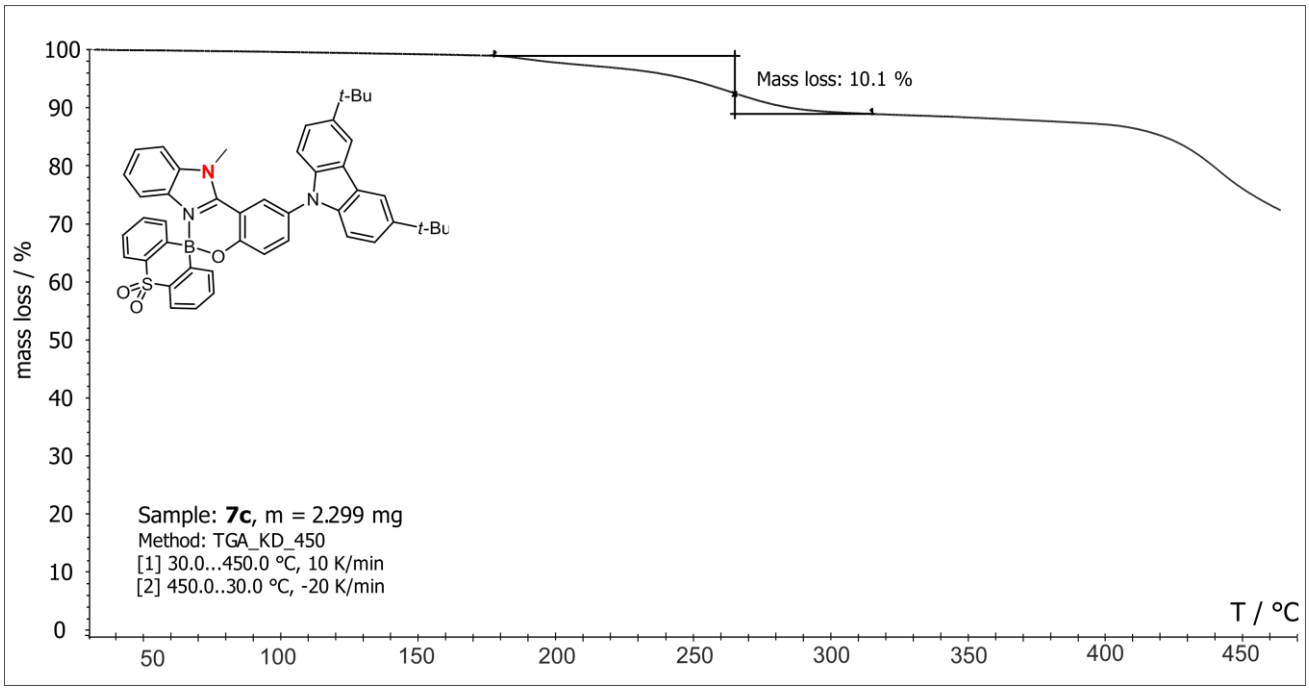

Figure S5.5. TGA curves of **7c**.

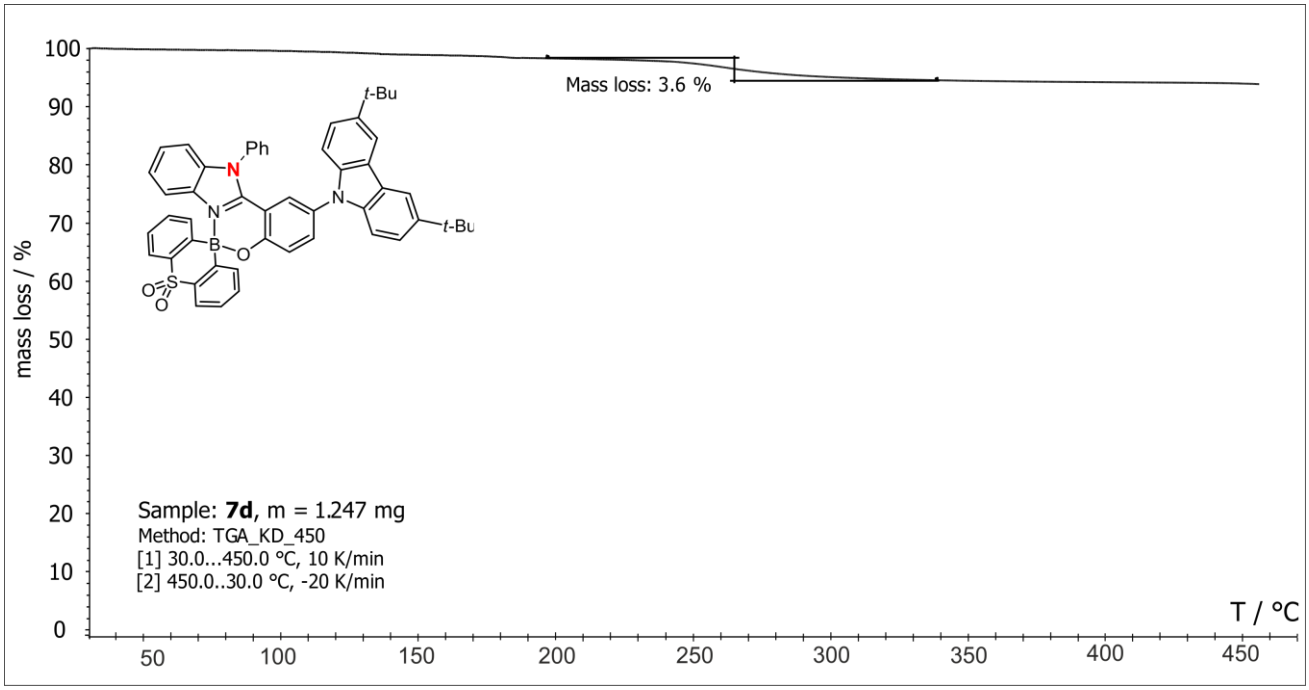

Figure S5.6. TGA curves of **7d**.

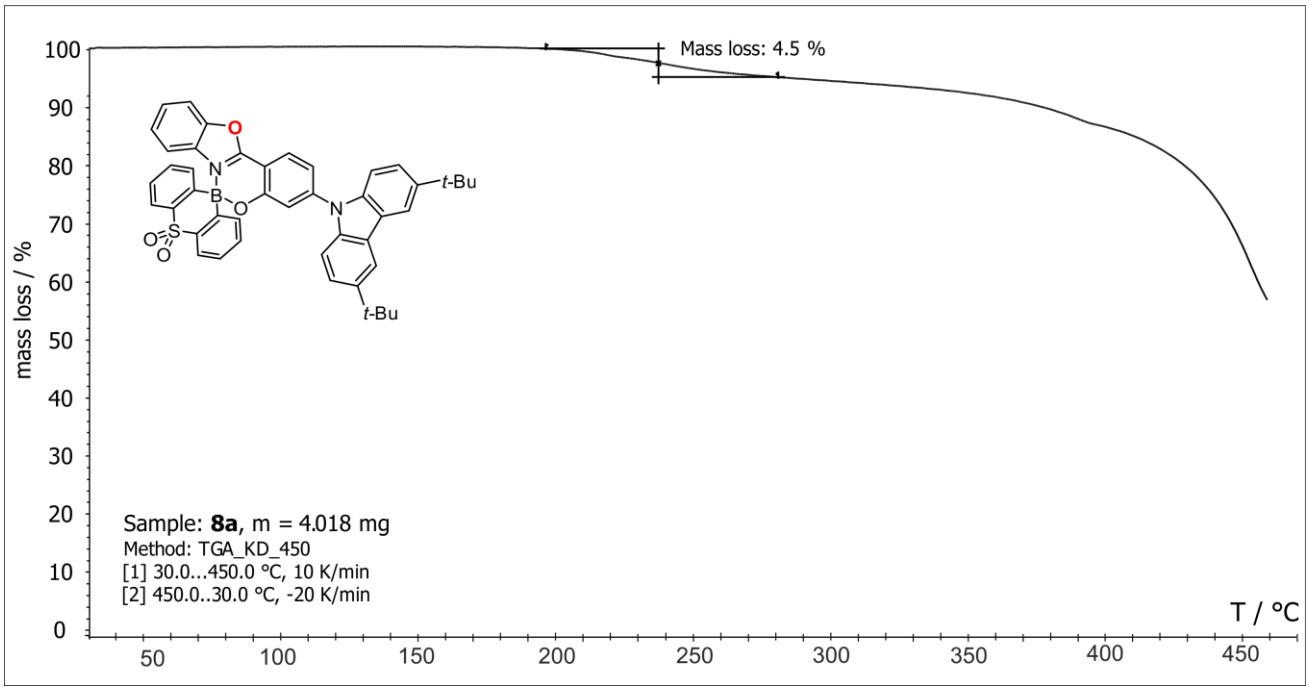

Figure S5.7. TGA curves of **8a**.

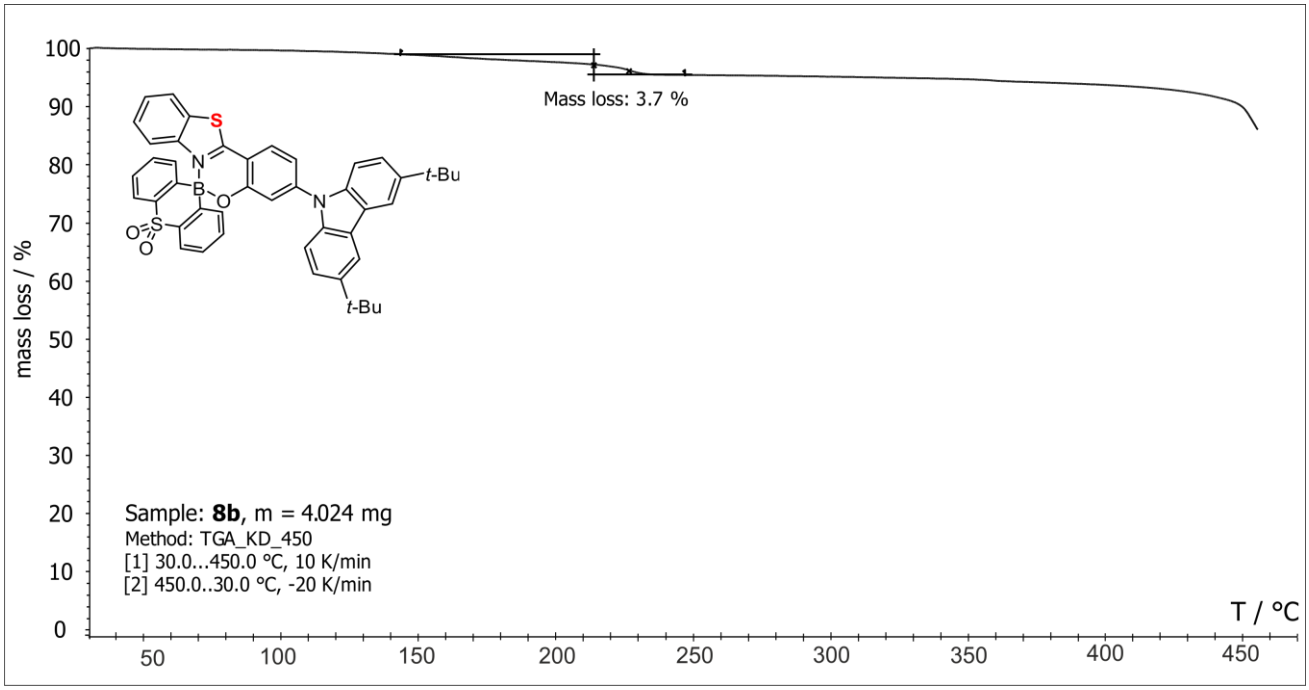

Figure S5.8. TGA curves of **8b**.

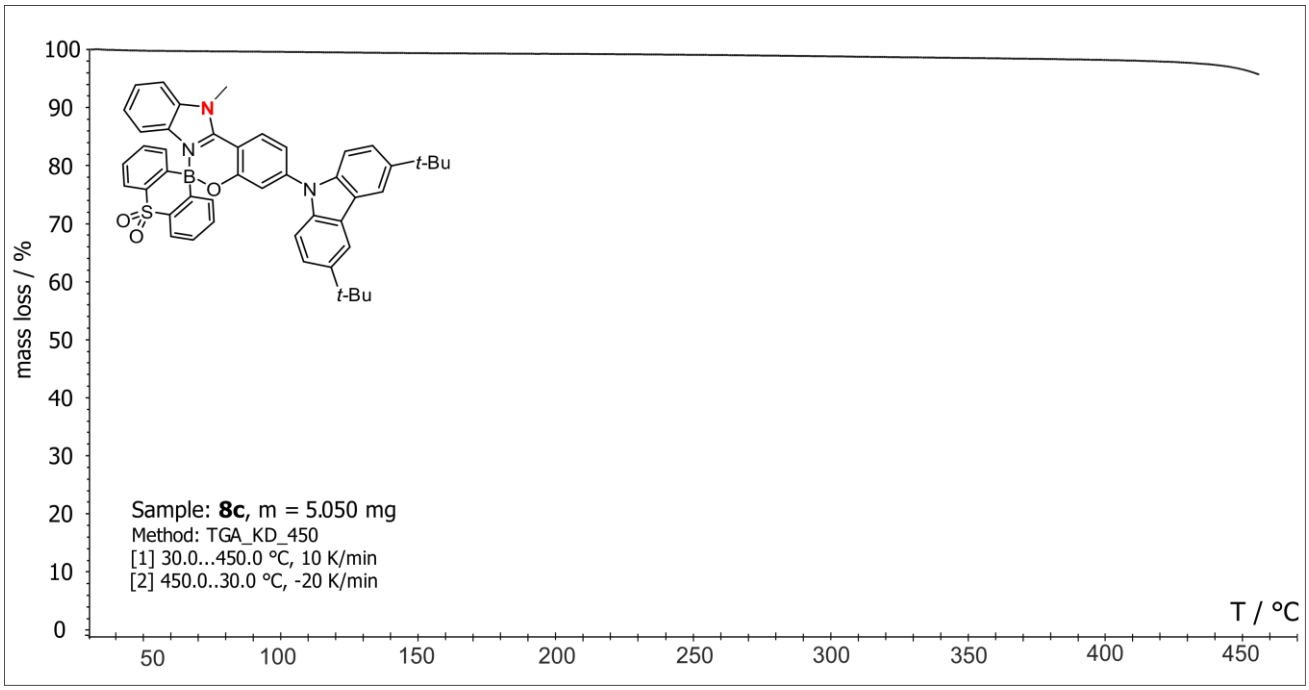

Figure S5.9. TGA curves of **8c**.

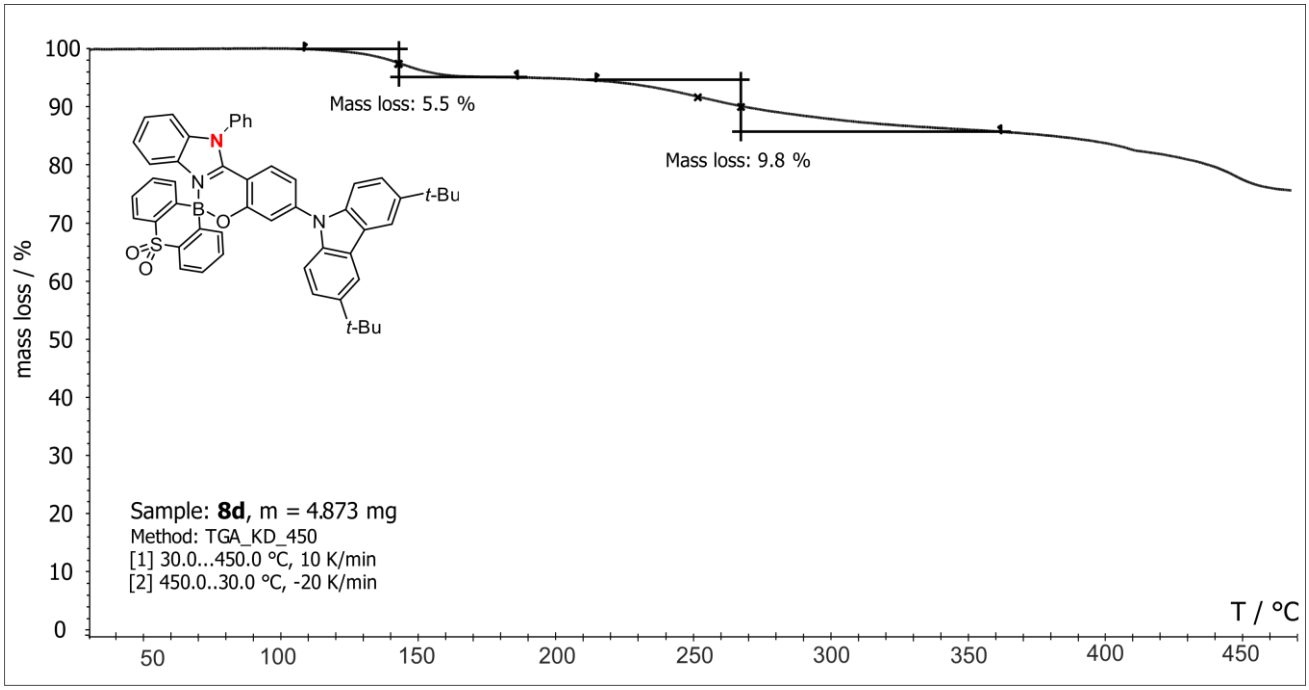

Figure S5.10. TGA curves of **8d**.

6. Quantum chemical calculations

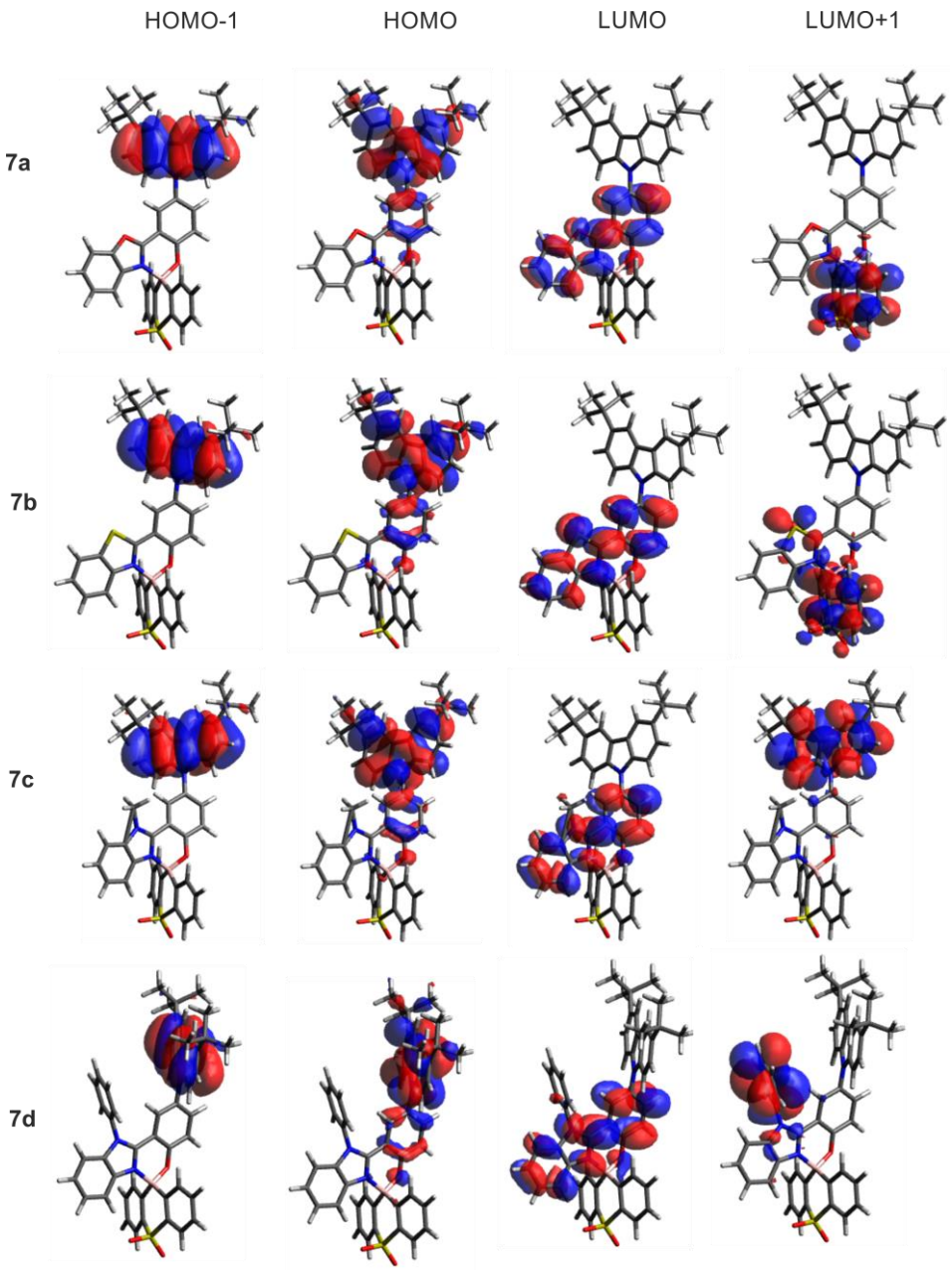

Figure 6.1. Distribution of frontiers molecular orbitals in **7a–7d**. Calculated at B3LYP/6-311++G(d,p) level of theory.

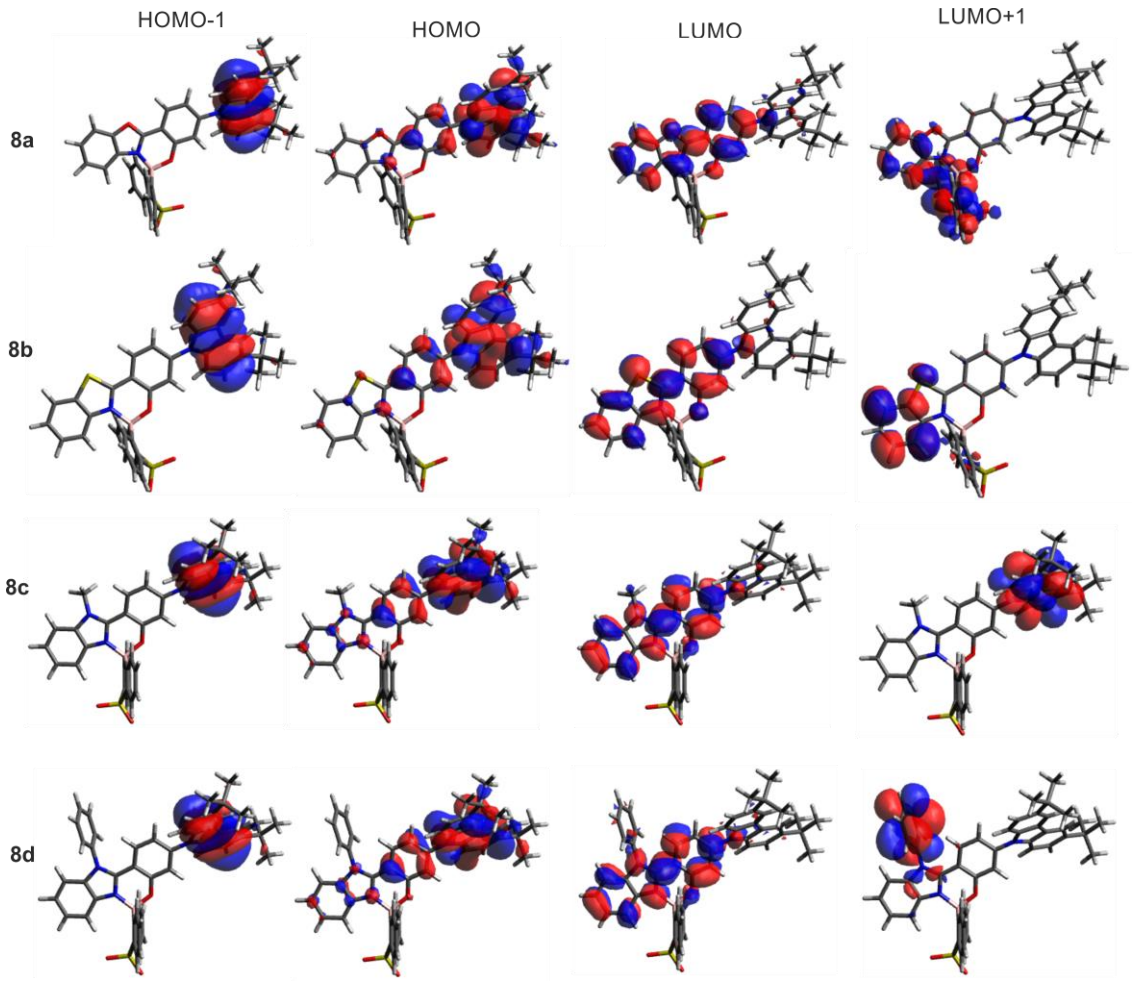

Figure 6.2. Distribution of frontiers molecular orbitals in **8a–8d**. Calculated at B3LYP/6-311++G(d,p) level of theory.

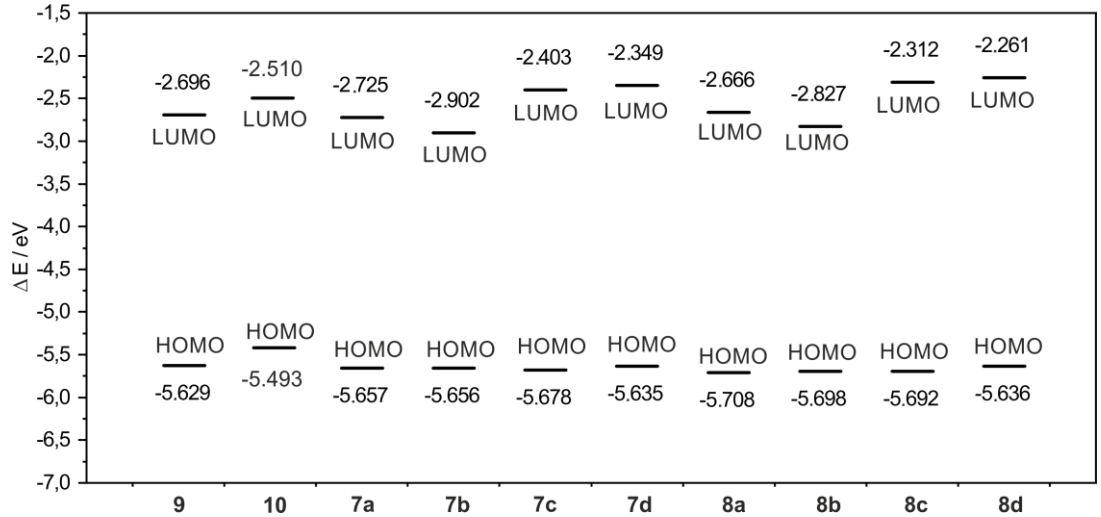

Figure 6.3. Diagram representing the energies of molecular orbitals (eV) for **7a–7d**, **8a–8d**, **9** and **10** derived from DFT calculations.

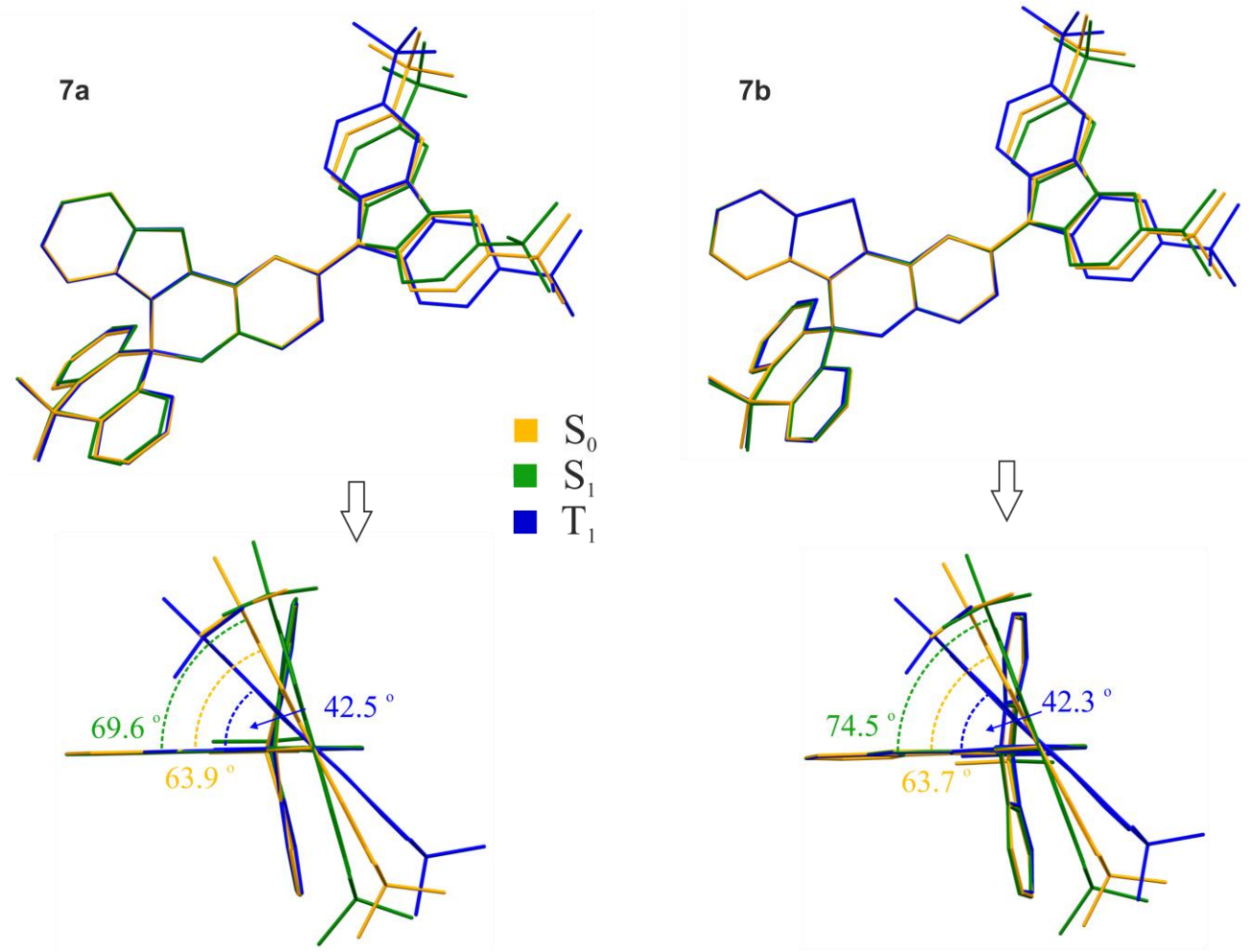

Figure S6.4. Overlay of the molecular geometries of S_0, S_1 and T_1 excited states in **7a** and **7b**.

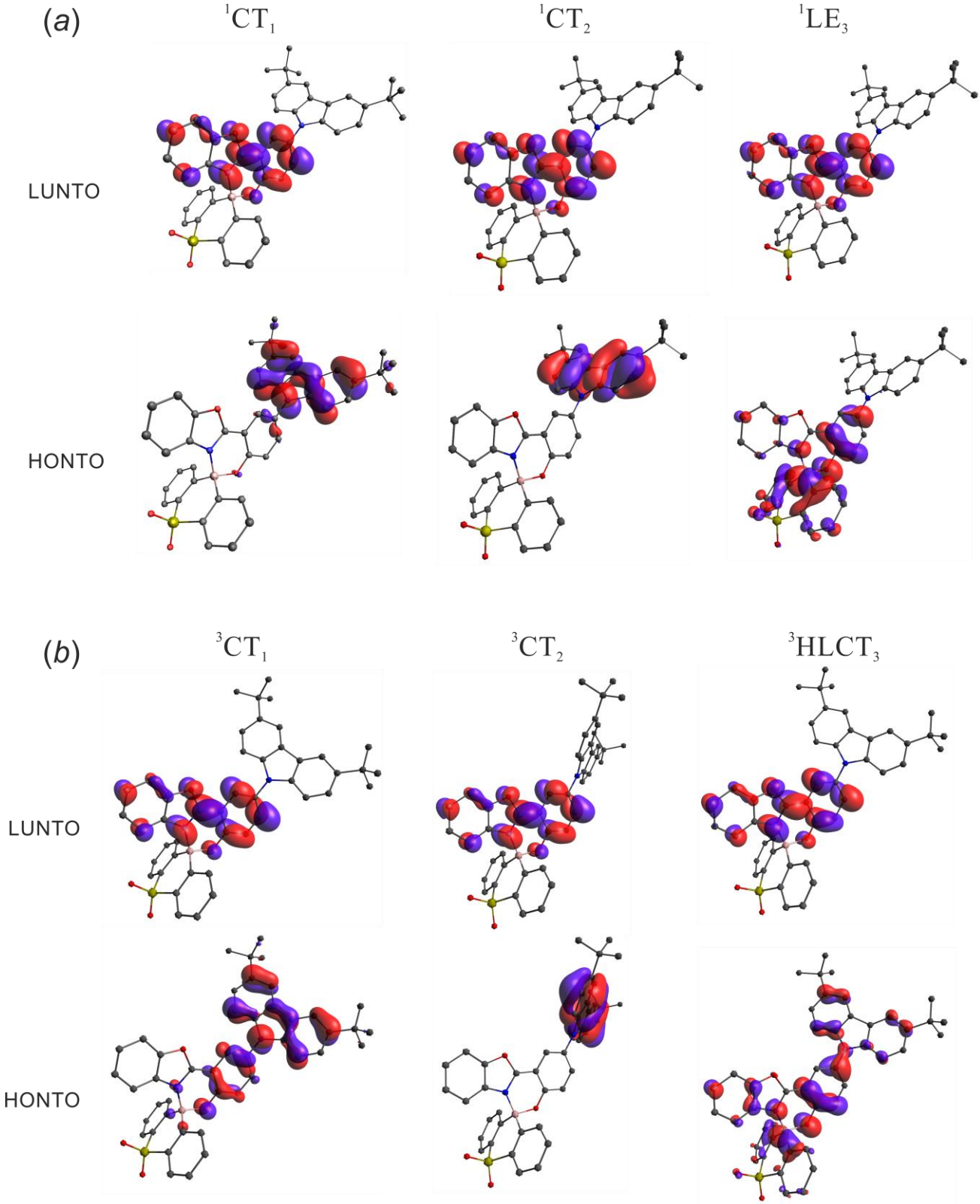

Figure S6.5. HONTO and LUNTO orbitals for S_1-S_3, T_1-T_3 states in **7a**.

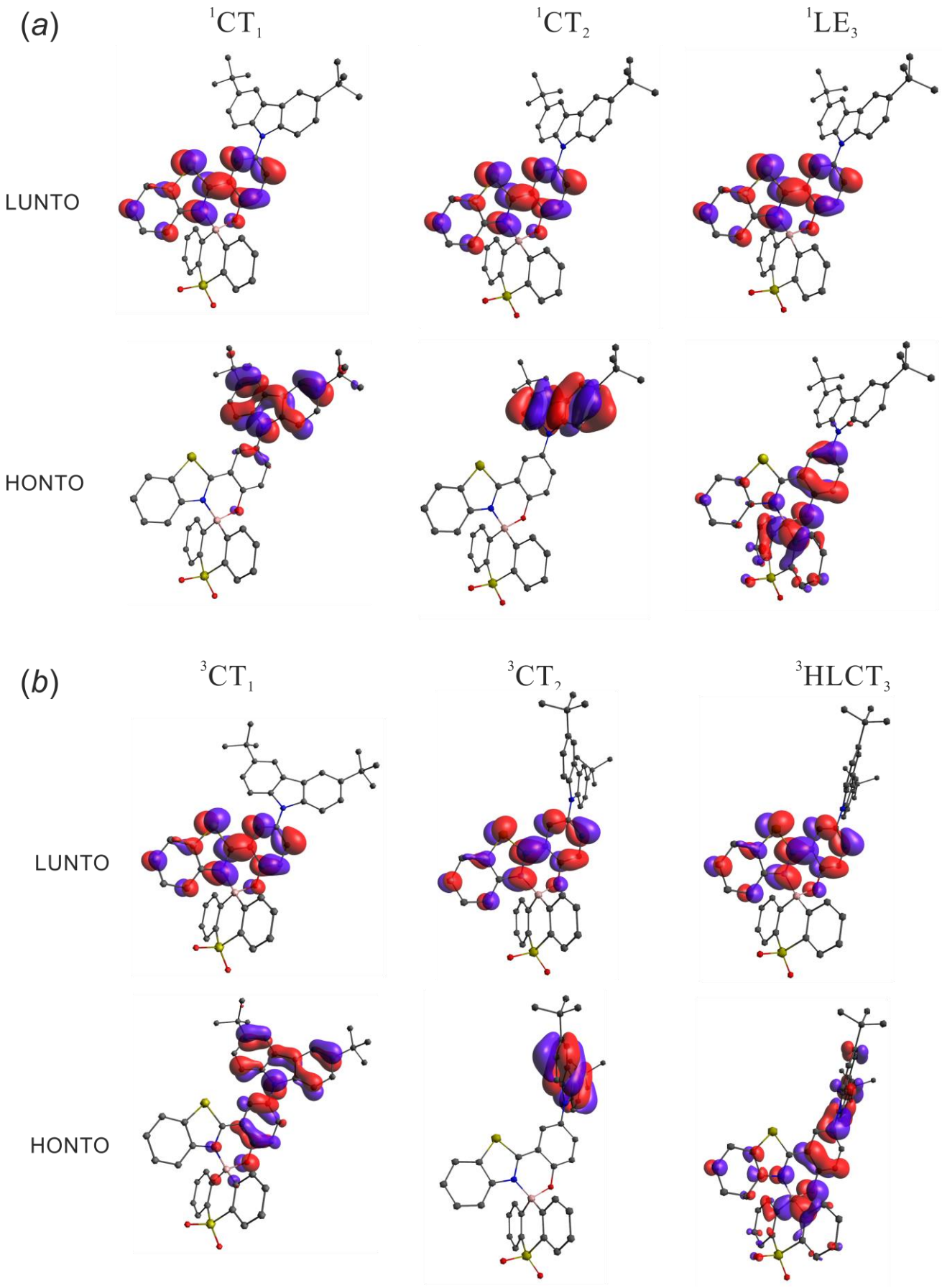

Figure S6.6. HONTO and LUNTO orbitals for S_1-S_3, T_1-T_3 states in **7b**.

Table S6.1. Overlap integrals between HOMO and LUMO orbitals (*O*) calculated for studied systems.

Compound	*O*
7a	0.280
7b	0.278
7c	0.285
7d	0.261
8a	0.421
8b	0.422
8c	0.431
8d	0.432
9	0.258
10	0.275

Table S6.2. Results of TD-DFT (PBE0/6-311++G(d,p)) calculations for studied compounds. The calculations were performed in toluene solvent field. The experimental absorption and emission wavelengths (toluene) have been provided for comparison.

	λ_{abs} (DFT)	*f*	λ_{abs} (exp.)	λ_{em} (DFT)	*f*	λ_{em} (exp.)
7a	430	0.0220	424	540	0.0384	522
7b	473	0.0518	451	588	0.0508	565
7c	412	0.0506	390	488	0.0595	476
7d	417	0.0577	406	501	0.0608	497
8a	437	0.6798	427	500	0.3107	489
8b	463	0.6779	456	530	0.2674	514
8c	399	0.7030	400	459	0.3377	436
8d	402	0.6931	410	472	0.3691	457

7. OLEDs

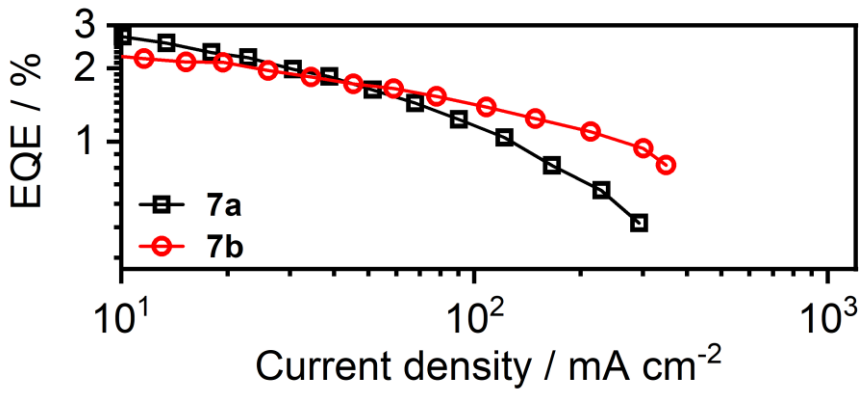

Figure S7.1. EQE *vs* current density for OLEDs featuring **7a** and **7b** as emitters.

8. Synthesis

General Comments.

Solvents used for reactions were dried by heating to reflux with sodium/benzophenone and distilled under argon. Starting materials and other reagents were used as received without further purification. Reactions involving air-sensitive compounds were carried out under an argon atmosphere. Detailed procedures for the synthesis of intermediates **1–4**, **5a–5d**, **6a–6d** and reference compounds **9** and **10** are given in the ESI, Section 7. ^{1}H and ^{13}C spectra were recorded on an Agilent NMR 400 MHz DDR2 spectrometer. In the ^{13}C NMR spectra the resonances of boron-bound carbon atoms were not observed in most cases as a result of their broadening by a quadrupolar boron nucleus. ^{1}H and ^{13}C NMR chemical shifts are given relative to TMS using residual solvent resonances.

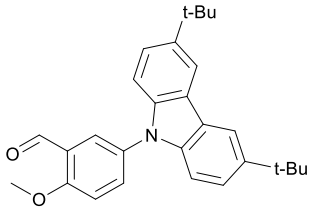

5-(3,6-di-*t*-butyl-9*H*-carbazol-9-yl)-2-methoxybenzadehyde (**1**). A 1-L 3-neck flask was charged with 3,6-di-*t*-butylcarbazole (13.95 g, 49.9 mmol), 5-bromo-2-methoxybenzaldehyde (8.95 g, 41.6 mmol), K_2CO_3 (17.30 g, 125 mmol). Solids were suspended in nitrobenzene (300 mL) and 18-crown-6 (1.14 g, 4.2 mmol) and CuI (0.80 g, 4.2 mmol) were added. The mixture was stirred at 180 °C under argon atmosphere for 4 days. The reaction mixture was cooled to rt, filtered through a thin Celite pad and the pad was washed with DCM (100 mL). Filtrate was washed with saturated NH_4Cl_{aq} solution (3 × 200 mL), 0.5 M HCl_{aq} (2 × 100 mL), water (100 mL) and the organic phase was dried over Na_2SO_4. After filtration volatile solvents were removed on rotary evaporator and nitrobenzene was distilled off under vacuum ($3 \cdot 10^{-3}$ mbar) to obtain thick oil. Hexane (150 mL) was added, and the mixture was warmed to boiling and left intensively stirring for 1 h. After cooling to rt precipitate was filtered off, washed with hexane (2 × 50 mL) and dried under vacuum to give **1** as pale yellow powder (11.38 g, 66%, TLC Rf = 0.50 (20% AcOEt/hexane)). ^{1}H NMR (400 MHz, $CDCl_3$) δ = 10.55 (s, 1H), 8.14 (d, *J* = 2.0 Hz, 2H), 8.02 (d, *J* = 2.7 Hz, 1H), 7.72 (dd, *J* = 8.8, 2.7 Hz, 1H), 7.46 (dd, *J* = 8.7, 2.0 Hz, 2H), 7.24 (d, *J* = 8.8 Hz, 2H), 7.20 (d, *J* = 8.8 Hz, 1H), 4.05 (s, 3H), 1.47 (s, 18H) ppm. $^{13}C\{^{1}H\}$ NMR (75 MHz, $CDCl_3$) δ = 189.1, 160.6, 143.1, 139.5, 134.4, 131.4, 126.9, 125.9, 123.8, 123.4, 116.4, 113.3, 109.0, 56.2, 34.9, 32.2 ppm.

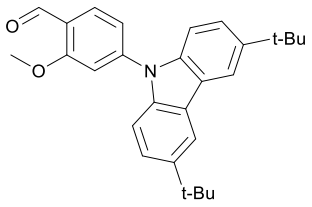

4-(3,6-di-*t*-butyl-9*H*-carbazol-9-yl)-2-methoxybenzadehyde (**2**).[4] The reaction was performed according to a protocol used for **1** using 3,6-di-*t*-butylcarbazole (3.35 g, 12.0 mmol), 4-bromo-2-methoxybenzaldehyde (2.25 g, 10.0 mmol), K_2CO_3 (4.15 g, 30 mmol), nitrobenzene (80 mL), 18-crown-6 (0.26 g, 0.10 mmol) and CuI (0.19 g, 0.10 mmol). Crude product was purified by column chromatography using toluene as eluent followed by hexane wash and drying under vacuum to yield **2** as pale yellow solid (3.07 g, 74%, TLC Rf = 0.45 (toluene)). ^{1}H NMR (300 MHz, $CDCl_3$) δ = 10.52

(d, *J* = 0.8 Hz, 1H), 8.15 (d, *J* = 1.6 Hz, 1H), 8.14 (d, *J* = 1.6 Hz, 1H), 8.06 (d, *J* = 8.2 Hz, 1H), 7.50 – 7.48 (m, 4H), 7.29 (ddd, *J* = 8.2, 1.8, 0.8 Hz, 1H), 7.24 (d, *J* = 1.8 Hz, 1H), 3.97 (s, 3H), 1.48 (s, 18H) ppm.

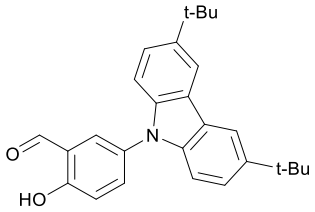

5-(3,6-di-*t*-butyl-9*H*-carbazol-9-yl)-2-hydroxybenzadehyde (**3**). 1 M BCl_3 in hexane (31 mL, 31 mmol) was added dropwise to solution of **1** (6.43 g, 15.5 mmol) and *n*-Bu_4NI (6.01 g, 16.3 mmol) in anh. DCM (130 mL) at –78 °C. After few minutes cooling bath was removed and mixture was warmed up to rt and stirred for 2.5 h. Ice cooling bath was placed and reaction was quenched with ice-cold water (10 mL), then sat. $NaHCO_3$ solution (ca. 50 mL) was added to reach pH = 7. Phases were separated, organic phase was washed with sat. $NaHCO_3$ solution (2 × 50 mL), water (30 mL) and dried over Na_2SO_4. After filtration volatilities were removed under vacuum. Crude (yellow solid) was purified by column chromatography using AcOEt/hexane eluent in 0–20% gradient. Combined fractions comprising the product were concentrated till dryness, and the residue was washed with a small amount of hexane, filtered and dried under vacuum to give **3** as pale yellow solid (3.16 g, 51%, TLC Rf = 0.77 (20% AcOEt/hexane)). ^{1}H NMR (400 MHz, $CDCl_3$) δ = 11.15 (s, 1H), 9.94 (d, *J* = 0.6 Hz, 1H), 8.15 (dd, *J* = 2.0, 0.6 Hz, 2H), 7.74 (dd, *J* = 2.6, 0.5 Hz, 1H), 7.70 (ddd, *J* = 8.7, 2.6, 0.5 Hz, 1H), 7.48 (dd, *J* = 8.6, 2.0 Hz, 2H), 7.23 (dd, *J* = 8.6, 0.6 Hz, 2H), 7.22 (dt, *J* = 8.7, 0.6 Hz, 1H), 1.47 (s, 18H) ppm. ^{13}C{^{1}H} NMR (101 MHz, $CDCl_3$) δ = 196.1, 160.6, 143.3, 139.6, 136.3, 131.7, 130.4, 123.9, 123.4, 121.3, 119.5, 116.5, 108.8, 34.9, 32.1 ppm.

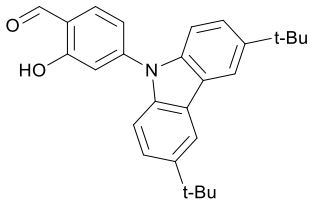

4-(3,6-di-*t*-butyl-9*H*-carbazol-9-yl)-2-hydroxybenzadehyde (**4**).[4] The reaction was performed according to a protocol used for **3** using 1 M BCl_3/hexane (6.3 mL, 6.3 mmol), **2** (1.30 g, 3.14 mmol), *n*-Bu_4NI (1.36 g, 3.45 mmol) and anh. DCM (25 mL). After the addition of BCl_3 mixture was stirred at –10 °C for 2h, then quenched with water (1 mL). Crude product was purified using DCVC method with $CHCl_3$/heptane eluent in 0–100% gradient. Compound **4** was obtained as yellow solid (0.96 g, 76%, TLC Rf = 0.43 (50% $CHCl_3$/heptane)). ^{1}H NMR (300 MHz, $CDCl_3$) δ = 11.35 (s, 1H), 9.95 (d, *J* = 0.6 Hz, 1H), 8.12 (dd, *J* = 1.9, 0.7 Hz, 2H), 7.75 (dd, *J* = 8.3, 0.4 Hz, 1H), 7.54 (dd, *J* = 8.7, 0.7 Hz, 2H), 7.49 (dd, *J* = 8.7, 1.9 Hz, 2H), 7.30 (dd, *J* = 8.2, 1.9 Hz, 1H), 7.27–7.25 (m, 1H), 1.47 (s, 18H) ppm.

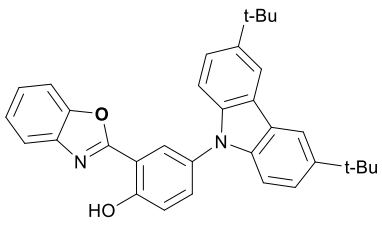

2-(2-hydroxy-5-(3,6-di-*t*-butyl-9*H*-carbazol-9-yl)-phenyl)-1,3-benzoxazole (**5a**). A mixture of 2-aminophenol (70 mg, 0.50 mmol), **3** (200 mg, 0.50 mmol) and activated molecular sieves 3Å (ca. 15 beads) in anh. DMF (5 mL) was stirred at 60 °C for 2h. After cooling to room temperature NaCN (4 mg, 0.08 mmol) was added and mixture was left intensively stirred in open flask. Progress of the reaction was monitored by TLC. Upon completion of the reaction (ca. 20 h) powdered molecular sieves were filtered off, DMF was distilled off under vacuum. Crude product was purified by column chromatography using 1% AcOEt/hexane eluent to give **5a** as yellowish solid (153 mg, 63%, TLC Rf = 0.80 (20% AcOEt/heptane)). ^{1}H NMR (400 MHz, $CDCl_3$) δ 11.67 (bs, 1H, OH), 8.23 (d, *J* = 2.4 Hz, 1H), 8.19 (dd, *J* = 2.0, 0.6 Hz, 2H), 7.81–7.76 (m, 1H), 7.62 (dd, *J* = 8.7, 2.6 Hz, 1H), 7.59–7.55 (m, 1H), 7.50 (dd, *J* = 8.6, 2.0 Hz, 2H), 7.45–7.37 (m, 2H), 7.34 (m, 3H), 1.50 (s, 18H) ppm. ^{13}C{^{1}H} NMR (101 MHz, $CDCl_3$) δ 162.2, 157.7, 149.2, 142.8, 139.9, 139.6, 132.5, 129.9, 125.8, 125.6, 125.2, 123.7, 123.2, 119.4, 118.9, 116.3, 111.5, 110.8, 109.0, 34.8, 32.1 ppm.

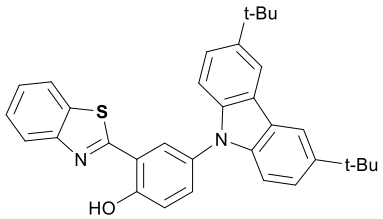

2-(2-hydroxy-5-(3,6-di-*t*-butyl-9*H*-carbazol-9-yl)-phenyl)-1,3-benzothiazole (**5b**). Mixture of 2-hydroxythiophenol (94 mg, 0.75 mmol), **3** (300 mg, 0.75 mmol) and $Na_2S_2O_5$ (143 mg, 0.75 mmol) in anh. DMF was stirred at 145 °C for 16 h. After cooling, water (10 mL) was slowly added to precipitate a bright solid. Precipitate was filtered off, washed with water and dried. Crude product was purified by column chromatography using 1% AcOEt/hexane eluent to give **5b** as pale yellow solid (246 mg, 65%, TLC Rf = 0.57 (10% AcOEt/heptane)). ^{1}H NMR (400 MHz, $CDCl_3$) δ 12.74 (bs, 1H, OH), 8.18 (dd, *J* = 2.0, 0.7 Hz, 2H), 8.06 (ddd, *J* = 8.2, 1.2, 0.6 Hz, 1H), 7.91–7.88 (m, 1H), 7.87 (d, *J* = 2.4 Hz, 1H), 7.58 – 7.52 (m, 2H), 7.50 (dd, *J* = 8.6, 1.9 Hz, 2H), 7.44 (ddd, *J* = 8.0, 7.2, 1.2 Hz, 1H), 7.33 (d, *J* = 8.8 Hz, 1 H), 7.31 (dd, *J* = 8.6, 0.7 Hz, 2H), 1.49 (s, 18H) ppm. ^{13}C NMR (101 MHz, $CDCl_3$) δ 168.5, 157.1, 151.8, 142.8, 139.7, 132.7, 131.8, 129.7, 126.9, 126.8, 125. 9, 123.7, 123.2, 122.4, 121.6, 119.4, 117.6, 116.3, 108.9, 34.8, 32.1 ppm.

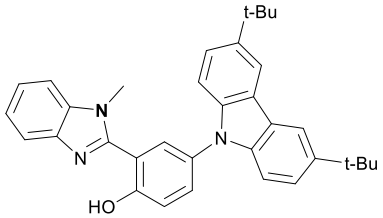

2-(2-hydroxy-5-(3,6-di-*t*-butyl-9*H*-carbazol-9-yl)-phenyl)-*N*-methyl-benzimidazole (**5c**). The reaction was performed according to a protocol developed for **5b** using 2-(*N*-methylamino)phenol (92 mg, 0.75 mmol), **3** (300 mg, 0.75 mmol), $Na_2S_2O_5$ (145 mg, 0.75 mmol), anh. DMF (7.5 mL). Crude product was purified by DCVC using AcOEt/heptane eluent in 0-10% gradient to give **5c** as beige solid (267 mg, 71%, TLC Rf = 0.57 (10% AcOEt/heptane)). ^{1}H NMR (400 MHz, $CDCl_3$) δ 13.31 (bs, 1H, OH), 8.18 (d, *J* = 1.9 Hz, 2H), 7.89 (d, *J* = 2.4 Hz, 1H), 7.85–7.79 (m, 1H), 7.52 (dd, *J* = 8.7, 2.5 Hz, 1H), 7.48 (dd, *J* = 8.6, 1.9 Hz, 2H), 7.44–7.34 (m, 4H), 7.29 (d, *J* = 8.6 Hz, 2H), 4.00 (s, 3H), 1.48 (s, 18H) ppm. ^{13}C{^{1}H} NMR (101 MHz, $CDCl_3$) δ 158.4, 150.8, 142.8, 140.2, 139.8, 135.6, 130.7,

128.7, 125.8, 123.7, 123.7, 123.3, 123.1, 119.5, 119.1, 116.3, 113.9, 109.6, 108.9, 34.8, 33.3, 32.0 ppm.

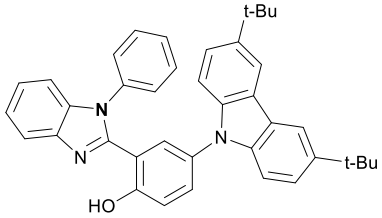

2-(2-hydroxy-5-(3,6-di-*t*-butyl-9*H*-carbazol-9-yl)-phenyl)-*N*-phenyl-benzimidazole (**5d**). The reaction was performed according to a protocol developed for **5b** using 2-(*N*-phenylamino)phenol (141 mg, 0.75 mmol), **3** (300 mg, 0.75 mmol), $Na_2S_2O_5$ (145 mg, 0.75 mmol), anh. DMF (7.5 mL). Crude product was purified by DCVC using AcOEt/heptane eluent in 0–10% gradient to give **5d** as a beige solid (326 mg, 77%, TLC Rf = 0.57 (10% AcOEt/heptane)). ^{1}H NMR (400 MHz, $CDCl_3$) δ 13.69 (bs, 1H, OH), 8.07 (dd, *J* = 2.0, 0.6 Hz, 2H), 7.87 (d, *J* = 8.1 Hz, 1H), 7.55–7.46 (m, 2H), 7.44–7.34 (m, 7H), 7.33–7.27 (m, 2H), 7.12 (d, *J* = 2.4 Hz, 1H), 7.05 (d, *J* = 8.1 Hz, 1H), 6.92 (dd, *J* = 8.6, 0.6 Hz, 2H), 1.48 (s, 18H) pmm. ^{13}C{^{1}H} NMR (101 MHz, $CDCl_3$) δ 158.5, 150.2, 142.5, 139.9, 139.2, 136.8, 136.8, 130.8, 130.2, 129.7, 128.4, 127.7, 125.8, 124.1, 123.7, 123.4, 122.8, 119.2, 118.8, 115.9, 113.2, 110.6, 109.1, 34.7, 32.0 ppm.

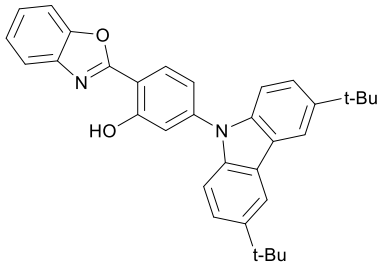

2-(2-hydroxy-4-(3,6-di-*t*-butyl-9*H*-carbazol-9-yl)-phenyl)-1,3-benzoxazole (**6a**). The reaction was performed according to a protocol used for **5a** using 2-aminophenol (103 mg, 0.75 mmol), **4** (300 mg, 0.75 mmol), activated molecular sieves 3A (c.a. 15 beads), anh. DMF (7.5 mL), NaCN (4 mg, 0.075 mmol). Crude product was purified by DCVC using $CHCl_3$/heptane eluent in 0–100% gradient. **6a** was obtained as beige solid (264 mg, 72%, TLC Rf = 0.60 (5% AcOEt/hexane)). ^{1}H NMR (400 MHz, $CDCl_3$) δ 11.75 (bs, 1H, OH), 8.22 (d, *J* = 8.5 Hz, 1H), 8.15 (dd, *J* = 1.9, 0.7 Hz, 2H), 7.81–7.75 (m, 1H), 7.69–7.63 (m, 1H), 7.55 (dd, *J* = 8.7, 0.7 Hz, 2H), 7.50 (dd, *J* = 8.7, 1.9 Hz, 2H), 7.45–7.40 (m, 3H), 7.29 (dd, *J* = 8.4, 2.0 Hz, 1H), 1.49 (s, 18H) ppm. ^{13}C{^{1}H} NMR (101 MHz, $CDCl_3$) δ 162.5, 160.0, 149.2, 143.5, 143.0, 140.0, 138.5, 128.3, 125.5, 125.1, 123.9, 123.9, 123.8, 119.3, 117.3, 116.3, 114.4, 110.7, 109.7, 108.8, 34.8, 32.0 ppm.

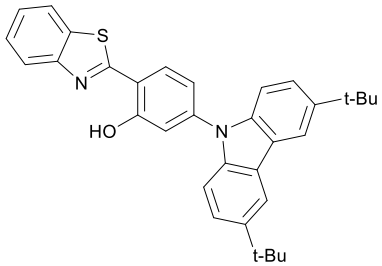

2-(2-hydroxy-4-(3,6-di-*t*-butyl-9*H*-carbazol-9-yl)-phenyl)-1,3-benzothiazole (6b). The reaction was performed according to a protocol used for **5b** using 2-hydroxythiophenol (95 mg, 0.75 mmol), **4**

(300 mg, 0.75 mmol), $Na_2S_2O_5$ (145 mg, 0.75 mmol), anh. DMF (7.5 mL). Crude product was purified by DCVC using $CHCl_3$/heptane eluent in 0-65% gradient. Compound **5b** was isolated as yellow solid (308 mg, 81%, TLC Rf = 0.45 (5% AcOEt/hexane)). ^{1}H NMR (400 MHz, $CDCl_3$) δ 12.80 (bs, 1H, OH), 8.14 (dd, *J* = 2.0, 0.7 Hz, 2H), 8.03 (ddd, *J* = 8.2, 1.2, 0.6 Hz, 1H), 7.94 (bd, *J* = 8.0 Hz, 1H), 7.88 (d, *J* = 8.3 Hz, 1H), 7.56–7.53 (m, 3H), 7.50 (dd, *J* = 8.7, 1.9 Hz, 2H), 7.45 (ddd, *J* = 8.3, 7.3, 1.2 Hz, 1H), 7.36 (d, *J* = 2.0 Hz, 1H), 7.22 (dd, *J* = 8.4, 2.0 Hz, 1H), 1.48 (s, 18H) ppm. ^{13}C{^{1}H} NMR (101 MHz, $CDCl_3$) δ 168.9, 159.4, 143.6, 142.4, 138.7, 132.6, 129.8, 127.0, 125.8, 124.0, 123.9, 122.3, 121.7, 117.4, 116.4, 115.2, 114.9, 109.8, 34.9, 32.1 ppm.

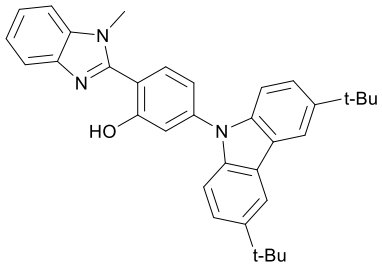

2-(2-hydroxy-4-(3,6-di-*t*-butyl-9*H*-carbazol-9-yl)-phenyl)-*N*-methyl-benzimidazole (6c). The reaction was performed according to a protocol used for **5b** using 2-hydroxythiophenol (92 mg, 0.75 mmol), **4** (300 mg, 0.75 mmol), $Na_2S_2O_5$ (145 mg, 0.75 mmol), anh. DMF (7.5 mL). Crude product was purified by DCVC using $CHCl_3$/heptane eluent in 0-65% gradient. Compound **5c** was isolated as a yellow solid (320 mg, 85%, TLC Rf = 0.45 (5% AcOEt/hexane)). ^{1}H NMR (400 MHz, $CDCl_3$) δ 13.42 (bs, 1H, OH), 8.15 (bs, 2H), 7.94 (d, *J* = 8.4 Hz, 1H), 7.86–7.77 (m, 1H), 7.55 (dd, *J* = 8.6, 0.7 Hz, 2H), 7.49 (dd, *J* = 8.7, 1.9 Hz, 2H), 7.47 – 7.34 (m, 4H), 7.22 (dd, *J* = 8.5, 2.1 Hz, 1H), 4.14 (s, 3H), 1.49 (s, 18H) ppm. ^{13}C{^{1}H} NMR (101 MHz, $CDCl_3$) δ 160.6, 151.3, 143.3, 141.0, 140.3, 138.7, 135.7, 128.0, 123.7, 123.7, 123.5, 123.2, 118.9, 116.3, 115.4, 111.5, 109.6, 109.6, 34.8, 33.2, 32.0 ppm.

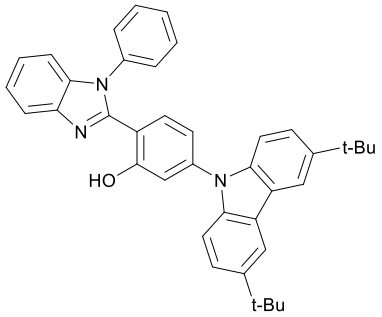

2-(2-hydroxy-4-(3,6-di-*t*-butyl-9*H*-carbazol-9-yl)-phenyl)-*N*-phenyl-benzimidazole (**6d**). The reaction was performed according to a protocol used for **5b** using 2-(*N*-phenylamino)phenol (138 mg, 0.75 mmol), **4** (300 mg, 0.75 mmol), $Na_2S_2O_5$ (145 mg, 0.75 mmol), anh. DMF (7.5 mL). Crude product was purified by DCVC using $CHCl_3$/heptane eluent in 0-100% gradient. Final compound was obtained as a white solid (342 mg, 81%, TLC Rf = 0.42 (50% $CHCl_3$/heptane)). ^{1}H NMR (400 MHz, $CDCl_3$) δ = 13.98 (bs, 1H, OH), 8.10 (dd, *J* = 1.8, 0.9 Hz, 2H), 7.85 (d, *J* = 7.8 Hz, 1H), 7.72–7.59 (m, 3H), 7.54–7.46 (m, 6H), 7.43–7.34 (m, 2H), 7.30 (ddd, *J* = 8.2, 7.1, 1.0 Hz, 1H), 7.12 (d, *J* = 8.1 Hz, 1H), 7.03 (d, *J* = 8.6 Hz, 1H), 6.78 (dd, *J* = 8.6, 2.2 Hz, 1H), 1.46 (s, 18H) ppm. ^{13}C{^{1}H} NMR (101 MHz, $CDCl_3$) δ = 161.2, 150.5, 143.4, 141.1, 138.7, 137.1, 136.6, 130.7, 130.0, 128.3, 128.2, 124.1, 123.8, 123.8, 118.7, 116.3, 115.8, 115.2, 110.7, 110.6, 109.9, 34.9, 32.1 ppm.

Synthesis of complexes 7a–7d and 8a–8d.

General procedure: Proligand **5a–5d**/**6a–6d** (1 equiv), 10-hydroxy-10*H*-dibenzo[*b*,*e*][1,4]thiaborinine 5,5-dioxide (SO2BOH, 1 equiv) and toluene (2 drops) were placed in 5 mL stainless steel vessel equipped with one 10 mm stainless steel ball. The mixture was ground at 30 Hz for 1 h. The powder was dissolved in DCM, filtered through a syringe filter (0.45 μm) and concentrated in vacuo. The residue was washed with hot EtOH to form a crystalline precipitate. It was filtered, washed with Et_2O, hexane and dried under vacuum to give a pure product.

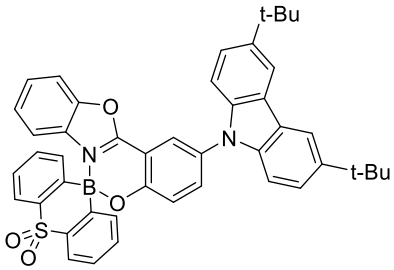

2-(3,6-Di-*tert*-butyl-9*H*-carbazol-9-yl)-6λ⁴,7λ⁴-spiro[benzo[e]benzo[4,5]oxazolo[3,2-*c*][1,3,2]oxazaborinine-6,10'-dibenzo[*b*,*e*][1,4]thiaborinine] 5',5'-dioxide (7a). Compound **7a** was obtained as a yellowish crystalline solid using **5a** (70 mg, 0.14 mmol) and SO2BOH (35 mg, 0.14 mmol). Yield: 60 mg (58%). ^{1}H NMR (400 MHz, $CDCl_3$) δ 8.25 (ddd, *J* = 7.9, 1.3, 0.6 Hz, 2H), 8.18 (d, *J* = 2.0, 1H), 8.18 (dd, *J* = 7.5, 2.3, 2H), 7.76 (dd, *J* = 8.9, 2.7 Hz, 1H), 7.65 (dt, *J* = 8.4, 0.9 Hz, 1H), 7.56–7.51 (m, 4H), 7.49 (ddd, *J* = 7.5, 1.5, 0.6 Hz, 2H), 7.46–7.38 (m, 5H), 7.29–7.23 (m, 3H), 1.50 (s, 18H) ppm. ^{13}C{^{1}H} NMR (101 MHz, $CDCl_3$) δ 161.1, 160.9, 148.9, 143.6, 143.3, 139.3, 137.4, 132.5, 131.8, 131.2, 129.9, 129.1, 127.6, 127.5, 123.8, 123.6, 123.4, 123.1, 122.2, 117.6, 116.5, 111.5, 108.9, 106.3, 34.8, 32.0 ppm. ^{11}B NMR (96 MHz, $CDCl_3$) δ = 1.1 ppm. HRMS (ESI, positive ion mode) Calcd. for $C_{45}H_{40}BN_2O_4S^+$ [MH^+]: 715.2796; found: 715.2779.

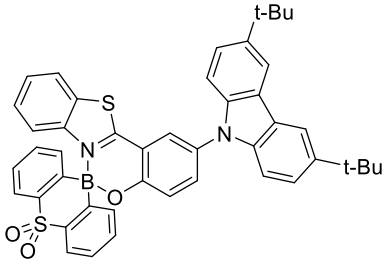

2-(3,6-Di-*tert*-butyl-9*H*-carbazol-9-yl)-6λ⁴,7λ⁴-spiro[benzo[e]benzo[4,5]thiazolo[3,2-*c*][1,3,2]oxazaborinine-6,10'-dibenzo[*b*,*e*][1,4]thiaborinine] 5',5'-dioxide (7b). Compound **7b** was obtained as a yellow crystalline solid from **5b** (97 mg, 0.19 mmol) and SO2BOH (48 mg, 0.19 mmol). Yield: 92 mg (65%). ^{1}H NMR (400 MHz, $CDCl_3$) δ 8.28 (dd, *J* = 8.0, 1.2 Hz, 2H), 8.18 (d, *J* = 2.0 Hz, 2H), 7.88 (d, *J* = 7.9 Hz, 1H), 7.84 (d, *J* = 2.5 Hz, 1H), 7.62 (dd, *J* = 8.9, 2.5 Hz, 1H), 7.54–7.45 (m, 4H), 7.40 (ddd, *J* = 8.2, 7.3, 1.1 Hz, 1H), 7.37–7.31 (m, 4H), 7.21–7.14 (m, 4H), 6.95 (d, *J* = 8.6 Hz, 1H), 1.49 (s, 18H) ppm. ^{13}C{^{1}H} NMR (101 MHz, $CDCl_3$) δ 169.1, 156.8, 143.9, 143.5, 143.2, 139.4, 136.9, 132.1, 131.8, 129.7, 129.2, 128.7, 128.5, 127.2, 125.1, 123.8, 123.4, 123.3, 122.7, 122.2, 121.2, 116.5, 113.1, 108.9, 34.8, 32.0 ppm. ^{11}B NMR (96 MHz, $CDCl_3$) δ = 0.5 ppm. HRMS (ESI, positive ion mode) Calcd. for $C_{45}H_{40}BN_2O_3S_2^+$ [MH^+]: 731.2568; found: 731.2554.

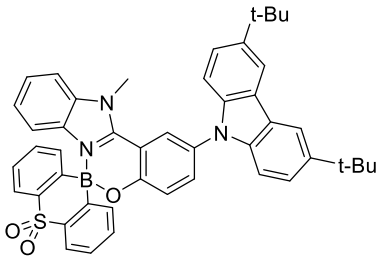

2-(3,6-Di-*tert*-butyl-9*H*-carbazol-9-yl)-12-methyl-12*H*-6λ⁴,7λ⁴-spiro[benzo[*e*]benzo[4,5]imidazo[1,2-*c*][1,3,2]oxazaborinine-6,10'-dibenzo[*b*,*e*][1,4]thiaborinine] 5',5'-dioxide (7c). Compound **7c** was obtained as a yellow crystalline solid from **5c** (90 mg, 0.18 mmol) and SO2BOH (45 mg, 0.18 mmol). Yield: 101 mg (77%). ^{1}H NMR (400 MHz, $CDCl_3$) δ 8.28–8.21 (m, 2H), 8.20–8.18 (m, 2H), 8.11 (d, *J* = 2.4 Hz, 1H), 7.60 (dd, *J* = 8.8, 2.5 Hz, 1H), 7.54–7.49 (m, 3H), 7.45 (ddd, *J* = 7.9, 7.3, 1.3 Hz, 2H), 7.38 (ddd, *J* = 8.3, 7.2, 1.0 Hz, 1H), 7.33 (dd, *J* = 8.6, 0.7 Hz, 2H), 7.31–7.27 (m, 3H), 7.17 (dd, *J* = 7.5, 0.8 Hz, 2H), 7.12 (ddd, *J* = 8.3, 7.2, 1.1 Hz, 1H), 6.99–6.91 (m, 1H), 4.27 (s, 3H), 1.49 (s, 18H) ppm. ^{13}C{^{1}H} NMR (101 MHz, $CDCl_3$) δ 159.8, 146.6, 143.8, 143.1, 139.6, 134.4, 134.3, 132.6, 132.35, 131.4, 128. 9, 128.3, 125.7, 125.6, 123.9, 123.7, 123.3, 123.3, 123.2, 117.5, 116.5, 110.2, 109.8, 108.7, 34.8, 34.3, 32.0 ppm. ^{11}B NMR (96 MHz, $CDCl_3$) δ = 0.3 ppm. HRMS (ESI, positive ion mode) Calcd. for $C_{46}H_{43}BN_3O_3S^+$ [MH^+]: 728.3113; found: 728.3106.

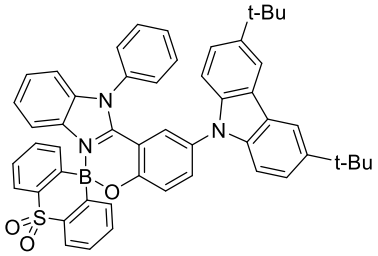

2-(3,6-Di-*tert*-butyl-9*H*-carbazol-9-yl)-12-phenyl-12*H*-6λ⁴,7λ⁴-spiro[benzo[e]benzo[4,5]imidazo[1,2-*c*][1,3,2]oxazaborinine-6,10'-dibenzo[*b*,*e*][1,4]thiaborinine] 5',5'-dioxide (7d). Compound was obtained as a beige crystalline solid from **5d** (105 mg, 0.19 mmol) and SO2BOH (46 mg, 0.19 mmol). Yield: 114 mg (78%). ^{1}H NMR (400 MHz, $CDCl_3$) δ 8.28 (dd, *J* = 7.9, 1.2 Hz, 2H), 8.07 (s, 2H), 7.68–7.59 (m, 4H), 7.55–7.46 (m, 3H), 7.42 (m, 3H), 7.36 (td, *J* = 7.3, 1.2 Hz, 2H), 7.33–7.28 (m, 2H), 7.28–7.24 (m, 1H), 7.20 (d, *J* = 8.9 Hz, 1H), 7.13 (t, *J* = 7.3 Hz, 1H), 7.08–7.01 (m, 4H), 6.99 (d, *J* = 8.4 Hz, 1H), 1.48 (d, *J* = 1.4 Hz, 18H) ppm. ^{13}C{^{1}H} NMR (101 MHz, $CDCl_3$) δ 159.4, 146.2, 143.8, 142.9, 138.8, 135.6, 134.5, 133.8, 132.5, 132.4, 131.5, 131.3, 128.6, 128.4, 127.4, 125.9, 125.9, 123.5, 123.4, 123.2, 123.1, 122.7, 117.2, 116.0, 111.2 109.1, 108.7, 34.7, 32.0 ppm. ^{11}B NMR (96 MHz, $CDCl_3$) δ = 2.0 ppm. HRMS (ESI, positive ion mode) Calcd. for $C_{51}H_{45}BN_3O_3S^+$ [MH^+]: 790.3269; found: 790.3264.

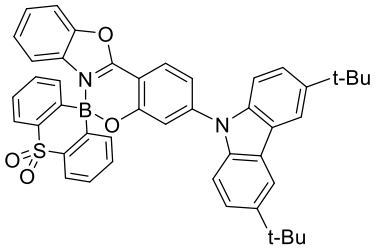

3-(3,6-Di-*tert*-butyl-9*H*-carbazol-9-yl)-6λ⁴,7λ⁴-spiro[benzo[e]benzo[4,5]oxazolo[3,2-*c*][1,3,2]oxazaborinine-6,10'-dibenzo[*b*,*e*][1,4]thiaborinine] 5',5'-dioxide (8a). Compound **8a** was

obtained as a yellowish crystalline solid from **6a** (150 mg, 0.31 mmol) and SO2BOH (76 mg, 0.31 mmol). Yield: 204 mg (92%). ^{1}H NMR (400 MHz, $CDCl_3$) δ 8.23 (ddd, *J* = 7.9, 1.3, 0.6 Hz, 2H), 8.17 (dd, *J* = 8.2, 0.6 Hz, 1H), 8.09 (dd, *J* = 2.0, 0.6 Hz, 2H), 7.70 (d, *J* = 8.3 Hz, 1H), 7.60 (dd, *J* = 8.7, 0.6 Hz, 2H), 7.55–7.46 (m, 6H), 7.46–7.38 (m, 3H), 7.37–7.31 (m, 2H), 7.25–7.20 (m, 2H), 1.45 (s, 18H) ppm. ^{13}C{^{1}H} NMR (101 MHz, $CDCl_3$) δ 163.4, 161. 2, 148.9, 147.8, 144.2, 143. 6, 137.9, 132.5, 131.8, 131.4, 129.0, 127.4, 127.3, 127.1, 124.4, 124.0, 123.1, 117.3, 116.8, 116.4, 116.0, 111.3, 110.2, 103.3, 34.8, 31.9 ppm. ^{11}B NMR (96 MHz, $CDCl_3$) δ = 0.3 ppm. HRMS (ESI, positive ion mode) Calcd. for $C_{45}H_{40}BN_2O_4S^+$ [MH^+]: 715.2794; found: 715.2800.

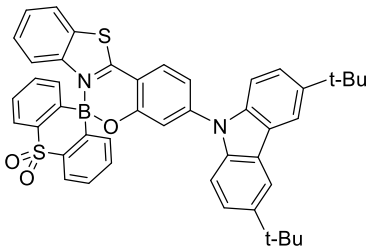

3-(3,6-Di-*tert*-butyl-9*H*-carbazol-9-yl)-6λ^4,7λ^4-spiro[benzo[*e*]benzo[4,5]thiazolo[3,2-*c*][1,3,2]oxazaborinine-6,10'-dibenzo[*b*,*e*][1,4]thiaborinine] 5',5'-dioxide (8b). Compound **8b** was obtained as a yellow crystalline solid from **6b** (150 mg, 0.30 mmol) and SO2BOH (74 mg, 0.30 mmol). Yield: **8b** (194 mg, 89%). ^{1}H NMR (400 MHz, $CDCl_3$) δ 8.26 (dd, *J* = 8.0, 1.2 Hz, 2H), 8.07 (d, *J* = 1.8 Hz, 2H), 7.90 (d, *J* = 8.1 Hz, 1H), 7.86 (d, *J* = 8.9 Hz, 1H), 7.55 (d, *J* = 8.7 Hz, 2H), 7.51–7.43 (m, 4H), 7.38 (ddd, *J* = 8.3, 7.3, 1.0 Hz, 1H), 7.32 (td, *J* = 7.4, 1.2 Hz, 2H), 7.25–7.21 (m, 2H), 7.18 (dd, *J* = 7.4, 1.3 Hz, 2H), 7.13 (dt, *J* = 7.3, 1.2 Hz, 1H), 6.89 (d, *J* = 8.6 Hz, 1H), 1.44 (s, 18H) ppm. ^{13}C{^{1}H} NMR (101 MHz, $CDCl_3$) δ 168.8, 159.2, 147.3, 144.1, 143.8, 143.4, 137.9, 132.3, 131.8, 129.0, 128.7, 128.6, 128.3, 126.8, 124.3, 124.0, 123.3, 122.1, 120.9, 116.8, 116.3, 116.3, 110.3, 110.2, 34.8, 31.9 ppm. ^{11}B NMR (96 MHz, $CDCl_3$) δ = 1.2 ppm. HRMS (ESI, positive ion mode) Calcd. for $C_{45}H_{40}BN_2O_3S_2^+$ [MH^+]: 731.2568; found: 731.2558.

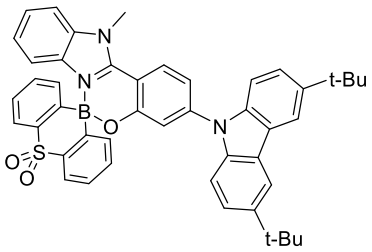

3-(3,6-Di-*tert*-butyl-9*H*-carbazol-9-yl)-12-methyl-12*H*-6λ^4,7λ^4-spiro[benzo[e]benzo[4,5]imidazo[1,2-*c*][1,3,2]oxazaborinine-6,10'-dibenzo[*b*,*e*][1,4]thiaborinine] 5',5'-dioxide (8c). Compound **8c** was obtained as a beige crystalline solid from **6c** (125 mg, 0.25 mmol) and SO2BOH (61 mg, 0.27 mmol) Yield: 164 mg (90%). ^{1}H NMR (400 MHz, $CDCl_3$) δ 8.23 (ddd, *J* = 7.9, 1.2, 0.6 Hz, 2H), 8.16 (d, *J* = 8.7 Hz, 1H), 8.09 (dd, *J* = 1.9, 0.7 Hz, 2H), 7.55 (dd, *J* = 8.7, 0.7 Hz, 2H), 7.52 (dt, *J* = 8.3, 0.7 Hz, 1H), 7.48–7.41 (m, 4H), 7.40–7.34 (m, 2H), 7.32–7.26 (m, 3H), 7.21 (ddd, *J* = 7.5, 1.4, 0.6 Hz, 2H), 7.11 (ddd, *J* = 8.3, 7.3, 1.1 Hz, 1H), 6.95 (d, *J* = 8.3 Hz, 1H), 4.41 (s, 3H), 1.44 (s, 18H) ppm. ^{13}C{^{1}H} NMR (101 MHz, $CDCl_3$) δ 162.3, 146.9, 144.8, 143.8, 143.7, 138.1, 134.3, 132.7, 132.4, 131.4, 128.3, 126.5, 125.5, 125.3, 124.1, 123.9, 123.1, 117.7, 117.3, 116.3, 116.1, 110.0, 110.0, 107.0, 34.7, 34.3, 31.9 ppm. ^{11}B NMR (96 MHz, $CDCl_3$) δ = 1.0 ppm. HRMS (ESI, positive ion mode) Calcd. for $C_{46}H_{42}BN_3O_3S$ [M]: 727.3034; found: 727.3036.

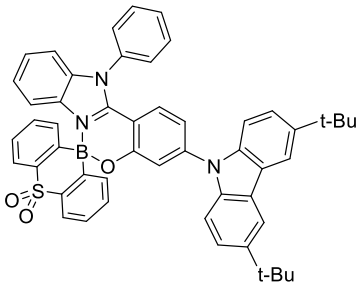

3-(3,6-Di-*tert*-butyl-9*H*-carbazol-9-yl)-12-phenyl-12*H*-6λ⁴,7λ⁴-spiro[benzo[e]benzo[4,5]imidazo[1,2-*c*][1,3,2]oxazaborinine-6,10'-dibenzo[*b*,*e*][1,4]thiaborinine] 5',5'-dioxide (8d). Compound **8d** was obtained as a beige crystalline solid from **6d** (150 mg, 0.27 mmol) and SO2BOH (66 mg, 0.27 mmol). Yield: 193 mg (92%). ^{1}H NMR (400 MHz, $CDCl_3$) δ 8.26 (dt, *J* = 7.9, 0.9 Hz, 2H), 8.04 (dd, *J* = 1.9, 0.6 Hz, 2H), 7.87–7.80 (m, 3H), 7.74–7.66 (m, 2H), 7.52–7.44 (m, 4H), 7.40 (dd, *J* = 8.7, 1.9 Hz, 2H), 7.37–7.35 (m, 4H), 7.30–7.24 (m, 2H), 7.16–7.06 (m, 2H), 7.00 (d, *J* = 8.3 Hz, 1H), 6.96 (d, *J* = 8.7 Hz, 1H), 6.84 (dd, *J* = 8.8, 2.1 Hz, 1H), 1.42 (s, 18H) ppm. ^{13}C{^{1}H} NMR (101 MHz, $CDCl_3$) δ 162.1, 146.4, 144.8, 143.7, 143.7, 138.0, 135.5, 134.9, 132.5, 132.5, 131.5, 131.4, 131.3, 128.4, 127.9, 126.8, 125.7, 125.6, 124.0, 123.8, 123.1, 117.1, 117.0, 116.2, 115.6, 111.0, 110.1, 105.9, 34.7, 31.9 ppm. ^{11}B NMR (96 MHz, $CDCl_3$) δ = –1.6 ppm. HRMS (ESI, positive ion mode) Calcd. for $C_{51}H_{44}BN_3O_3S$ [M]: 789.3191; found: 789.3202.

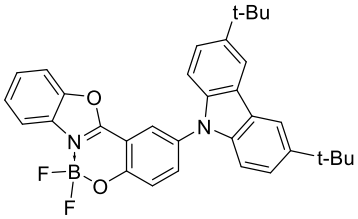

2-(3,6-di-tert-butyl-9*H*-carbazol-9-yl)-6,6-difluoro-6*H*-6λ⁴,7λ⁴-benzo[*e*]benzo[4,5]oxazolo[3,2-c][1,3,2]oxazaborinine (**9**).A solution of **5a** (0.244 g, 0.5 mmol) in THF (10 mL) was added to a suspension of NaH (60% oil dispersion, 0.015 g, 0.6 mmol) in anhydrous THF (10 mL) at 0 °C. After 30 min of stirring, $BF_3{\cdot}Et_2O$ (0.075 mL, 0.6 mmol) was added dropwise. A cooling bath was removed and a mixture was left to warm up to the room temperature. After 2 hours of stirring a mixture was concentrated in vacuo. The solid was washed with water (3 × 10 mL), cold EtOH (2 × 5 mL) and hexane (15 mL), and dried under vacuum to obtain pure compound **9** as a light yellow powder (0.188 g, 70%). ^{1}H NMR (400 MHz, $CDCl_3$) δ = 8.21 (d, *J* = 2.6, 1H), 8.16 (dd, *J* = 1.9, 0.7 Hz, 2H), 7.80–7.76 (m, 1H), 7.60 (dd, *J* = 8.8, 2.6 Hz, 1H), 7.58–7.54 (m, 1H), 7.49 (dd, *J* = 8.6, 2.0 Hz, 2H), 7.44–7.37 (m, 2H), 7.33 (dd, *J* = 8.7, 0.4 Hz, 1H), 7.31 (dd, *J* = 8.6, 0.7 Hz, 2H), 1.48 (s, 18H). ^{11}B NMR (96 MHz, $CDCl_3$) δ = 0.9 ppm; ^{19}F NMR (376 MHz, $CDCl_3$) δ = –130.43 ppm.

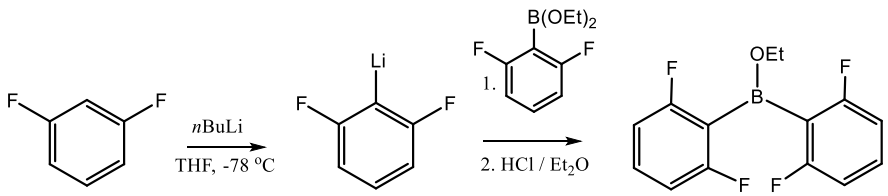

Ethoxy(bis(2,6-difluoro)phenyl)borane. The solution of 1,3-difluorobenzene (2.28 g, 20 mmol) in 20 mL THF was added to a solution of *n*-BuLi (20.2 mmol) in 50 mL THF at –78 °C. After 1h of stirring the solution of diethoxy((2,6-difluoro)phenyl)borane[5] (4.28 g, 20 mmol) was added. After 1 h

of stirring, the mixture was slowly heated to -20 °C followed by addition of 2 M HCl in Et_2O (10 mL, 20 mmol). The mixture was stirred for 2h at 35 °C. Then, the residual solvents were evaporated under reduced pressure and the crude compound was subjected to distillation (80 °C, 3 mbar) to give the product as a colourless oil (4.64 g, 82%). The compound readily hydrolyzes in contact with water thus it must be stored under argon. ^{1}H NMR (400 MHz, $CDCl_3$) δ = 7.35 (tt, *J* = 8.3, 6.6 Hz, 2H), 6.93–6.78 (m, 4H), 4.26 (q, *J* = 7.1 Hz, 2H), 1.40 (t, *J* = 7.1 Hz, 3H) ppm. ^{13}C NMR (101 MHz, $CDCl_3$) δ = 164.8 (dd, *J* = 246.9, 13.8 Hz), 132.3 (t, *J* = 10.5 Hz), 112.3 – 107.5 (m), 65.4, 17.0 ppm. ^{19}F NMR (376 MHz, $CDCl_3$) δ = –102.86 ppm.

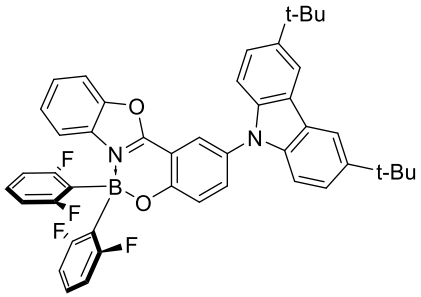

2-(3,6-di-tert-butyl-9*H*-carbazol-9-yl)-6,6-bis(2,6-difluorophenyl)-6*H*-6λ^4,7λ^4-benzo[*e*]benzo[4,5]oxazolo[3,2-*c*][1,3,2]oxazaborinin (**10**). Ethoxy(bis(2,6-difluoro)phenyl)borane (0.284 g, 1 mmol) was dissolved in anhydrous EtOH (10 mL) followed by the addition of **5a** (0.488 g, 1 mmol). Immediately, the resulting solution turned yellow. A mixture was stirred for 15 hours and the precipitation of the **10** was observed. The obtained thick slurry was filtered. The solid was washed with water (20 mL), EtOH (30 mL), Et_2O (10 mL) and hexane (20 mL). A crude product was transferred to a small flask, and stirred vigorously with Et_2O (20 mL) for 4 hours. Then it was filtered, washed with Et_2O (20 mL) and dried under vacuum to give **10** as a yellow powder (0.666 g, 92% yield). ^{1}H NMR (400 MHz, $CDCl_3$) δ = 8.15 (dd, *J* = 2.0, 0.6 Hz, 2H), 8.04 (d, *J* = 2.7, 1H), 7.69 (dd, *J* = 8.9, 2.6 Hz, 1H), 7.65 (dt, *J* = 8.4, 0.9 Hz, 1H), 7.52–7.42 (m, 3H), 7.38–7.29 (m, 4H), 7.25–7.17 (m, 3H), 6.82–6.73 (m, 4H), 1.48 (s, 18H) ppm; ^{13}C NMR (101 MHz, $CDCl_3$) δ = 166.22 (dd, *J* = 244.5, 14.8 Hz), 160.67, 160.45, 149.06, 143.01, 139.40, 136.67, 132.80, 129.50, 129.55 (t, *J* = 11.5 Hz), 126.83, 126.73, 123.71, 123.66, 123.28, 122.12, 116.86, 116.33, 111.49, 111.05 (d, *J* = 21.6 Hz), 109.02, 107.64, 34.8, 32.0 ppm. ^{11}B NMR (96 MHz, $CDCl_3$) δ = 2.4 ppm; ^{19}F NMR (376 MHz, $CDCl_3$) δ = –103.86 ppm.

9. NMR spectra

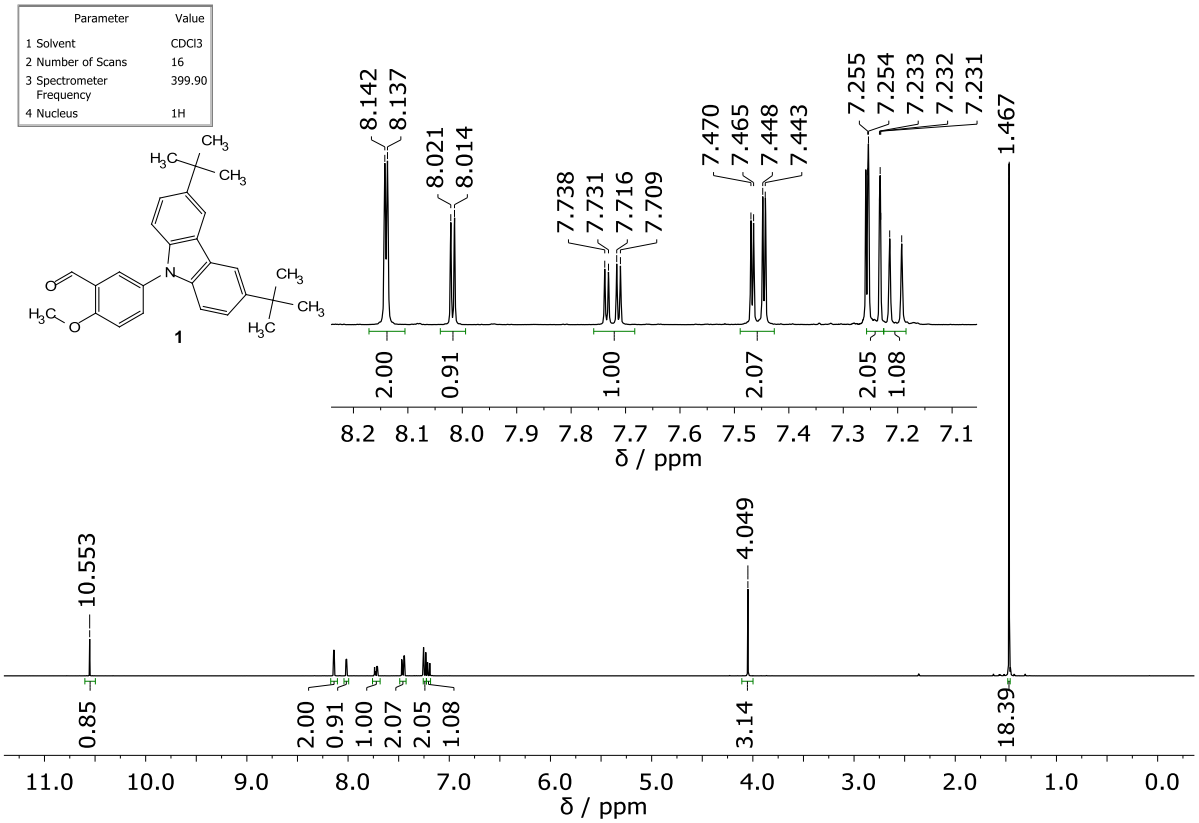

Figure S9.1. ^{1}H NMR spectrum (400 MHz, $CDCl_3$) of **1**.

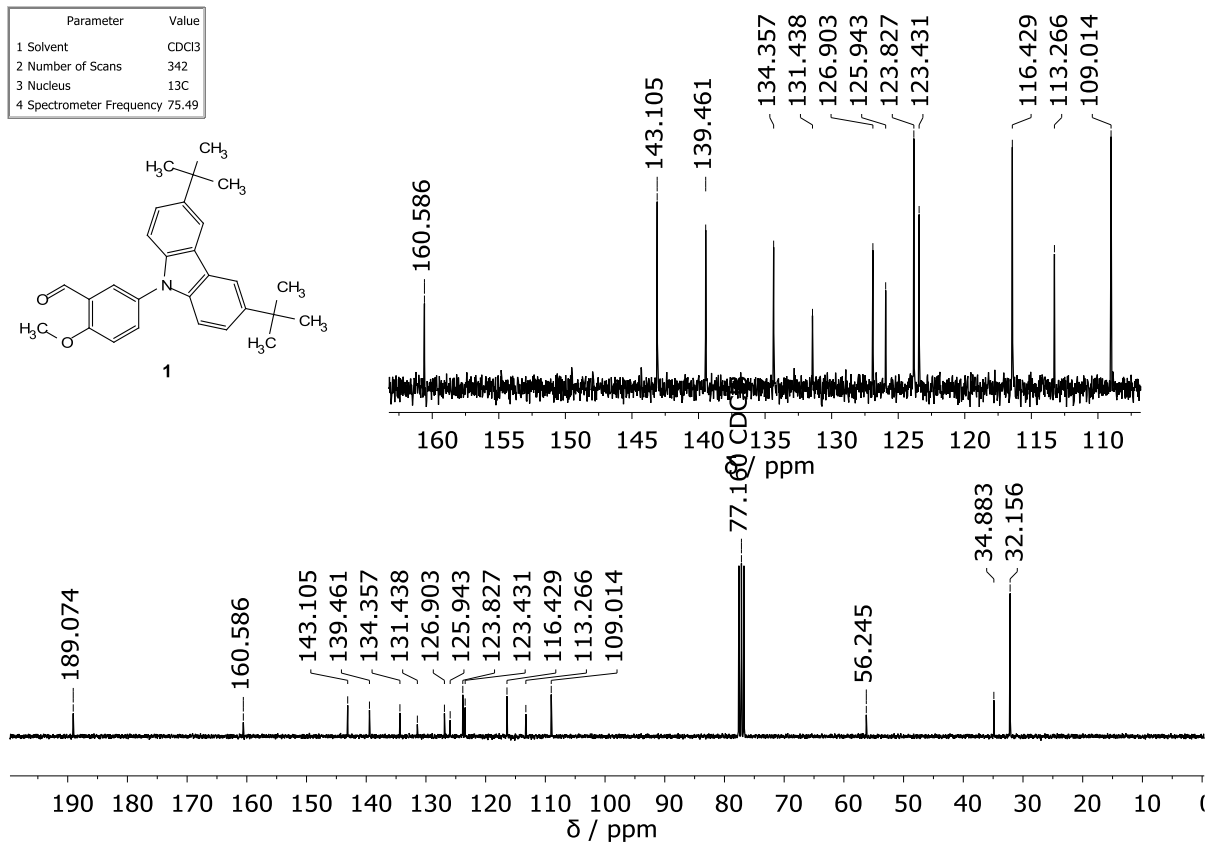

Figure S9.2. $^{13}C\{^{1}H\}$ NMR spectrum (75 MHz, $CDCl_3$) of **1**.

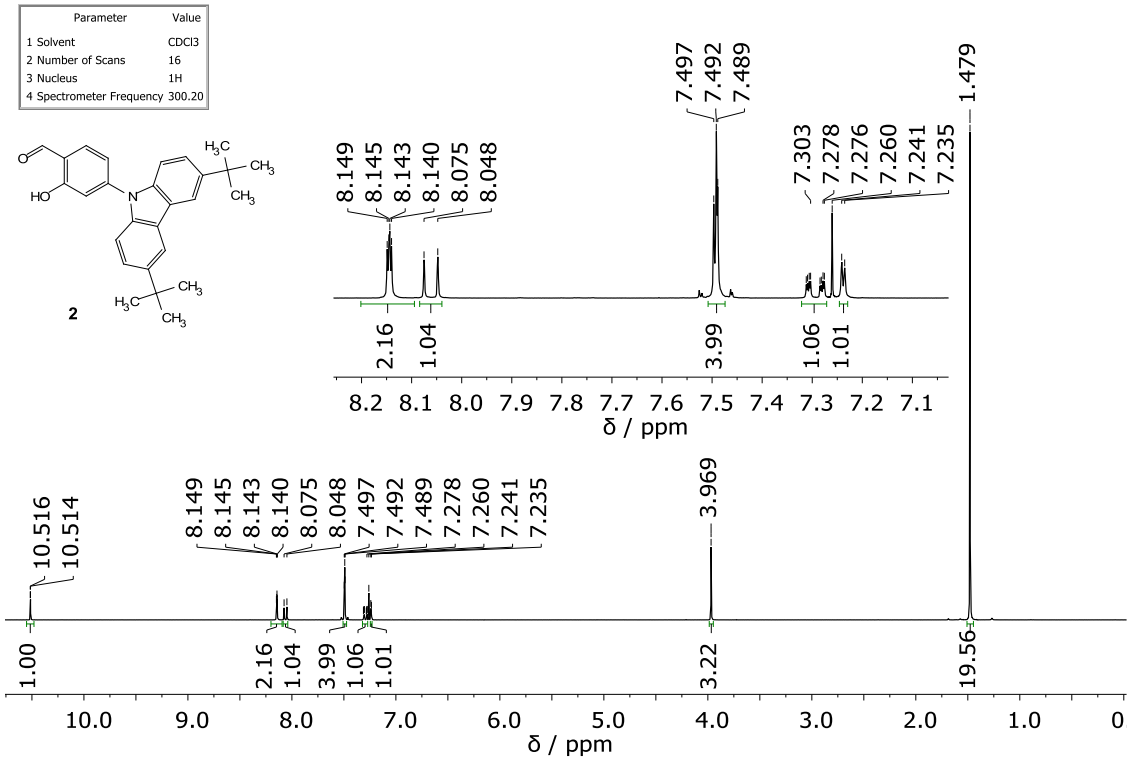

Figure S9.3. ^{1}H NMR spectrum (300 MHz, $CDCl_3$) of **2**.

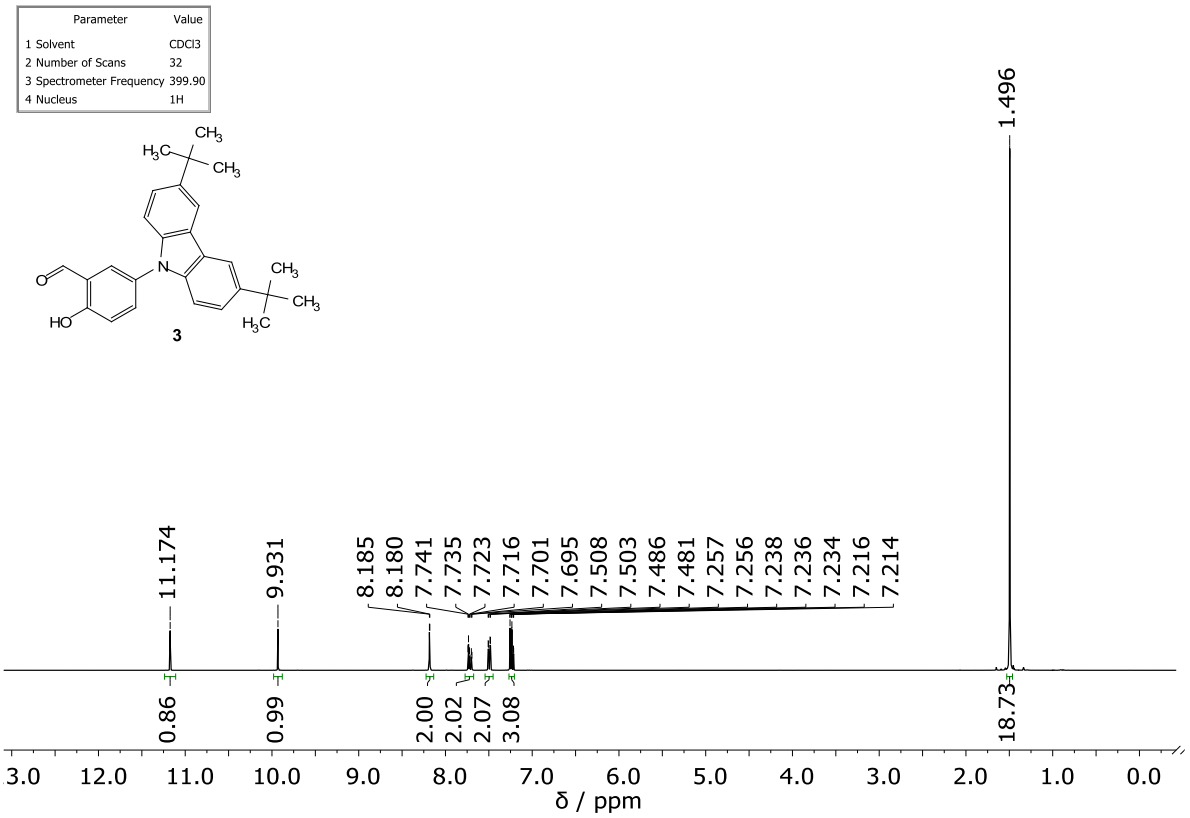

Figure S9.4. ^{1}H NMR spectrum (400 MHz, $CDCl_3$) of **3**.

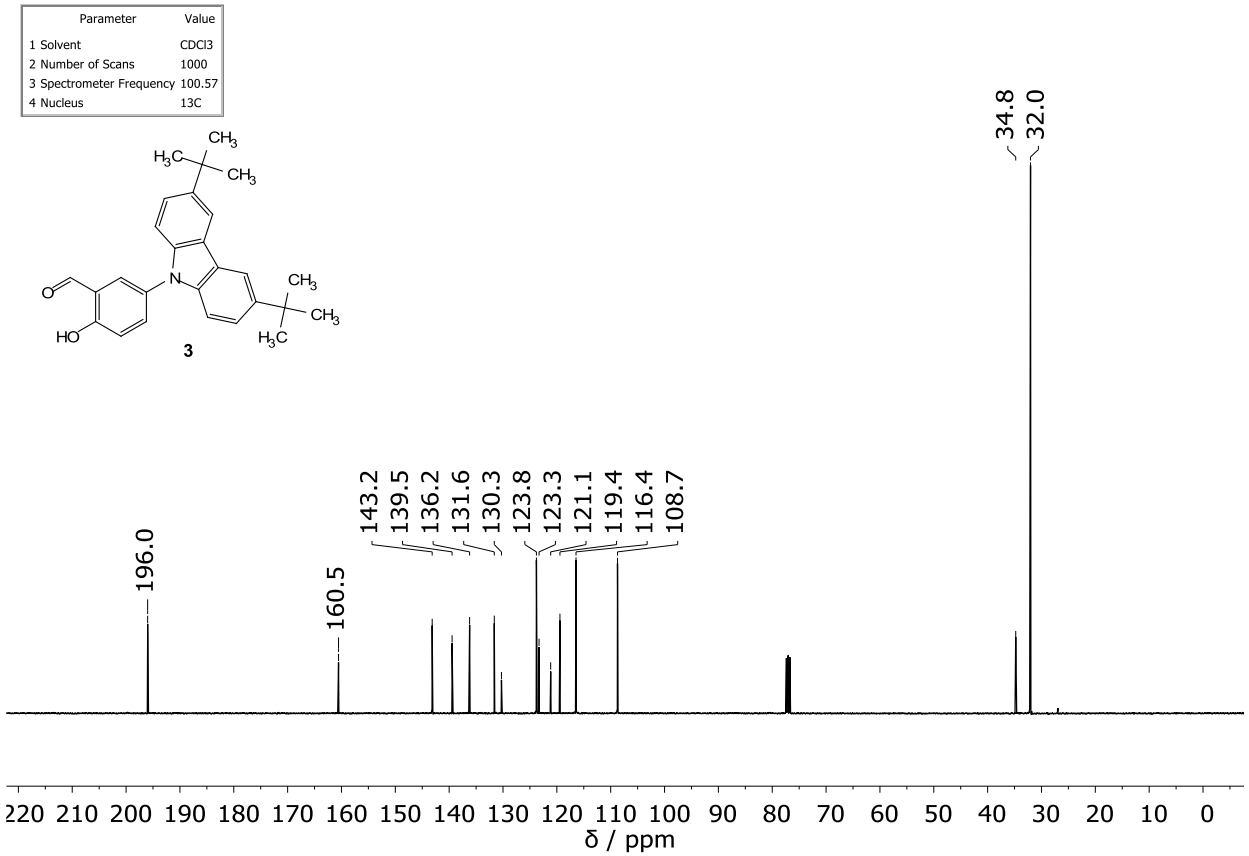

Figure S9.5. $^{13}C\{^{1}H\}$ NMR spectrum (101 MHz, $CDCl_3$) of **3**.

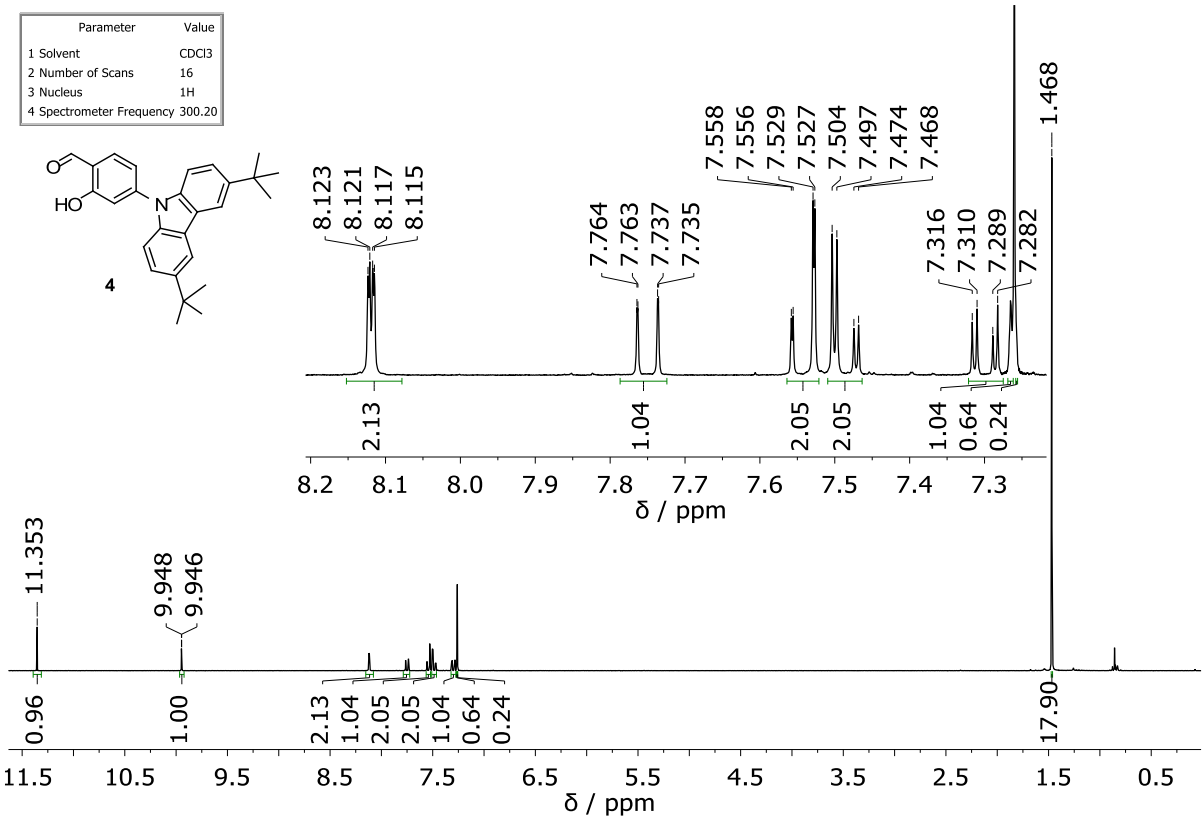

Figure S9.6. ^{1}H NMR spectrum (300 MHz, $CDCl_3$) of **4**.

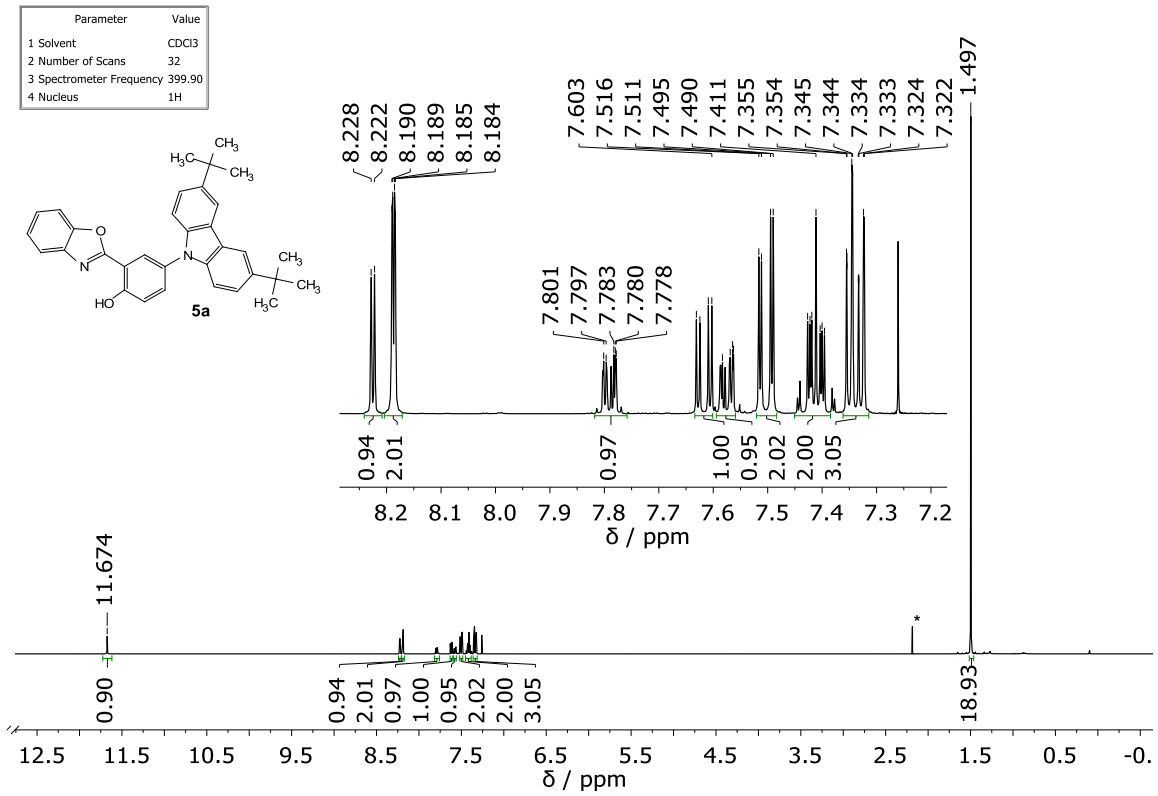

Figure S9.6. ^{1}H NMR spectrum (400 MHz, $CDCl_3$) of **5a**. Residual solvent (acetone) impurity is marked with an asterisk (*).

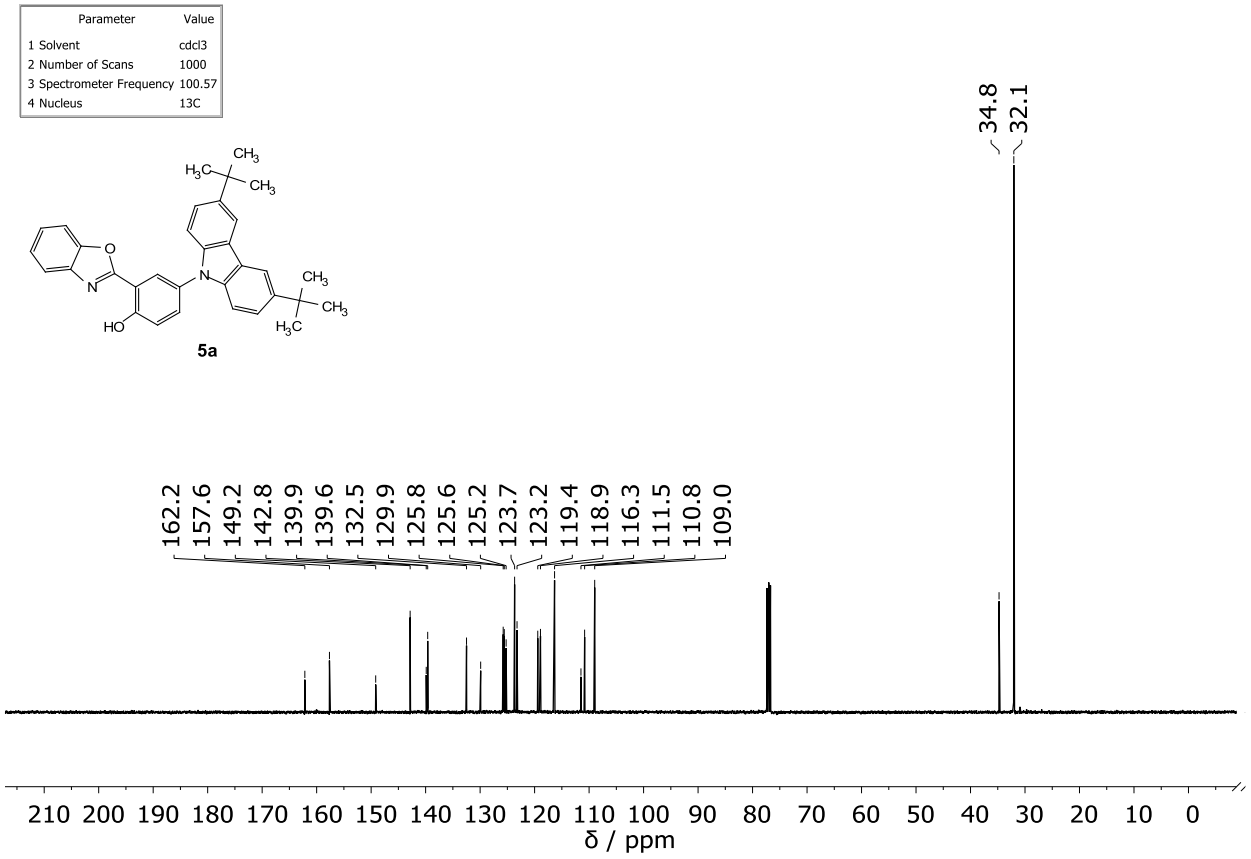

Figure S9.7. $^{13}C\{^{1}H\}$ NMR spectrum (101 MHz, $CDCl_3$) of **5a**.

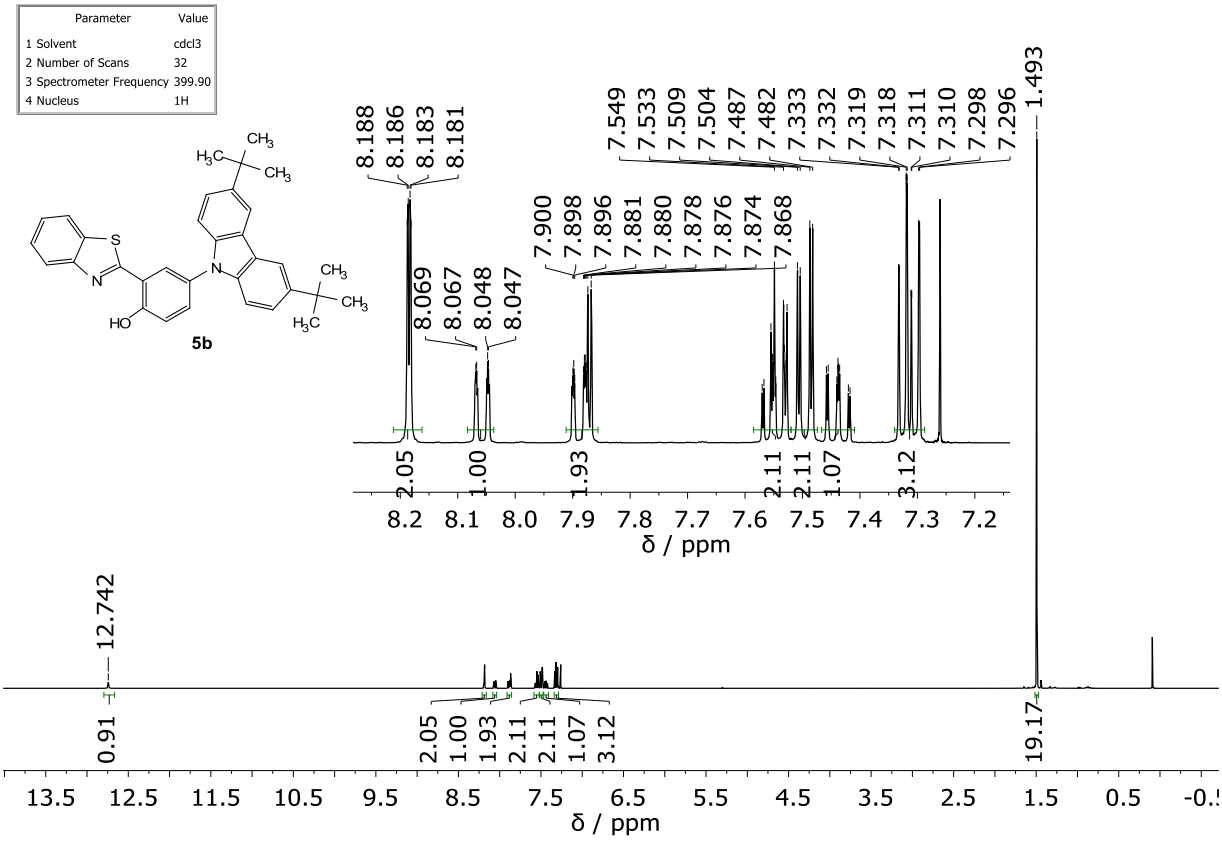

Figure S9.8. ^{1}H NMR spectrum (400 MHz, $CDCl_3$) of **5b**.

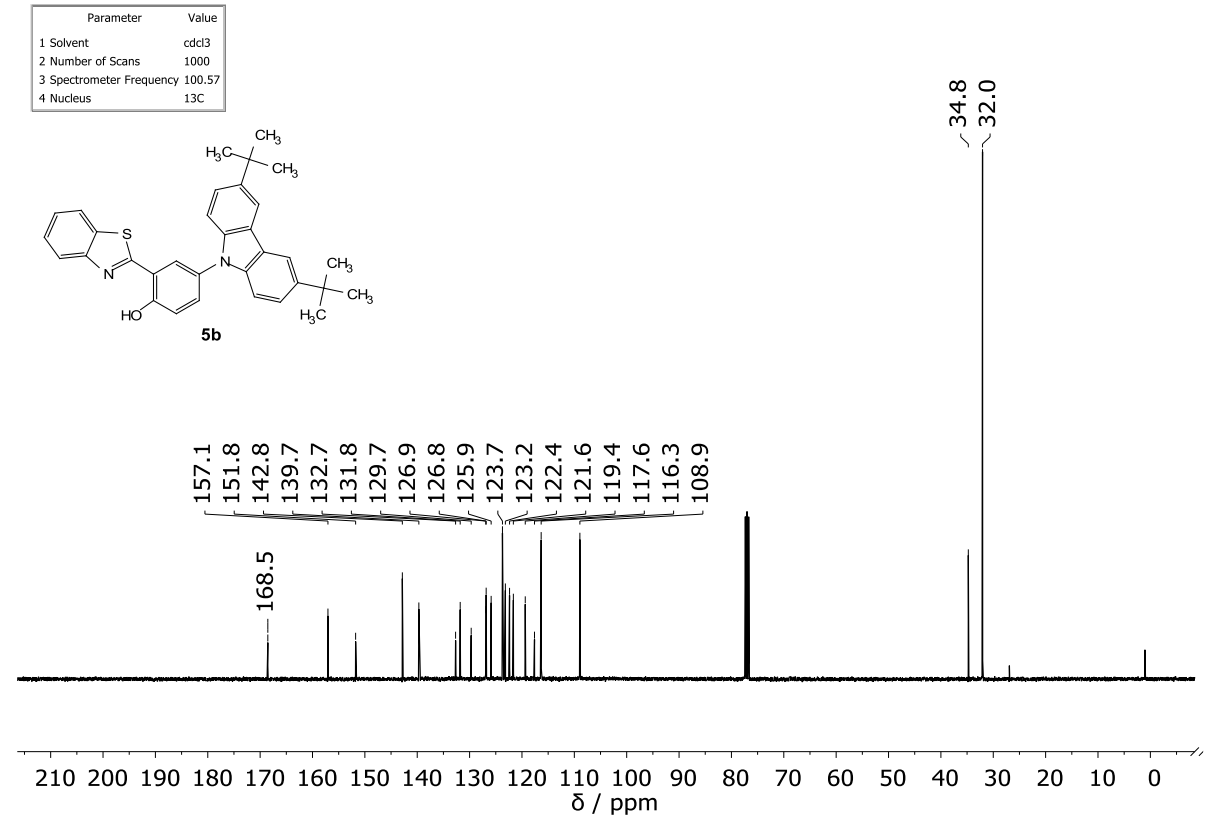

Figure S9.9. $^{13}C\{^{1}H\}$ NMR spectrum (101 MHz, $CDCl_3$) of **5b**.

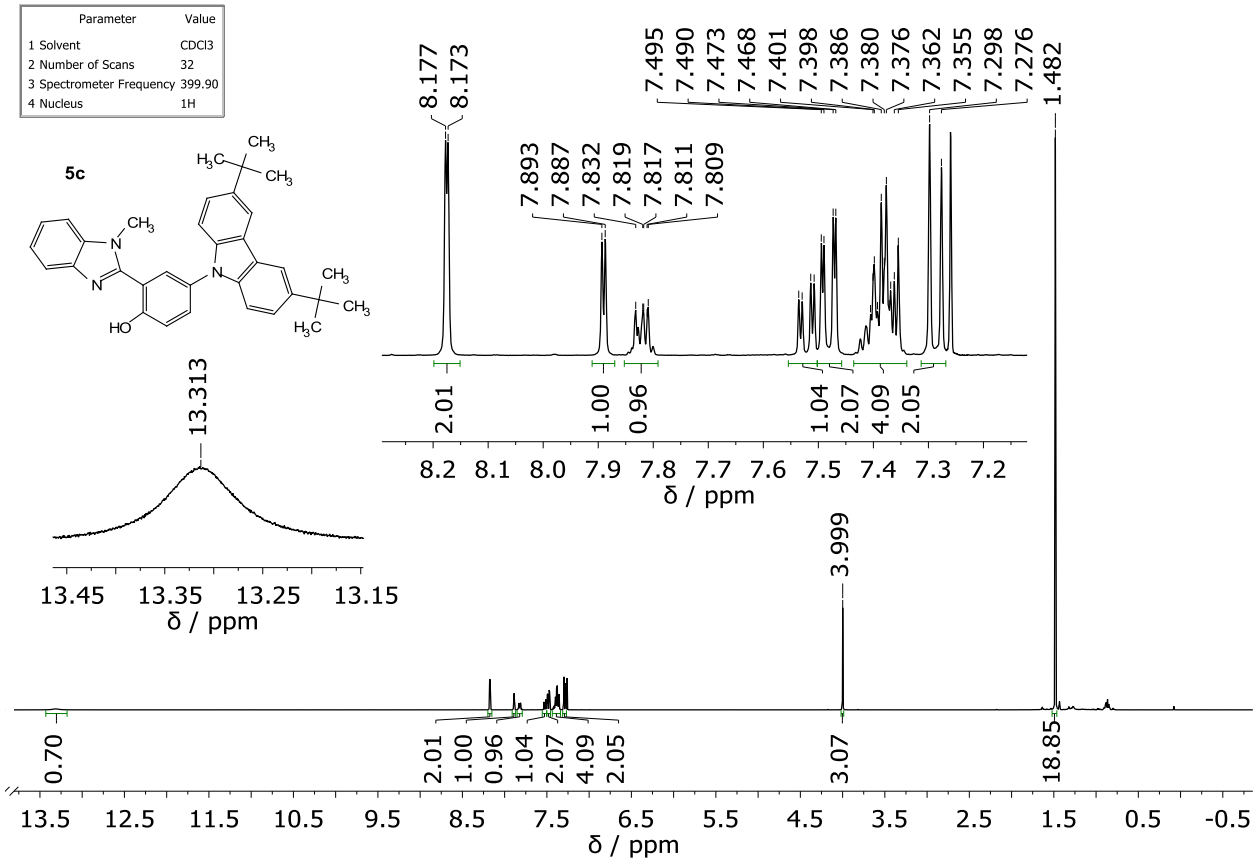

Figure S9.10. ^{1}H NMR spectrum (400 MHz, $CDCl_3$) of **5c**.

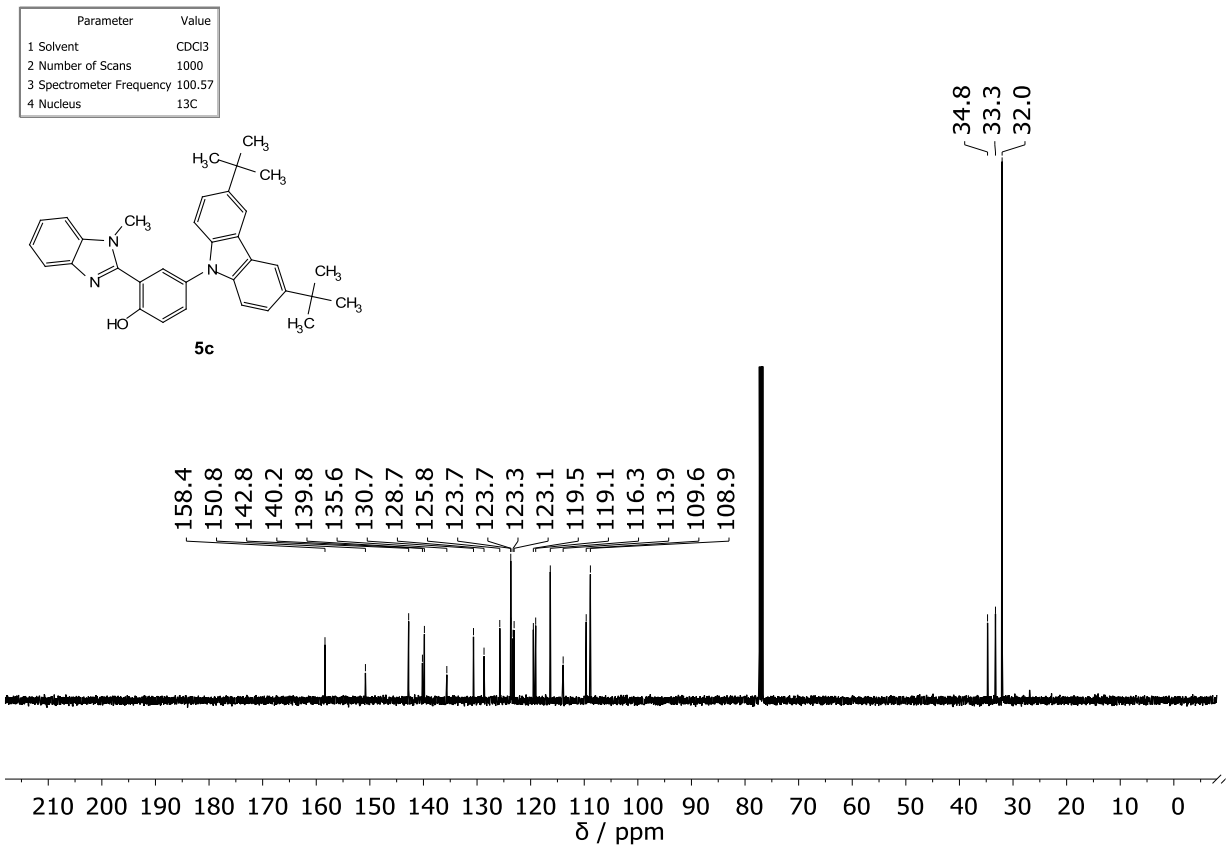

Figure S9.11. $^{13}C\{^{1}H\}$ NMR spectrum (101 MHz, $CDCl_3$) of **5c**.

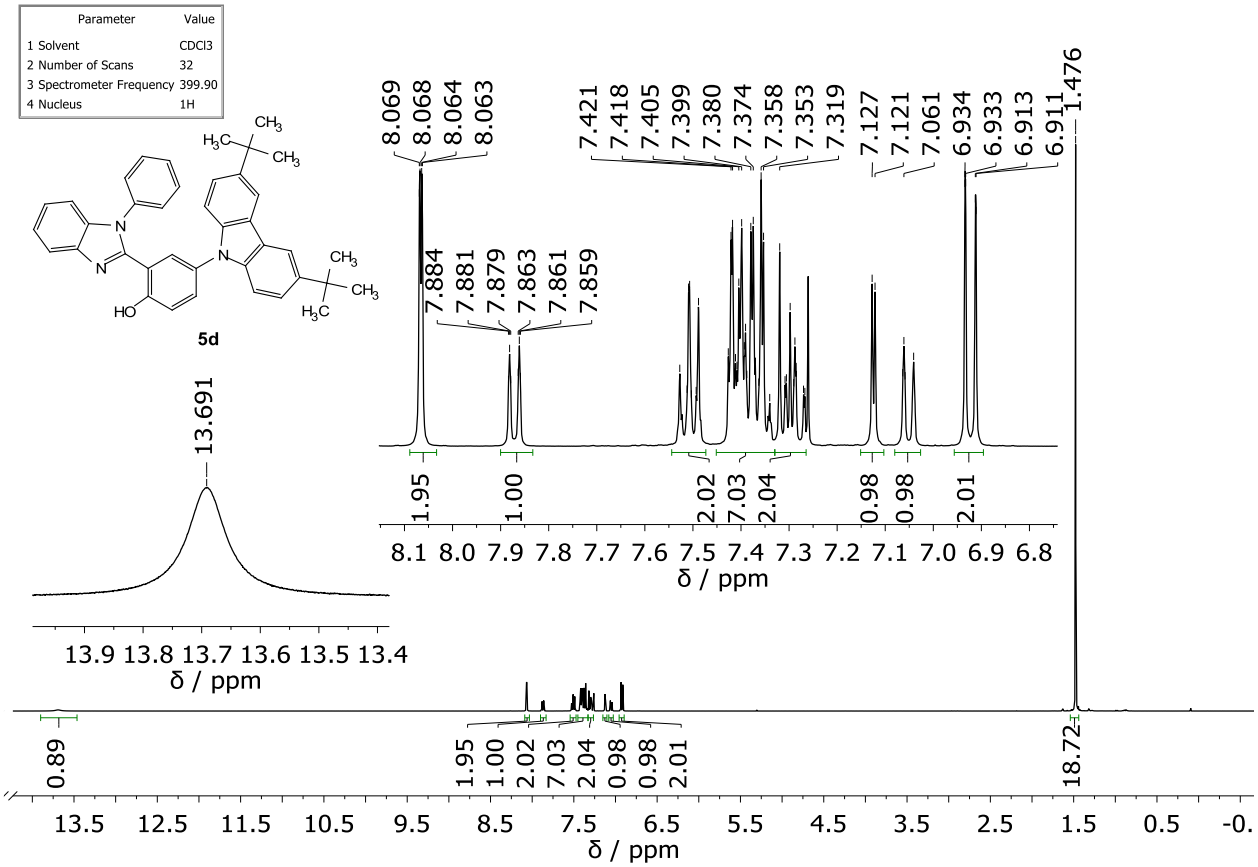

Figure S9.12 ^{1}H NMR spectrum (400 MHz, $CDCl_3$) of **5d**.

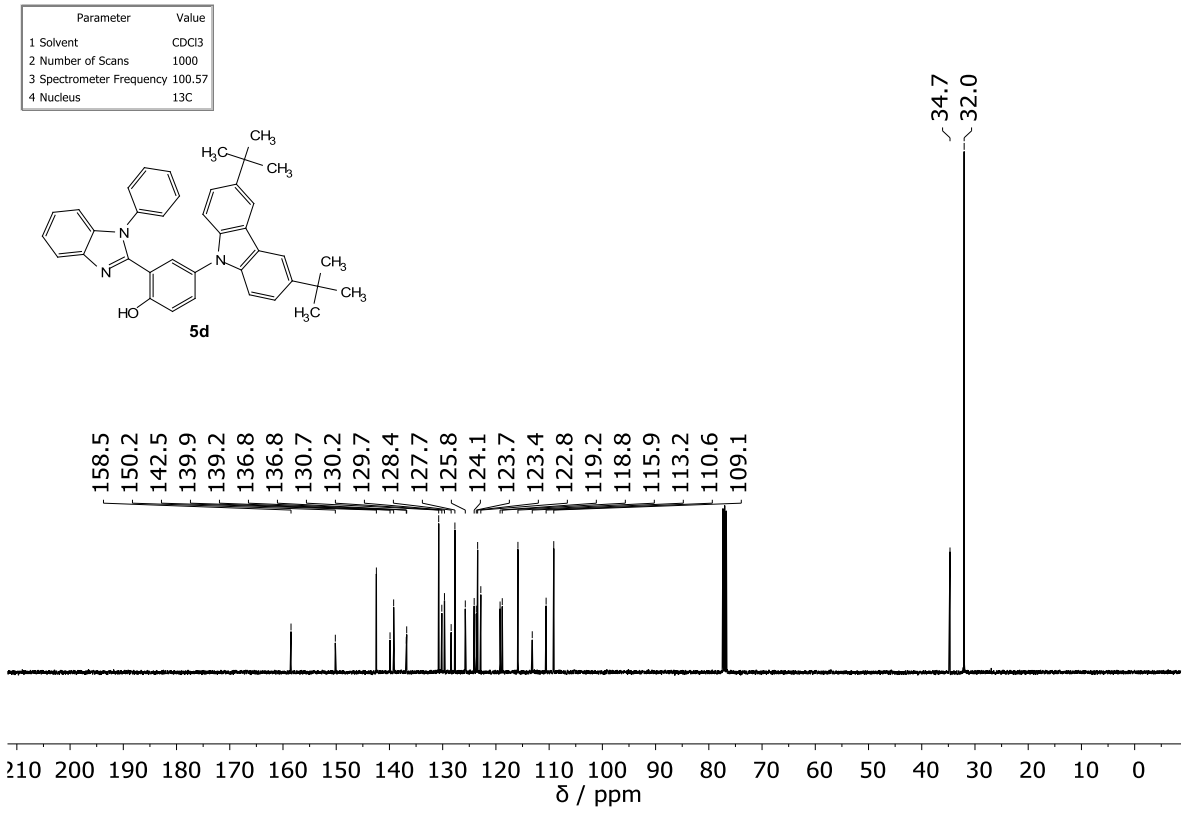

Figure S9.13. $^{13}C\{^{1}H\}$ NMR spectrum (101 MHz, $CDCl_3$) of **5d**.

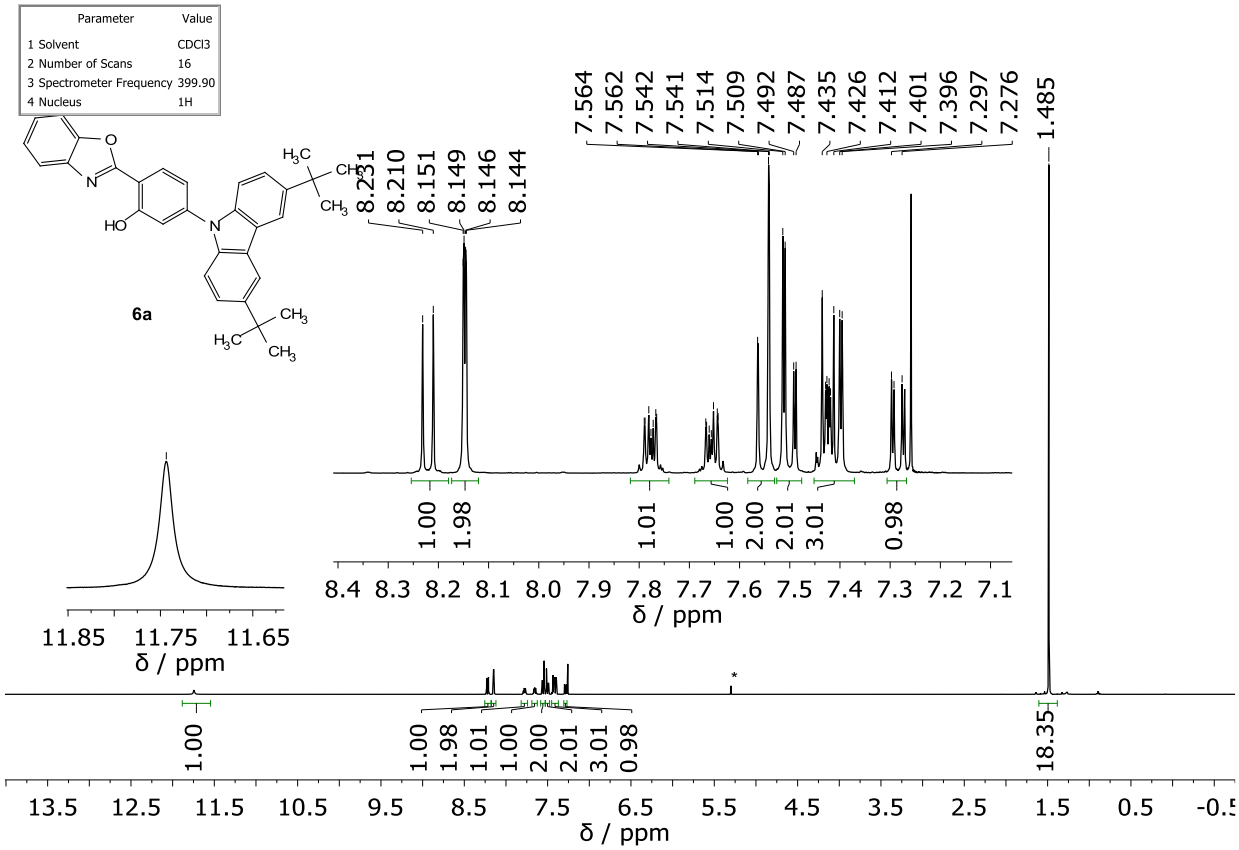

Figure S9.14. ^{1}H NMR spectrum (400 MHz, $CDCl_3$) of **6a**. Residual solvent (DCM) impurity is marked with an asterisk (*).

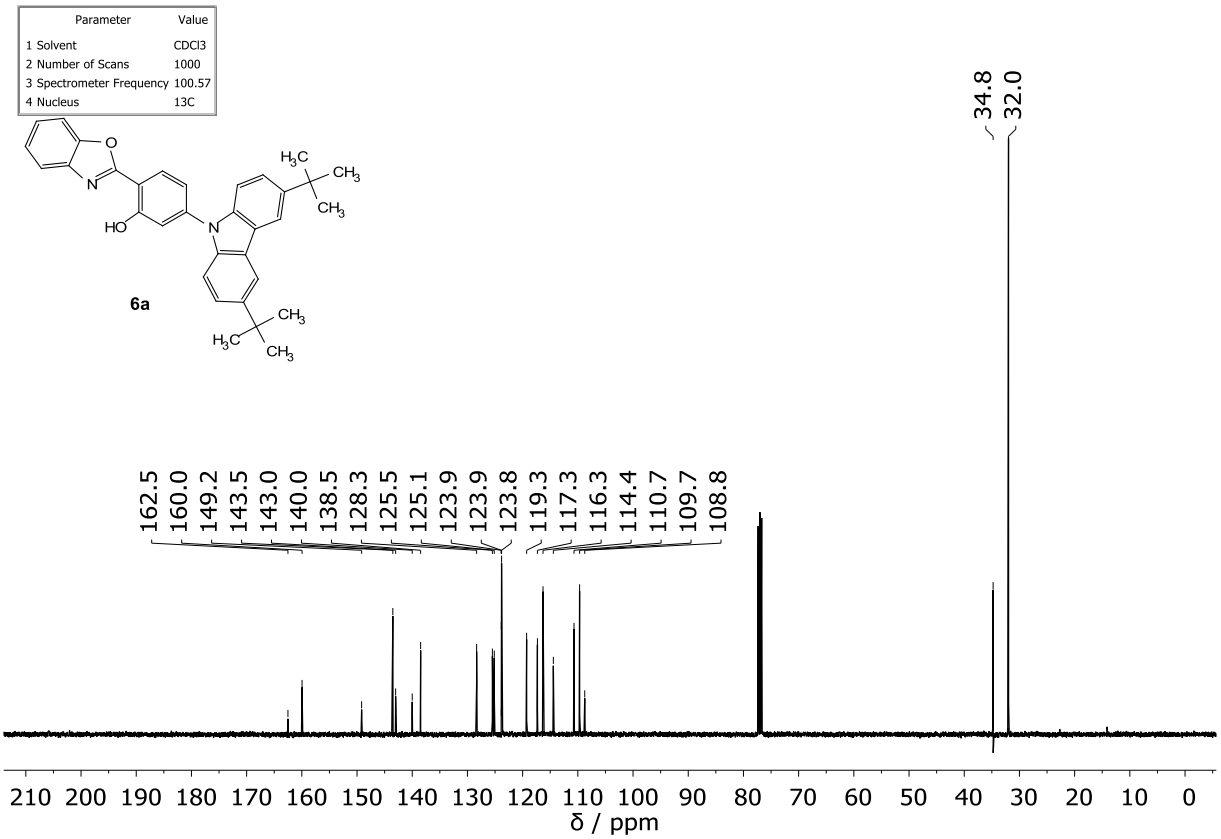

Figure S9.15. $^{13}C\{^{1}H\}$ NMR spectrum (101 MHz, $CDCl_3$) of **6a**.

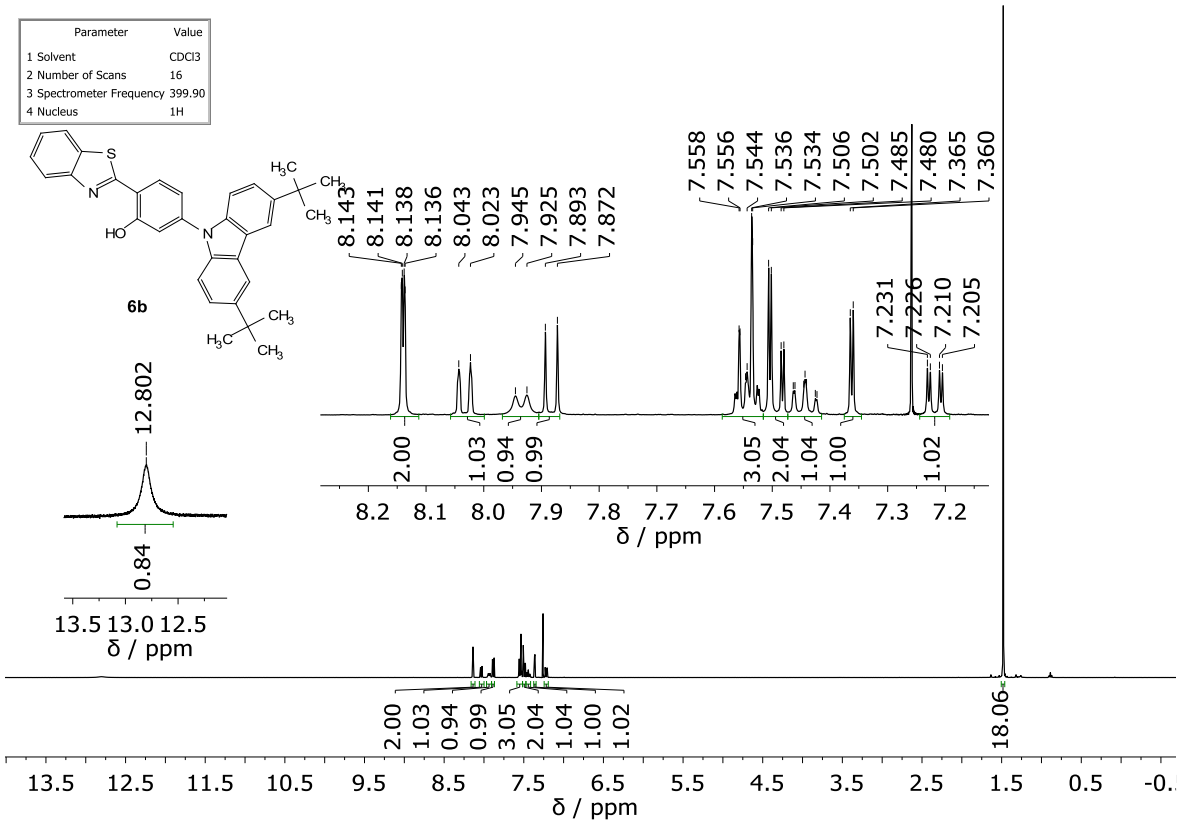

Figure S9.16. ^{1}H NMR spectrum (400 MHz, $CDCl_3$) of **6b**.

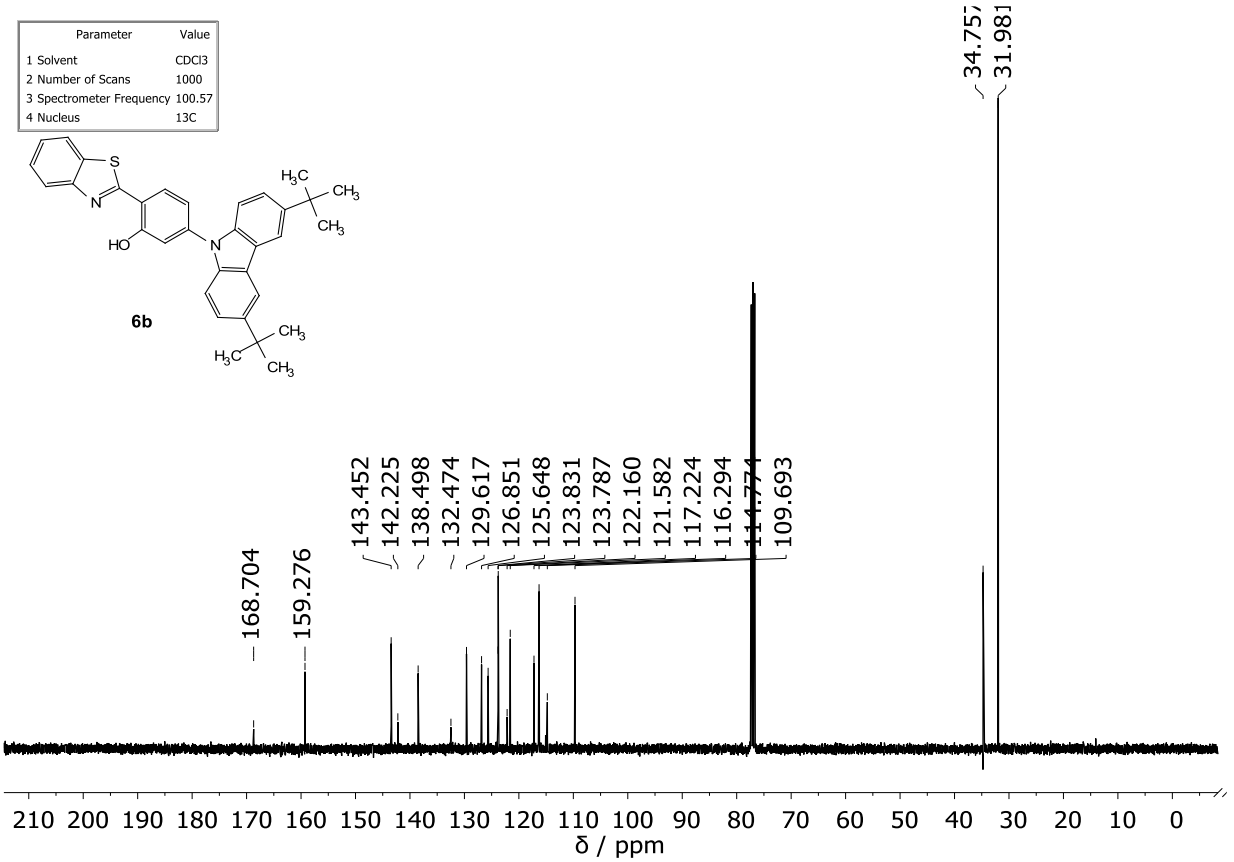

Figure S9.17. $^{13}C\{^{1}H\}$ NMR spectrum (101 MHz, $CDCl_3$) of **6b**.

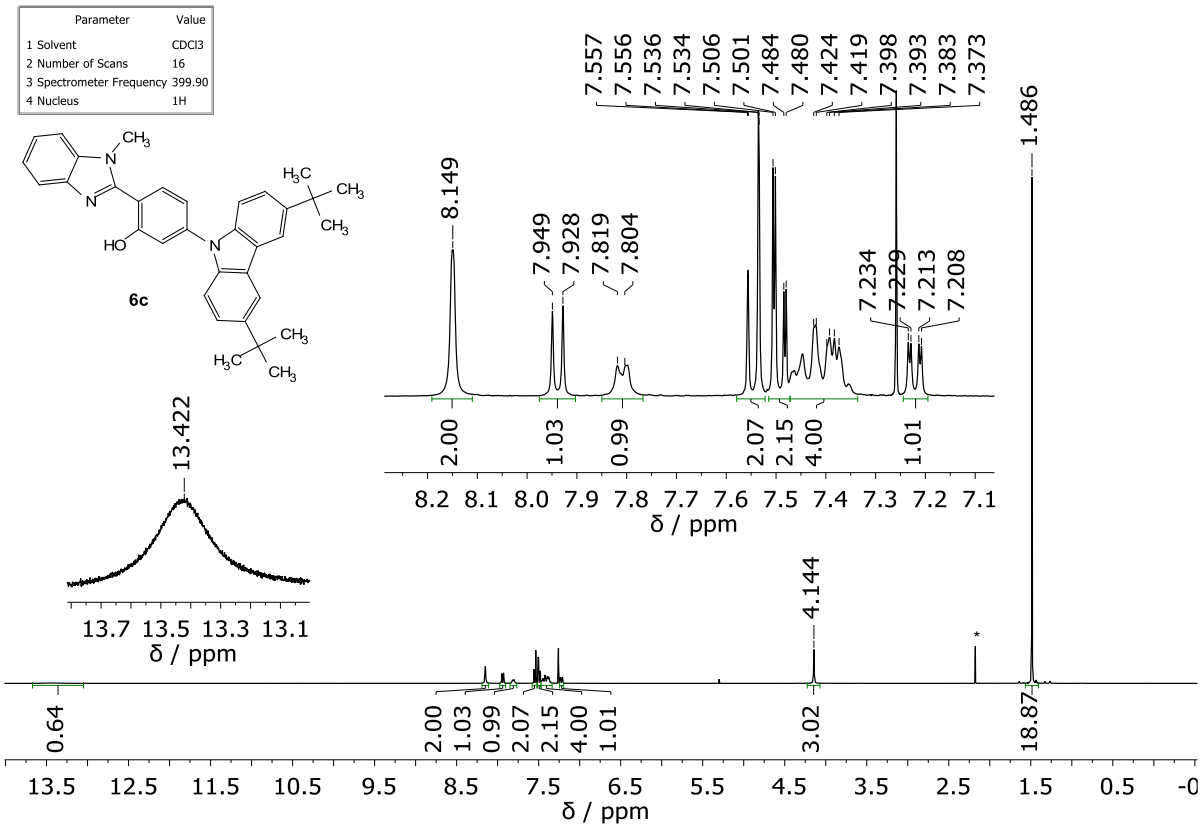

Figure S9.18. ^{1}H NMR spectrum (400 MHz, $CDCl_3$) of **6c**. Residual solvent (acetone) impurity is marked with an asterisk (*).

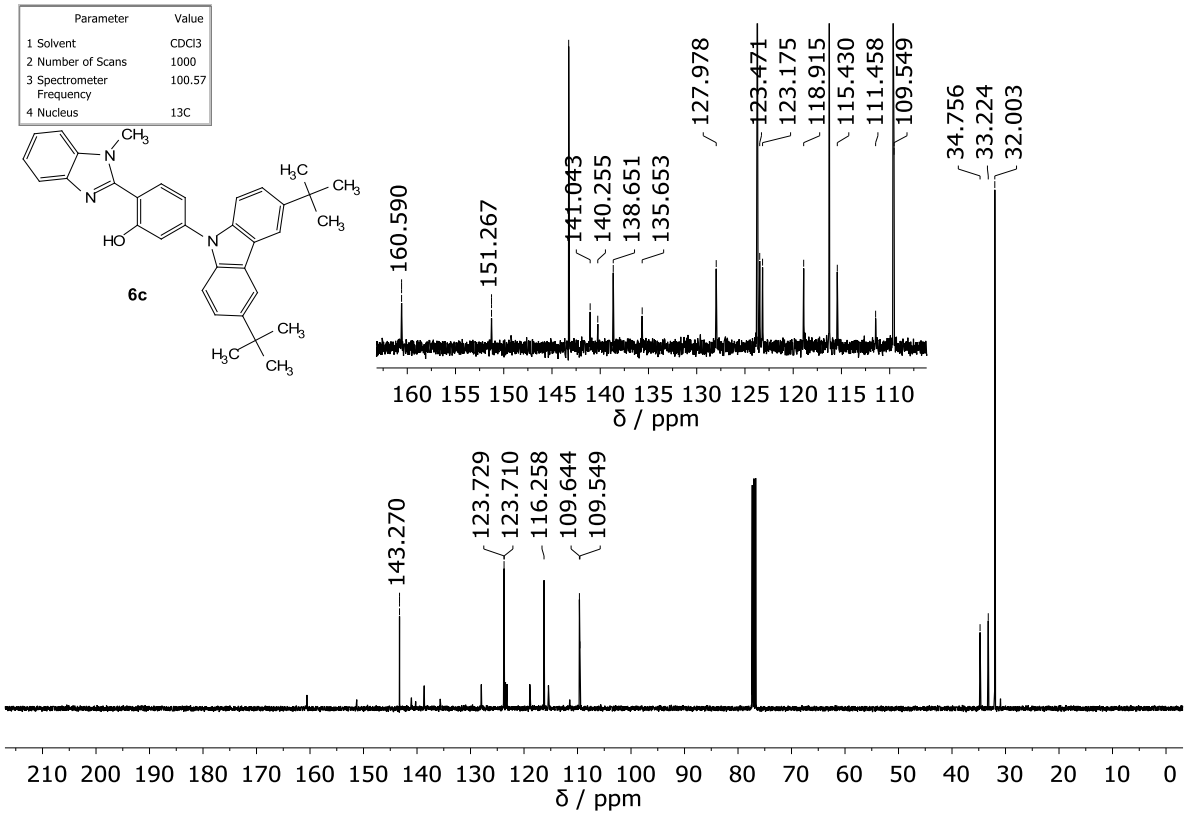

Figure S9.19. $^{13}C\{^{1}H\}$ NMR spectrum (101 MHz, $CDCl_3$) of **6c**.

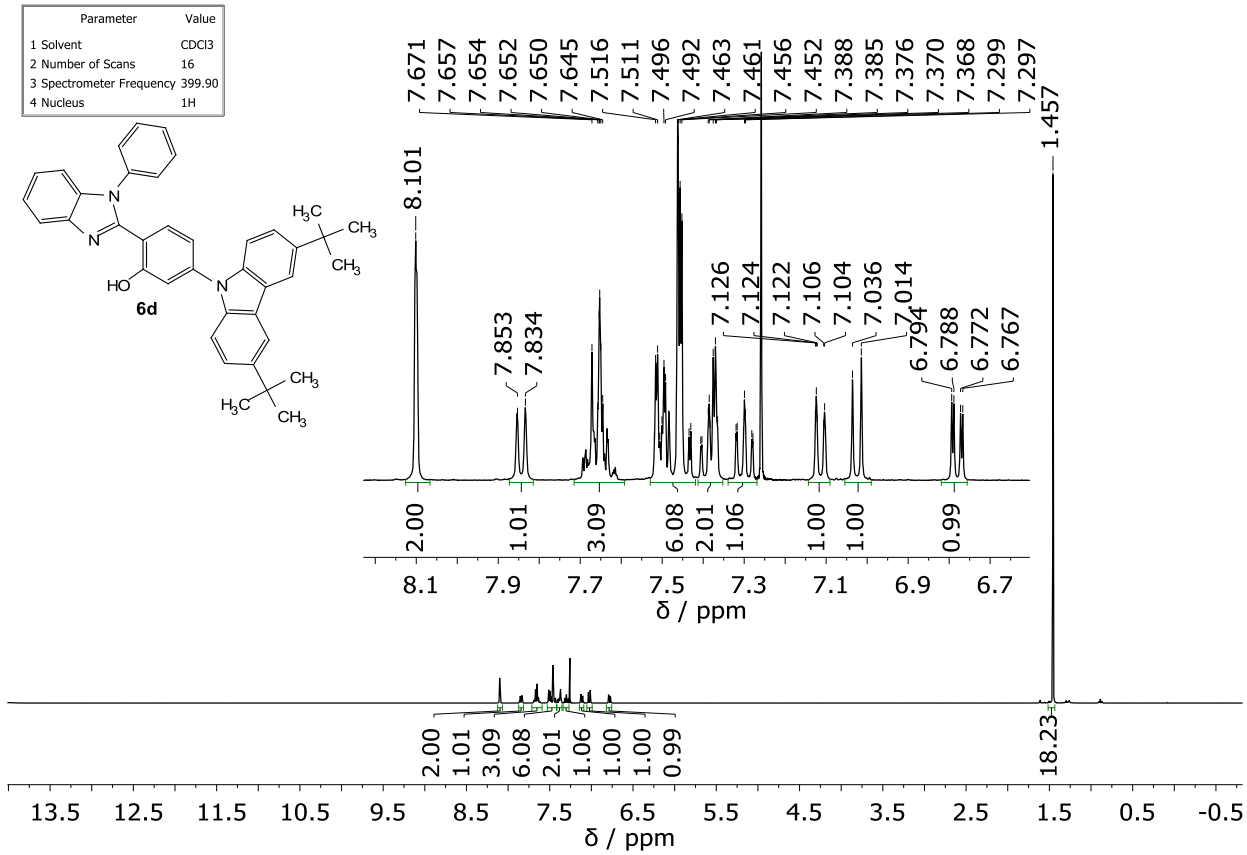

Figure S9.20. ^{1}H NMR spectrum (400 MHz, $CDCl_3$) of **6d**.

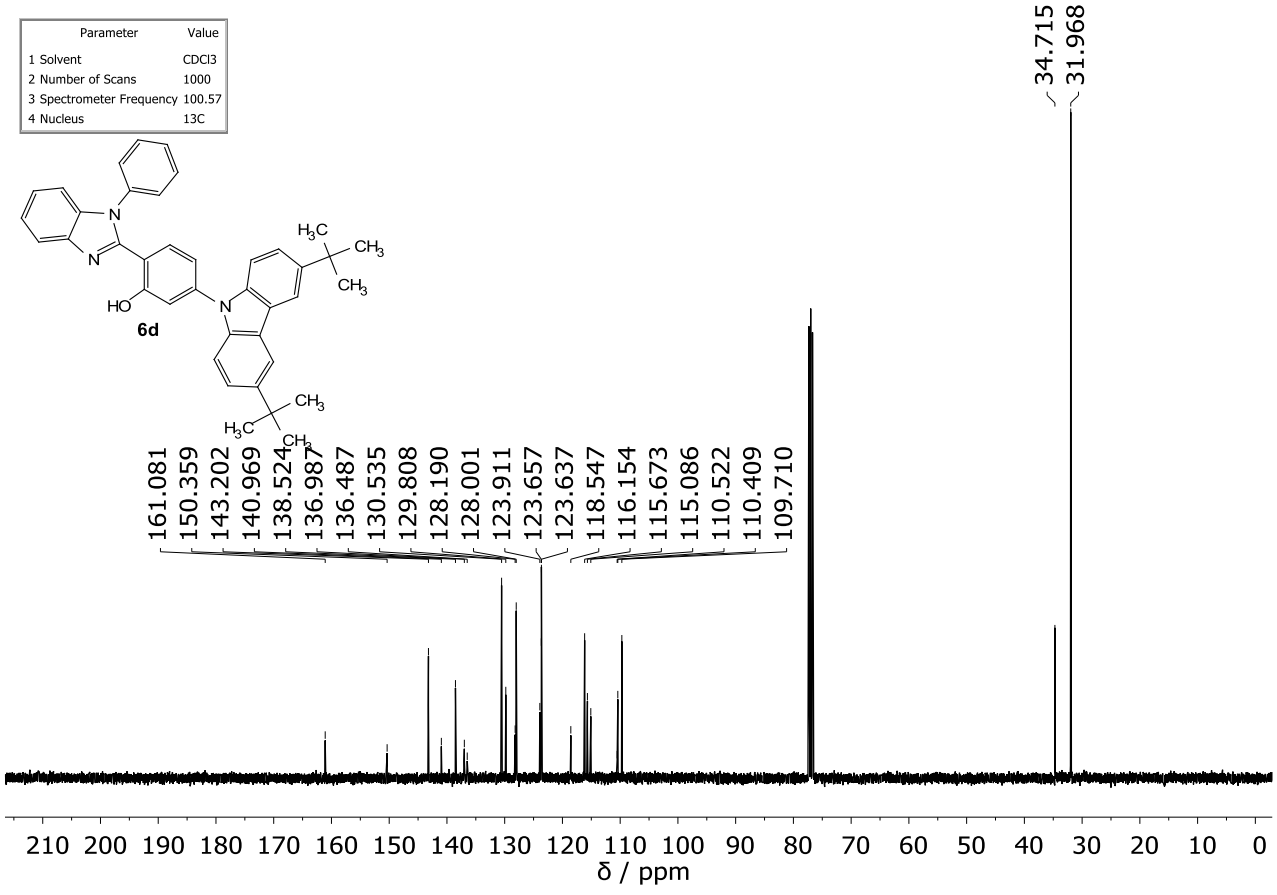

Figure S9.21. $^{13}C\{^{1}H\}$ NMR spectrum (101 MHz, $CDCl_3$) of **6d**.

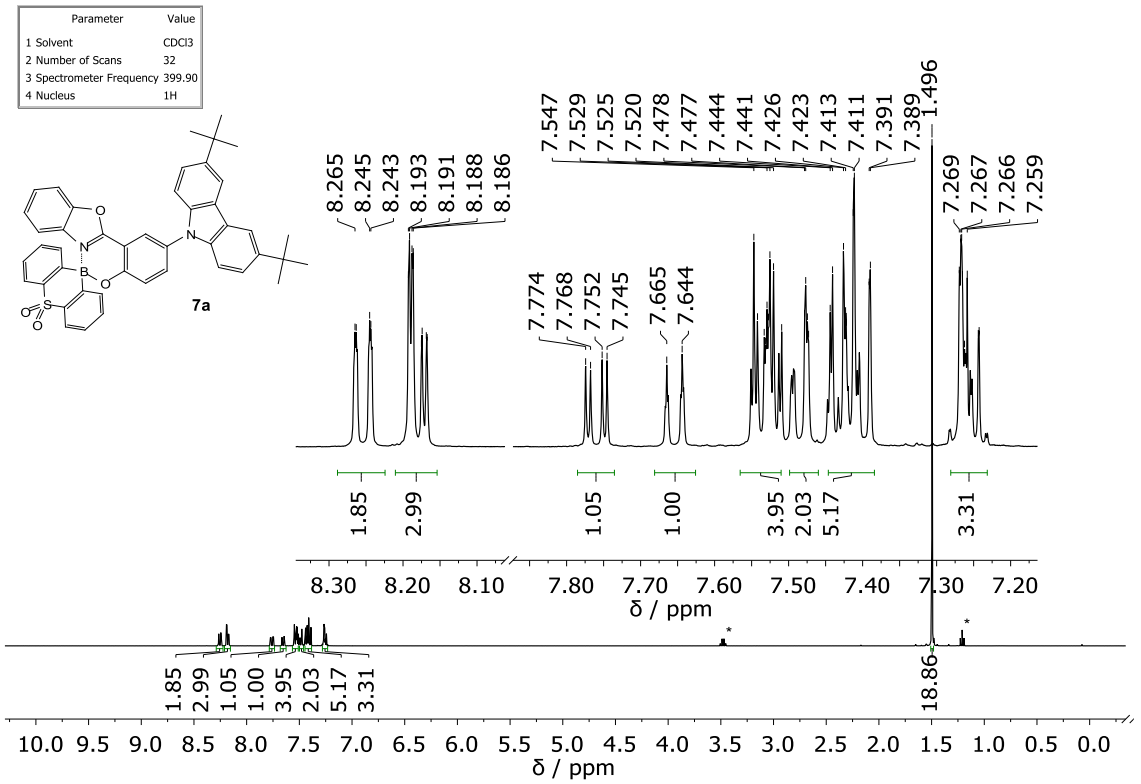

Figure S9.22. ^{1}H NMR spectrum (400 MHz, $CDCl_3$) of **7a**. Residual solvent (diethyl eter) impurity is marked with an asterisk (*).

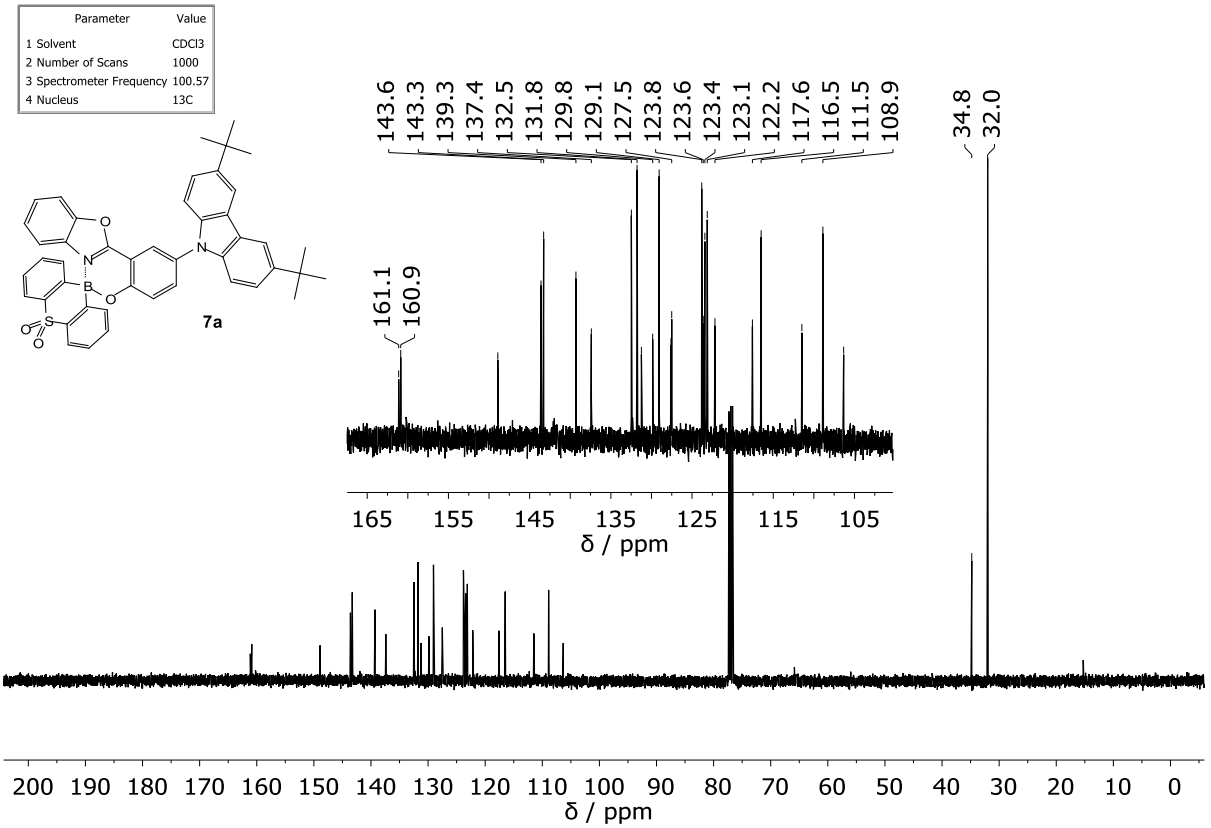

Figure S9.23. $^{13}C\{^{1}H\}$ NMR spectrum (101 MHz, $CDCl_3$) of **7a**.

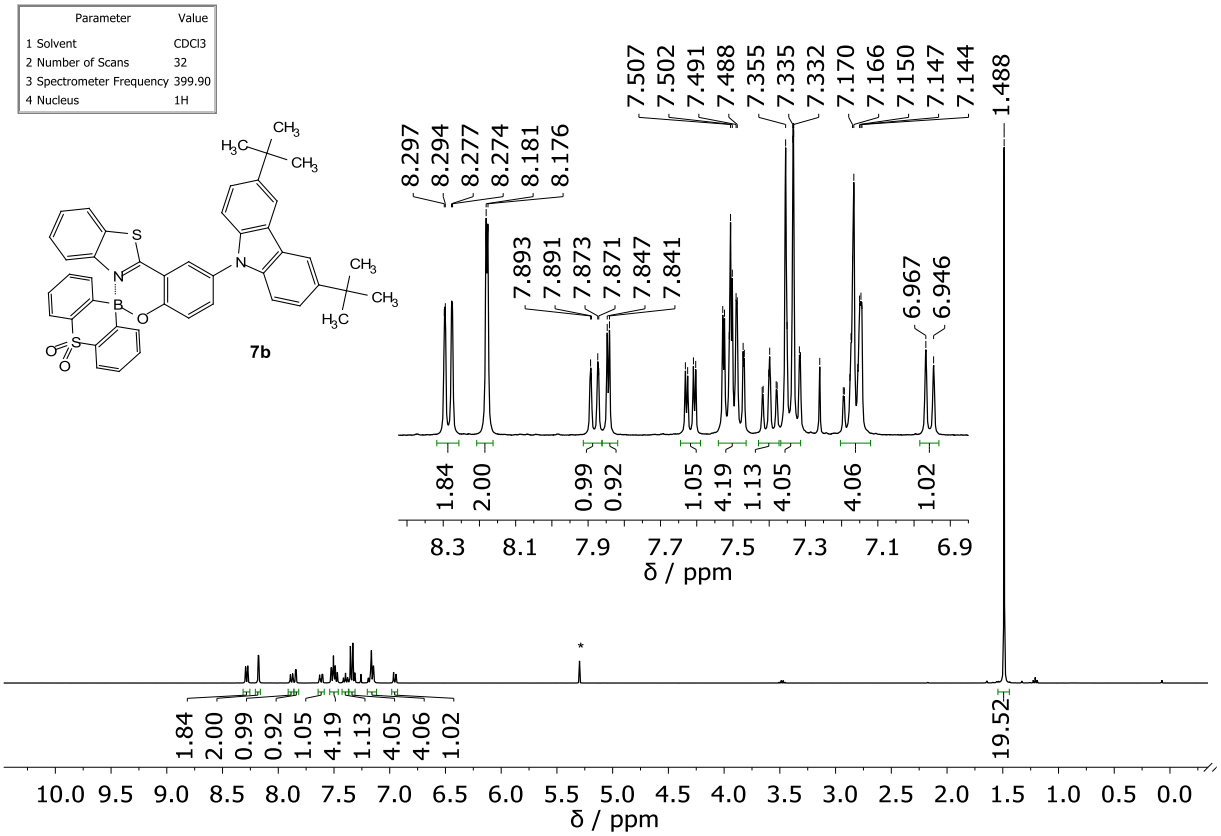

Figure S9.24. ^{1}H NMR spectrum (400 MHz, $CDCl_3$) of **7b**. Residual solvent (DCM) impurity is marked with an asterisk (*).

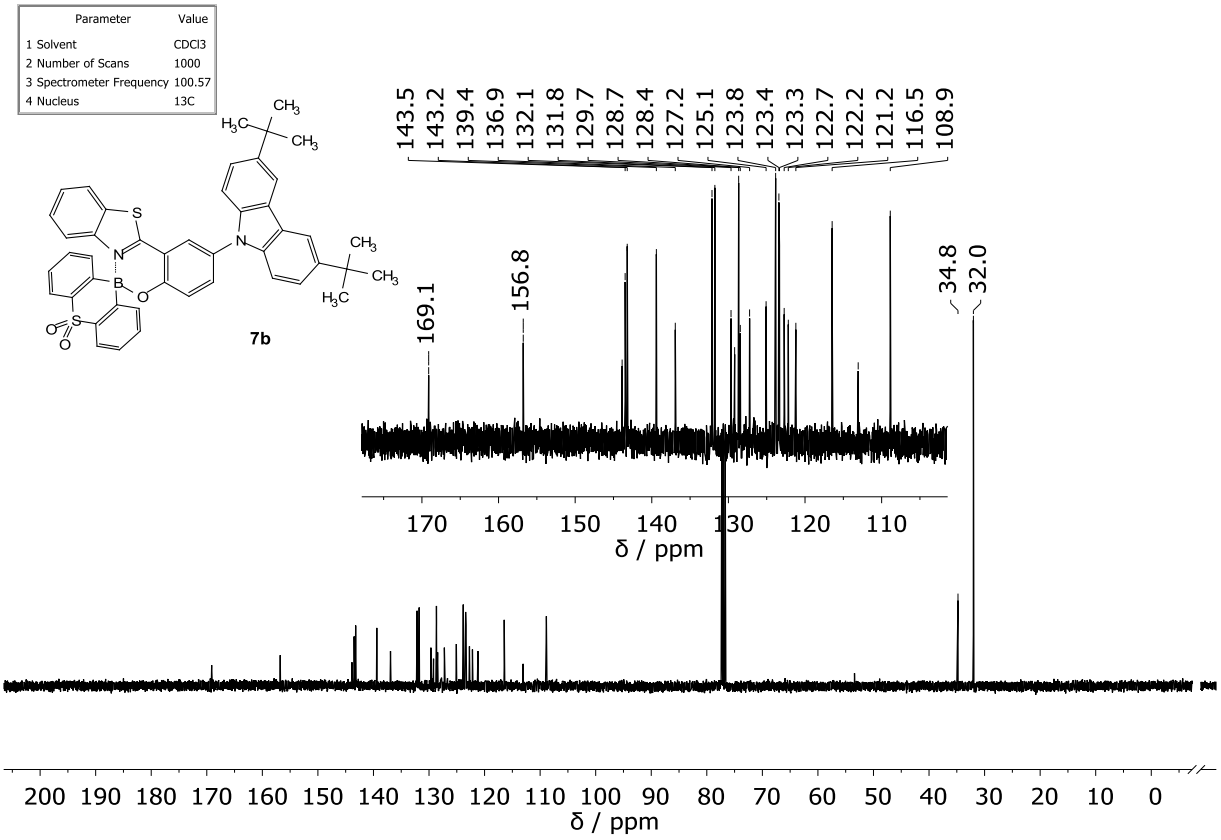

Figure S9.25. $^{13}C\{^{1}H\}$ NMR spectrum (101 MHz, $CDCl_3$) of **7b**.

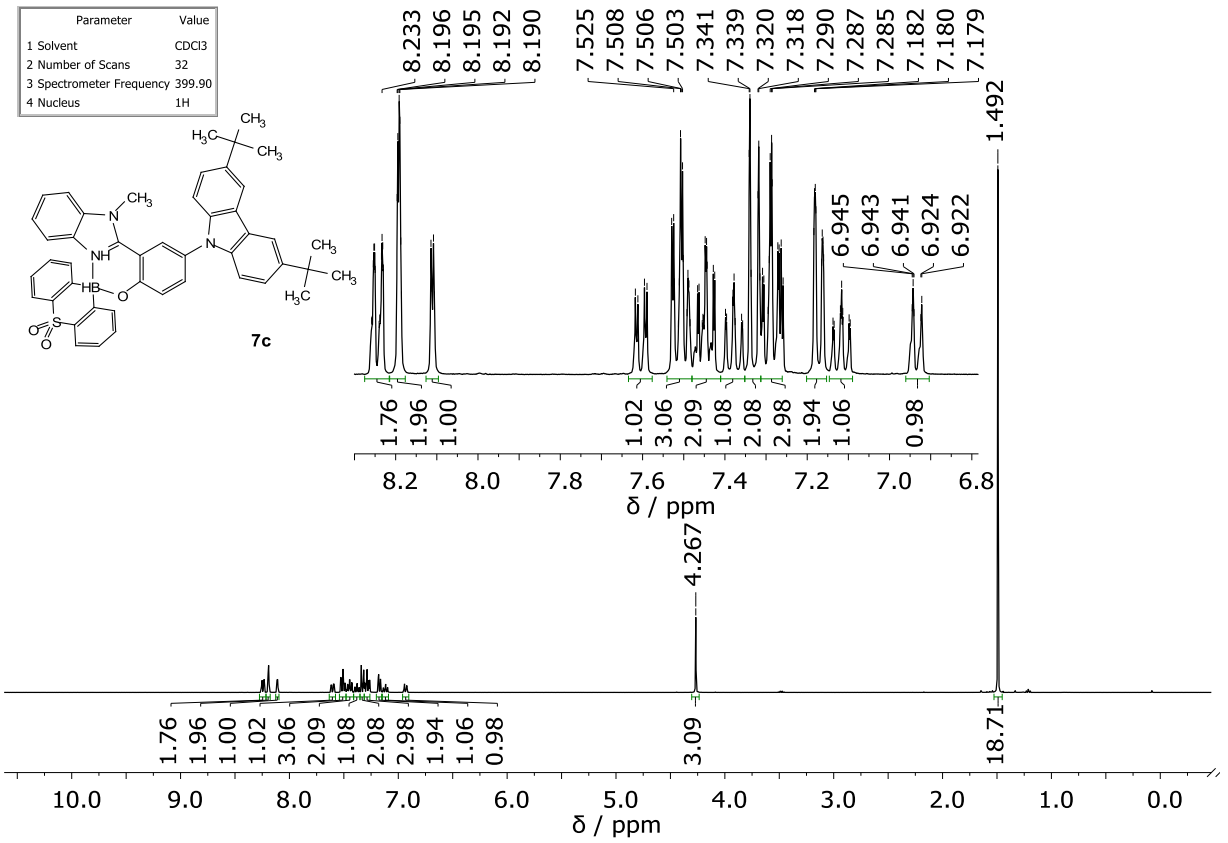

Figure S9.26. ^{1}H NMR spectrum (400 MHz, $CDCl_3$) of **7c**.

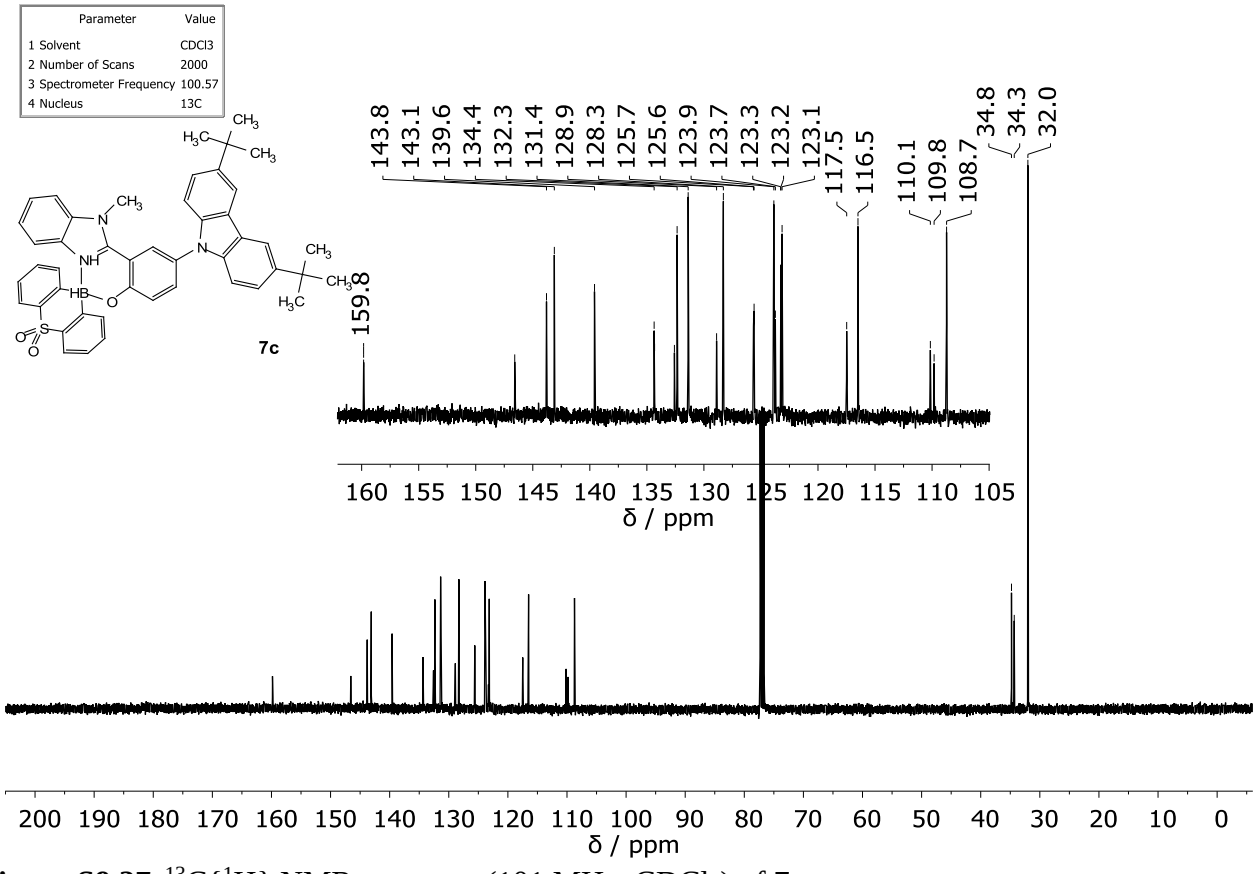

Figure S9.27. $^{13}C\{^{1}H\}$ NMR spectrum (101 MHz, $CDCl_3$) of **7c**.

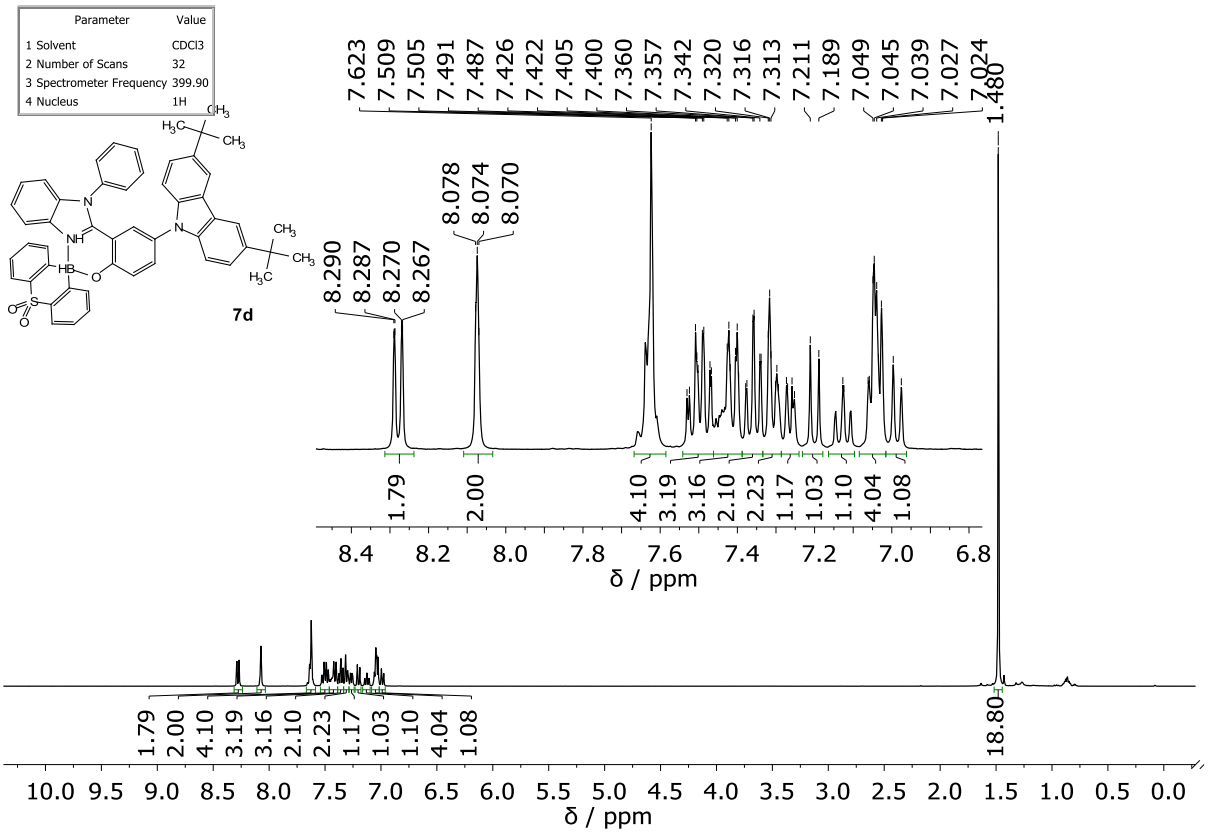

Figure S9.28. ^{1}H NMR spectrum (400 MHz, $CDCl_3$) of **7d**.

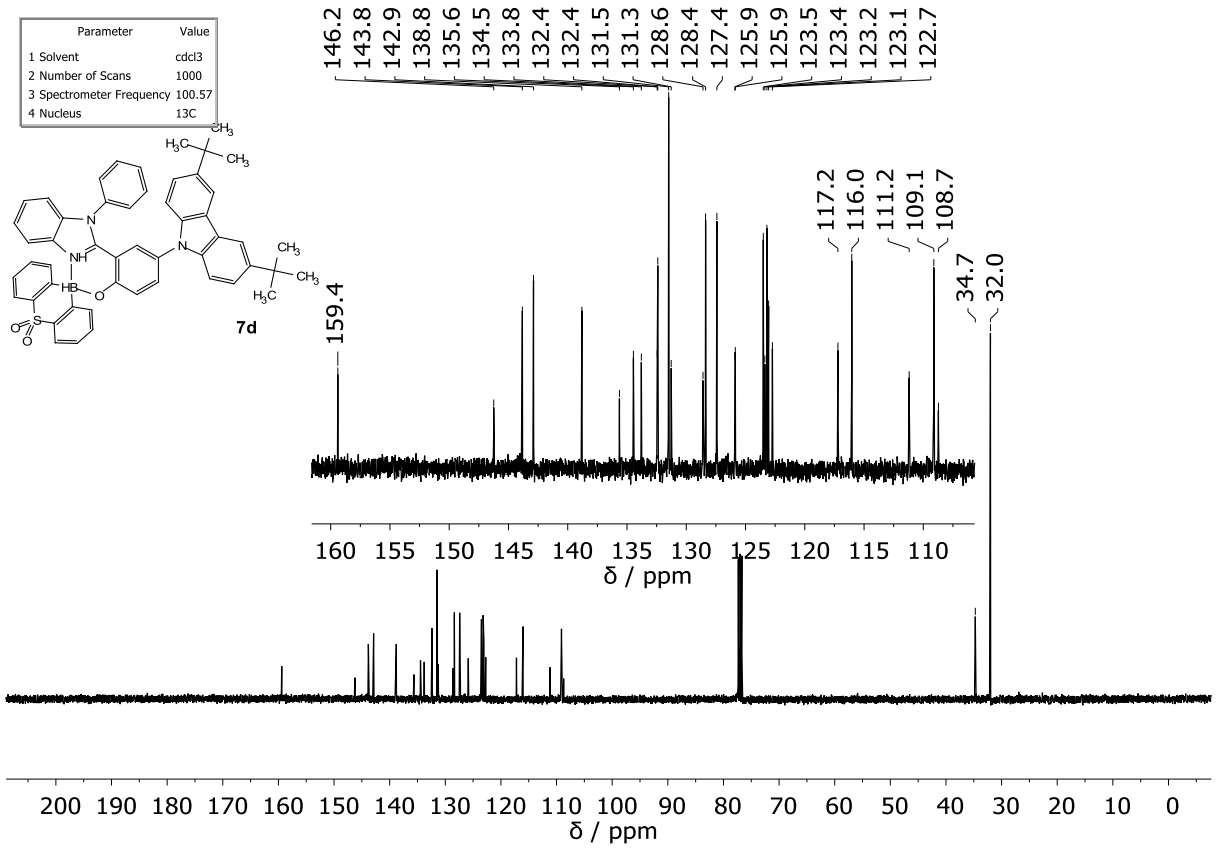

Figure S9.29. $^{13}C\{^{1}H\}$ NMR spectrum (101 MHz, $CDCl_3$) of **7d**.

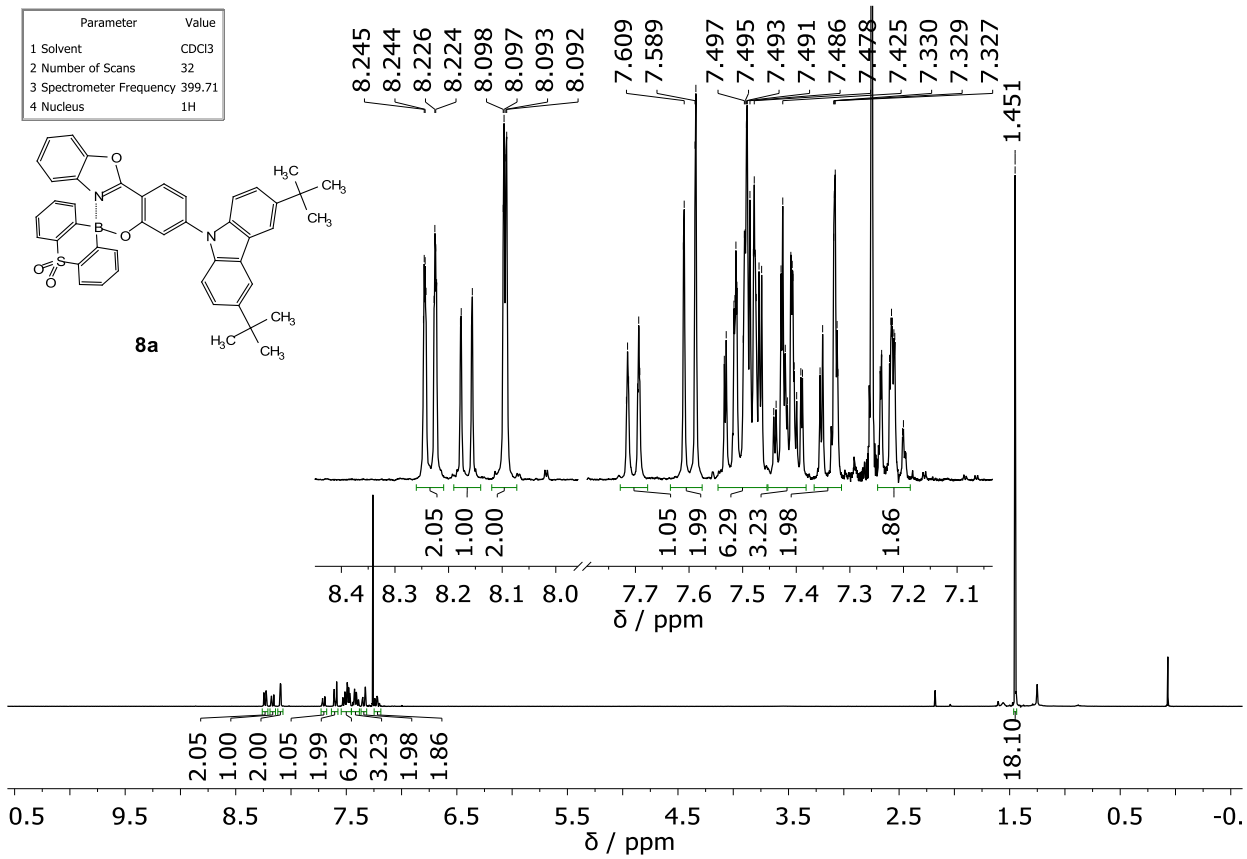

Figure S9.30. ^{1}H NMR spectrum (400 MHz, $CDCl_3$) of **8a**.

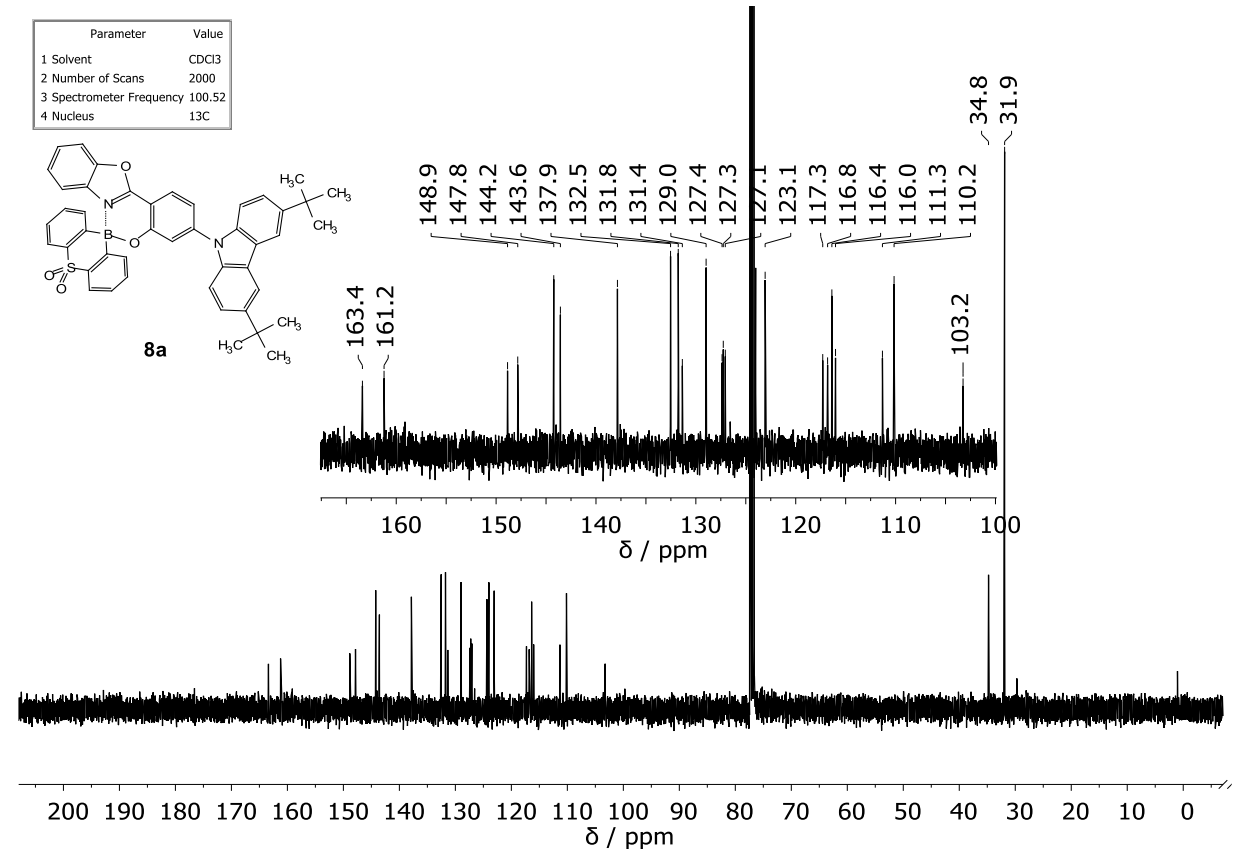

Figure S9.31. $^{13}C\{^{1}H\}$ NMR spectrum (101 MHz, $CDCl_3$) of **8a**.

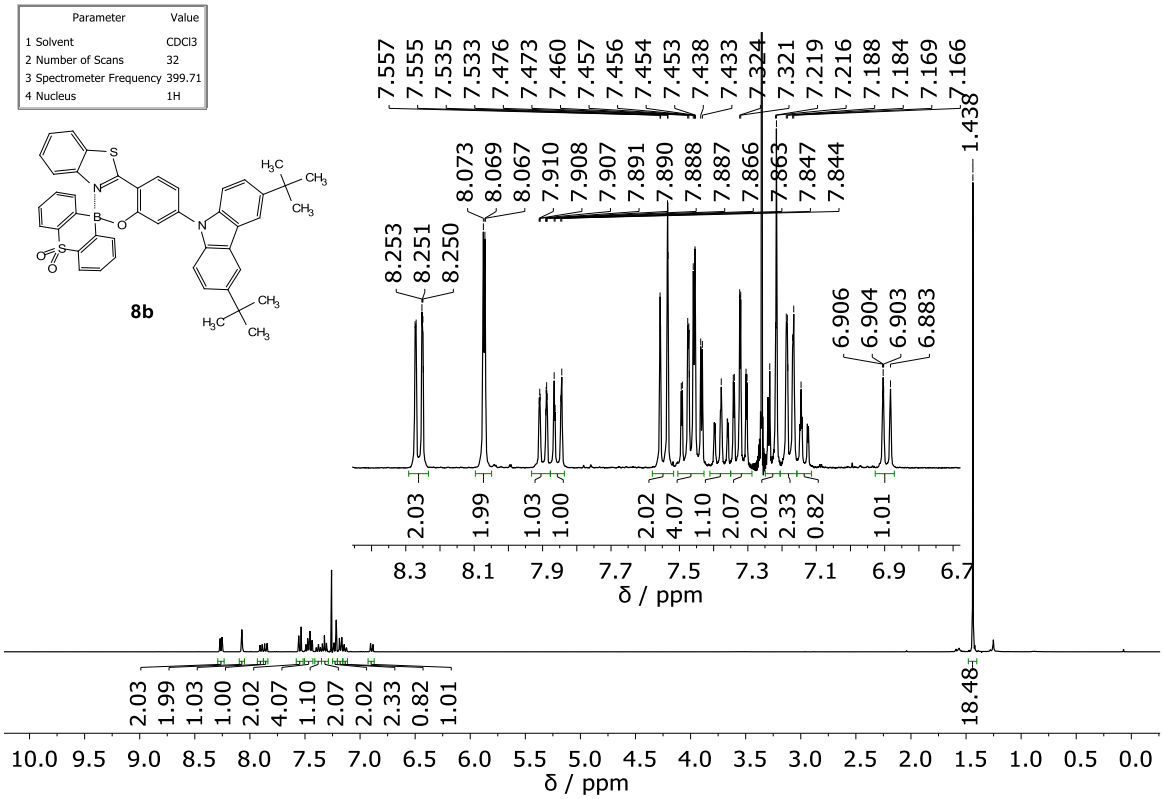

Figure S9.32. ^{1}H NMR spectrum (400 MHz, $CDCl_3$) of **8b**.

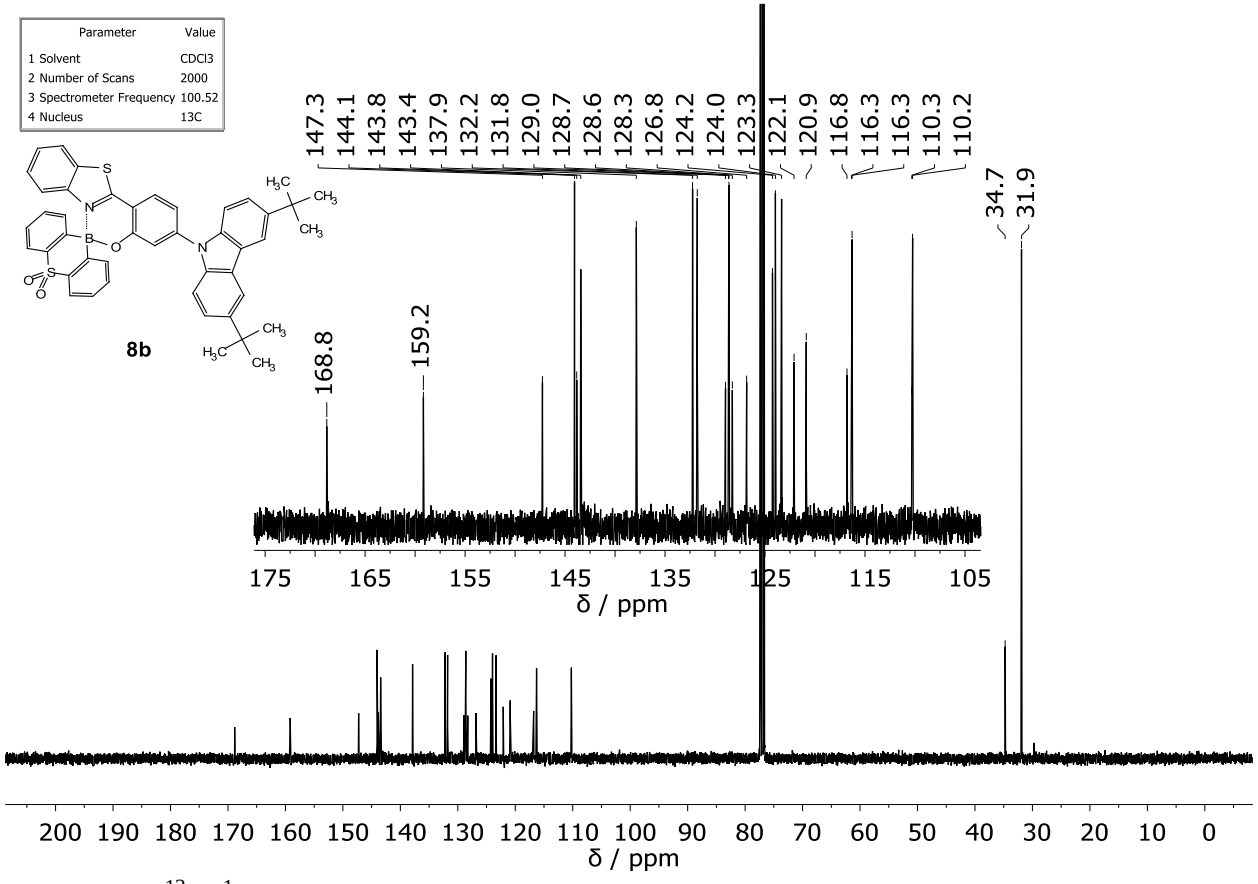

Figure S9.33. $^{13}C\{^{1}H\}$ NMR spectrum (101 MHz, $CDCl_3$) of **8b**.

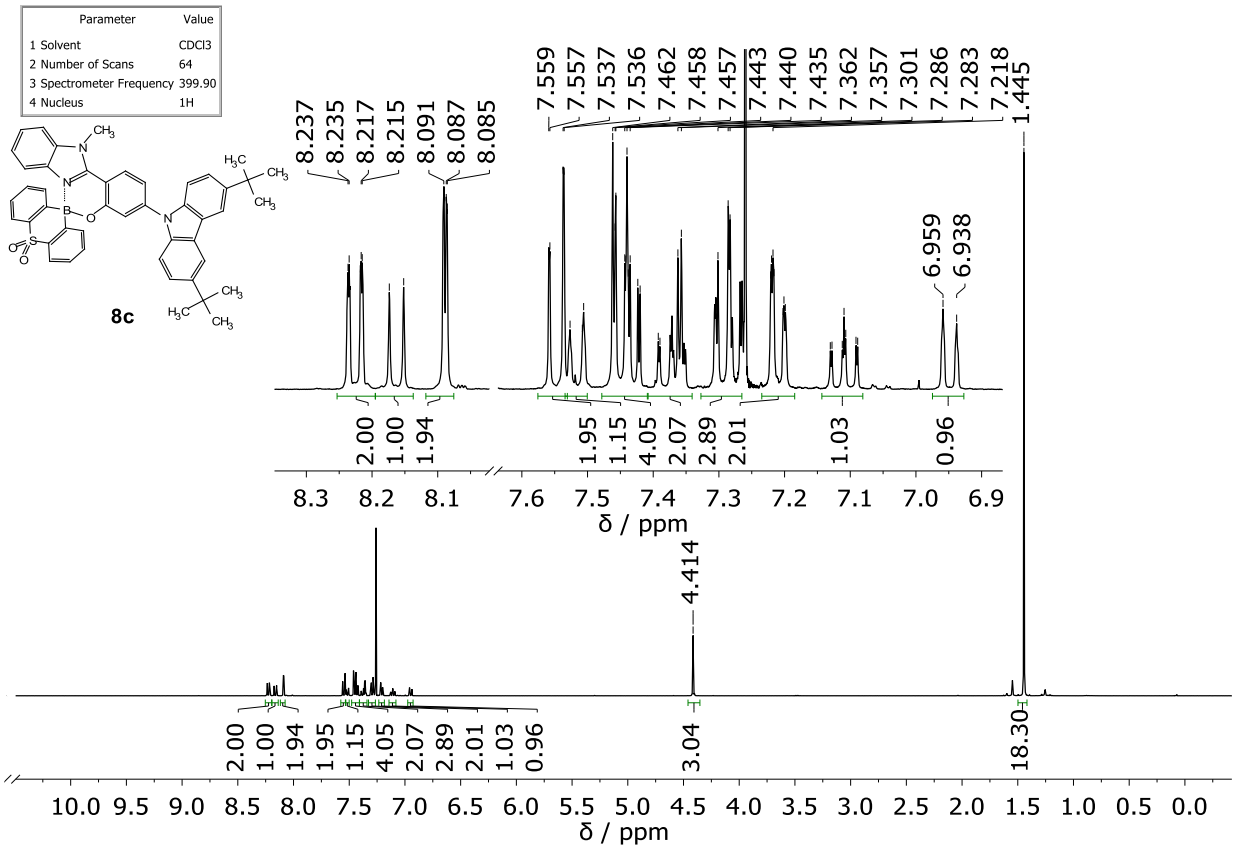

Figure S9.34. ^{1}H NMR spectrum (400 MHz, $CDCl_3$) of **8c**.

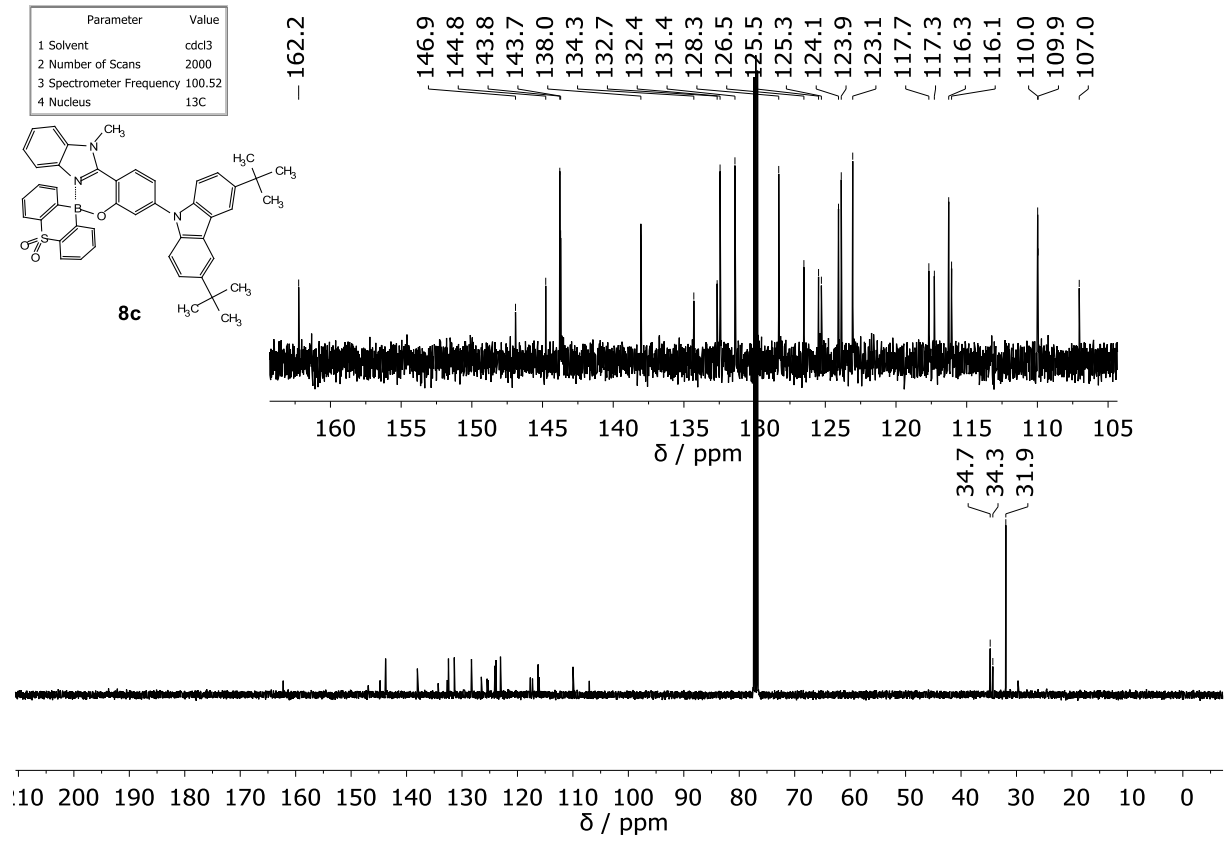

Figure S9.35. $^{13}C\{^{1}H\}$ NMR spectrum (101 MHz, $CDCl_3$) of **8c**.

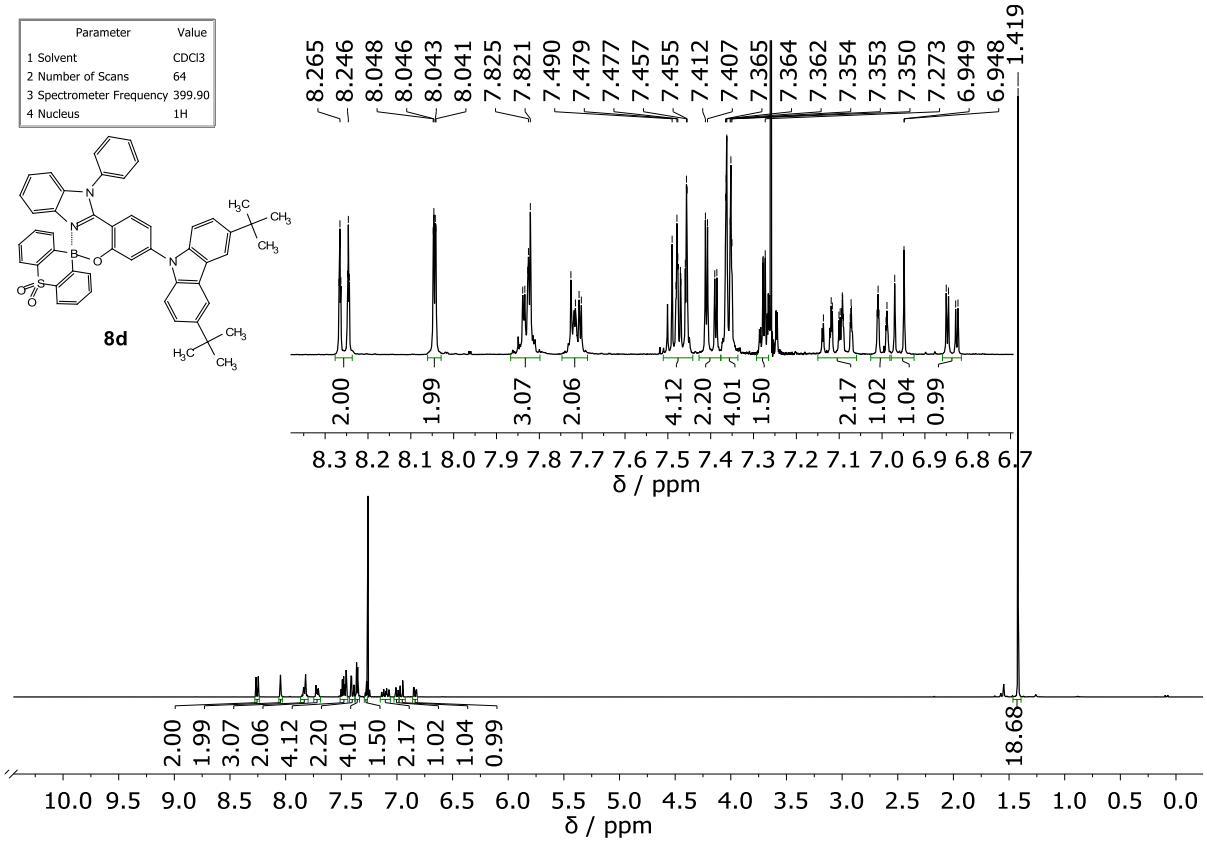

Figure S9.36. ^{1}H NMR spectrum (400 MHz, $CDCl_3$) of **8d**.

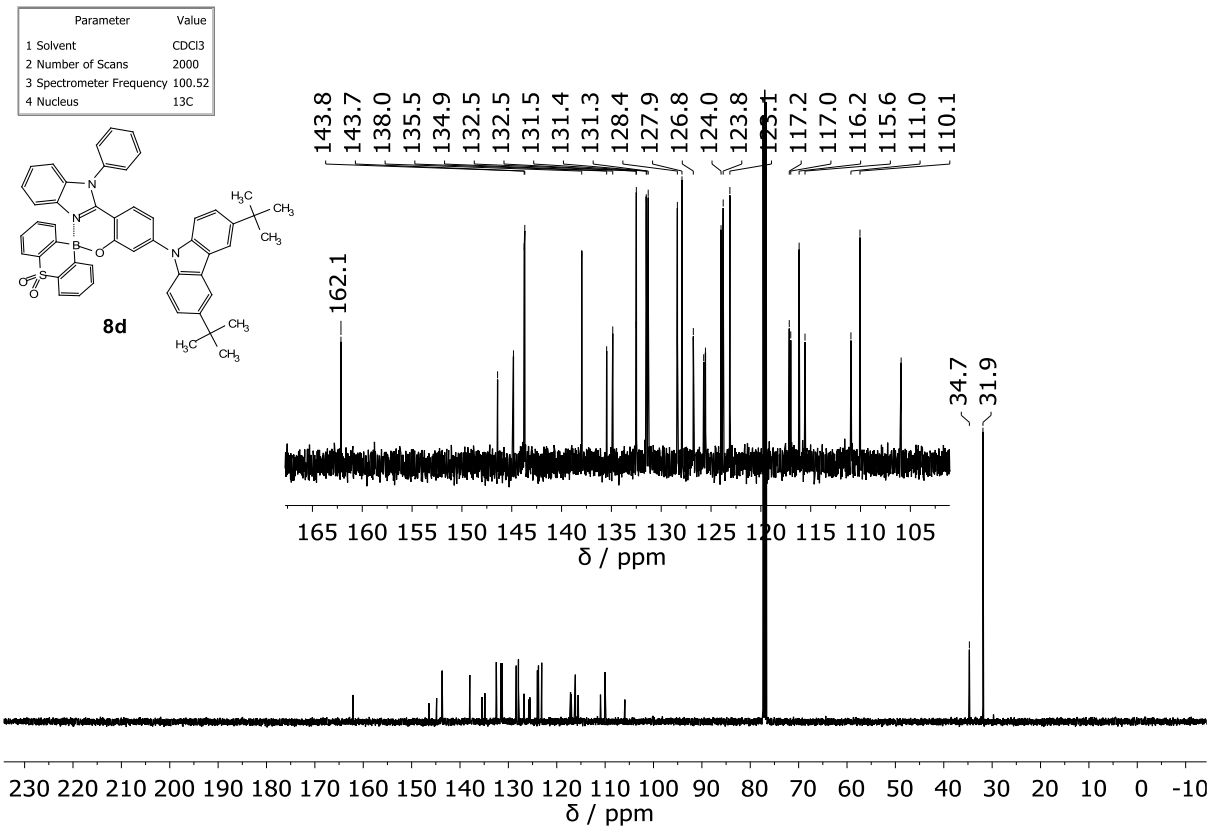

Figure S9.37. $^{13}C\{^{1}H\}$ NMR spectrum (101 MHz, $CDCl_3$) of **8d**.

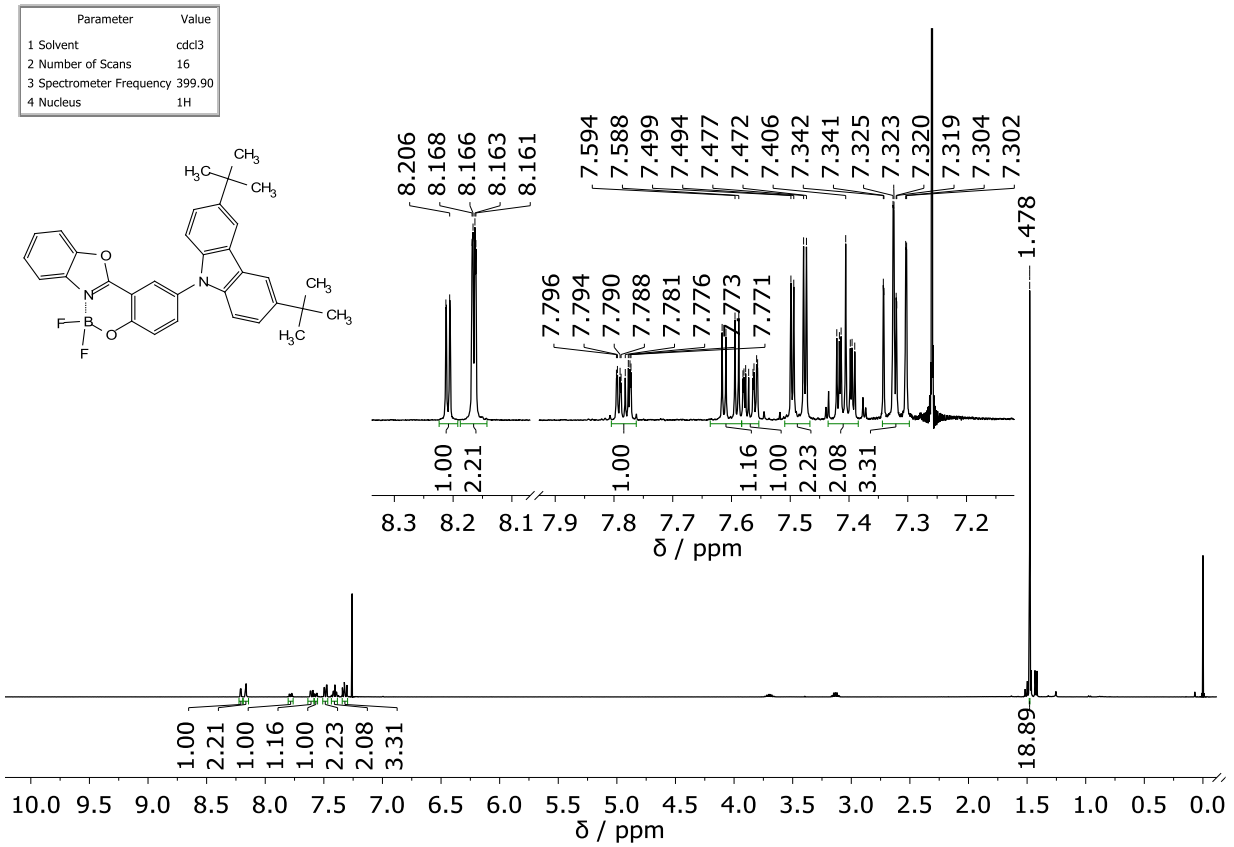

Figure S9.38. ^{1}H NMR spectrum (400 MHz, $CDCl_3$) of **9**.

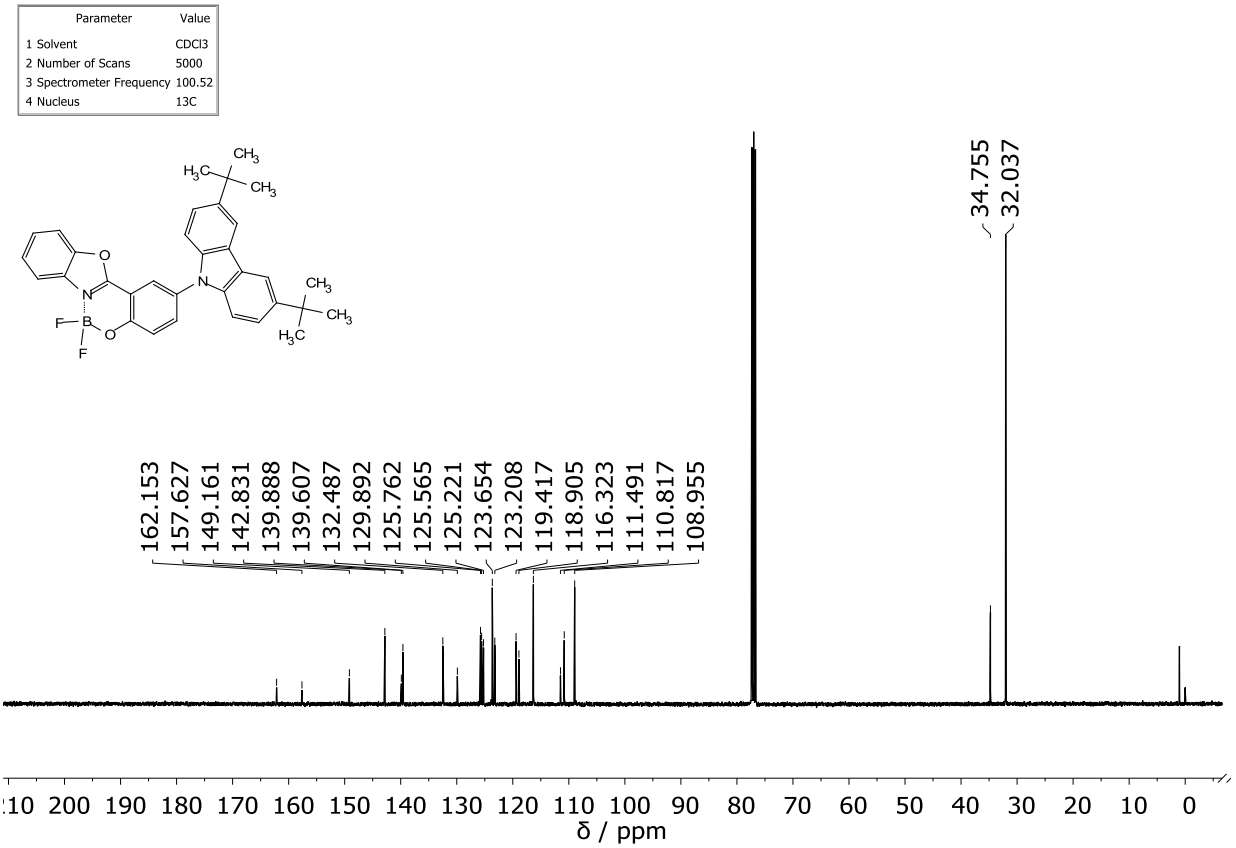

Figure S9.39. $^{13}C\{^{1}H\}$ NMR spectrum (101 MHz, $CDCl_3$) of **9**.

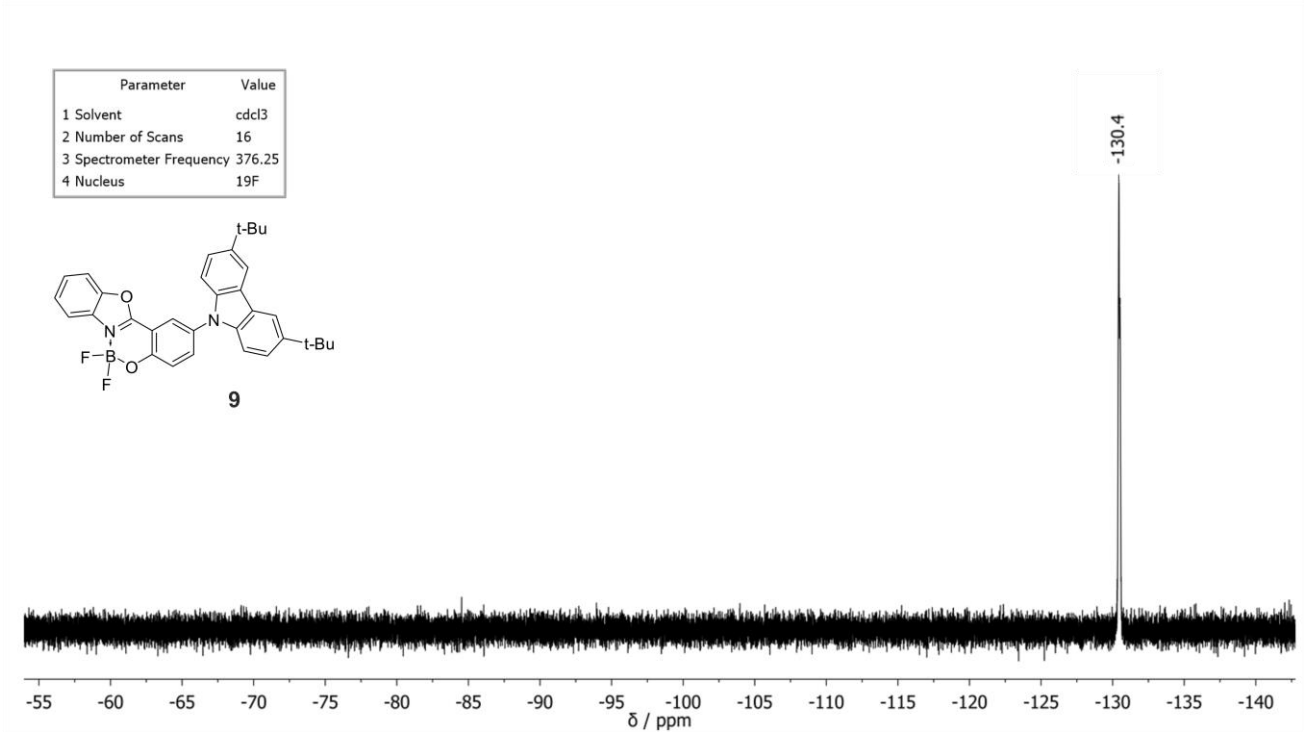

Figure S9.40. $^{19}F\{^{1}H\}$ NMR spectrum (376 MHz, $CDCl_3$) of **10**.

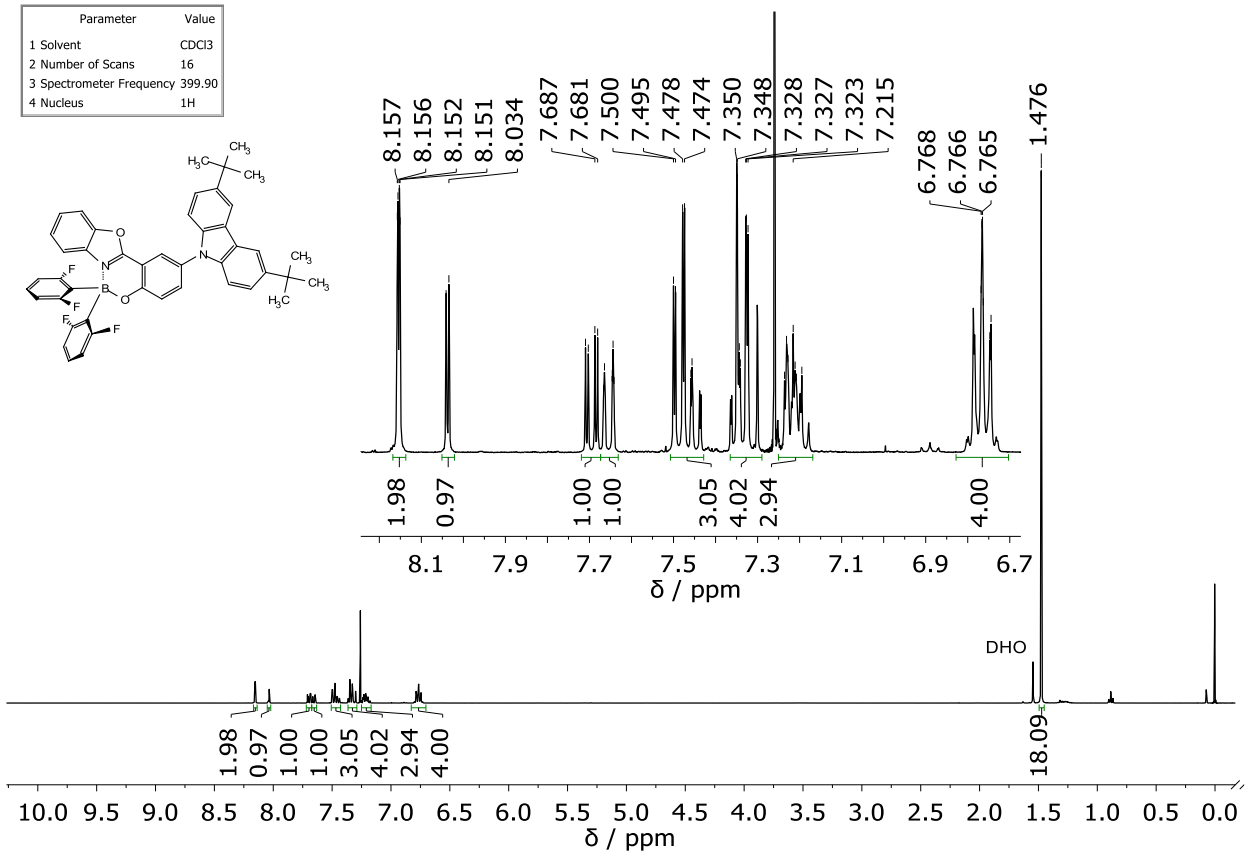

Figure S9.41. ^{1}H NMR spectrum (400 MHz, $CDCl_3$) of **10**.

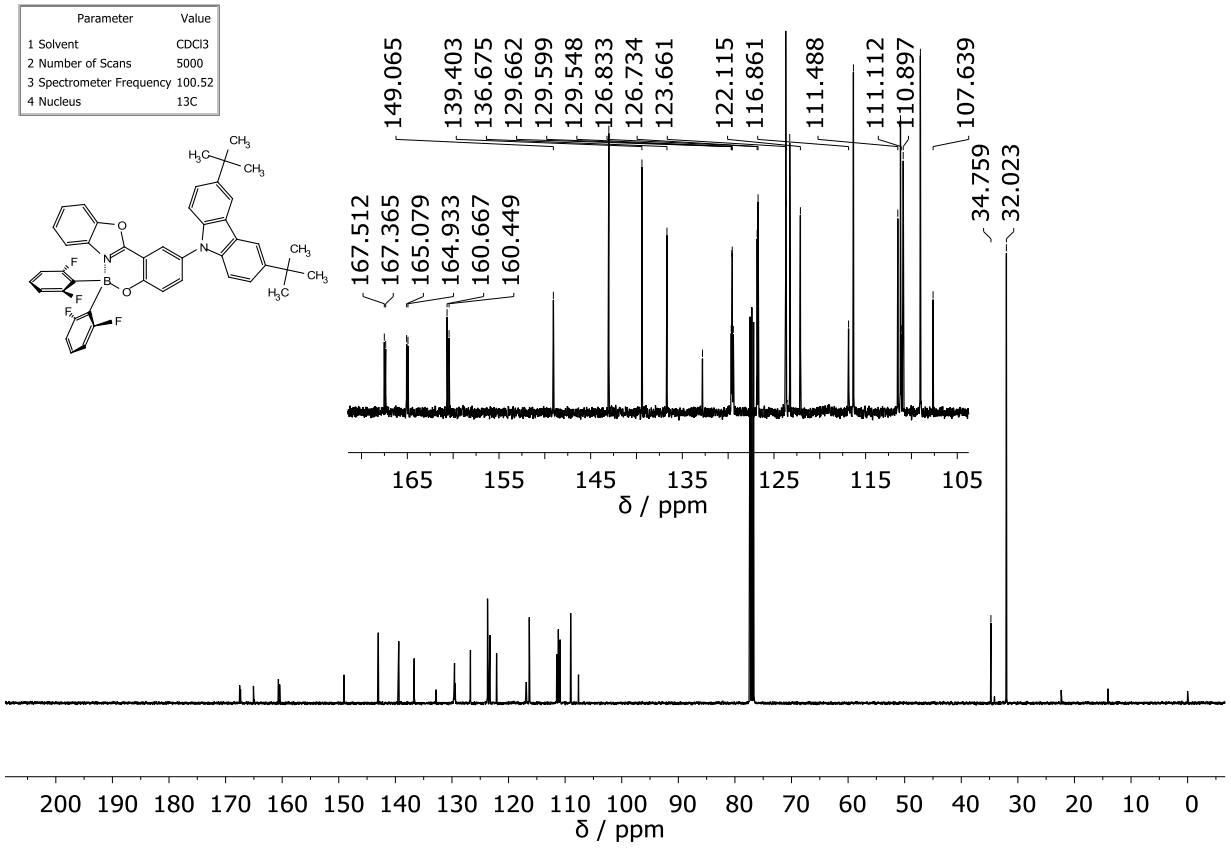

Figure S9.42. $^{13}C\{^{1}H\}$ NMR spectrum (101 MHz, $CDCl_3$) of **10**.

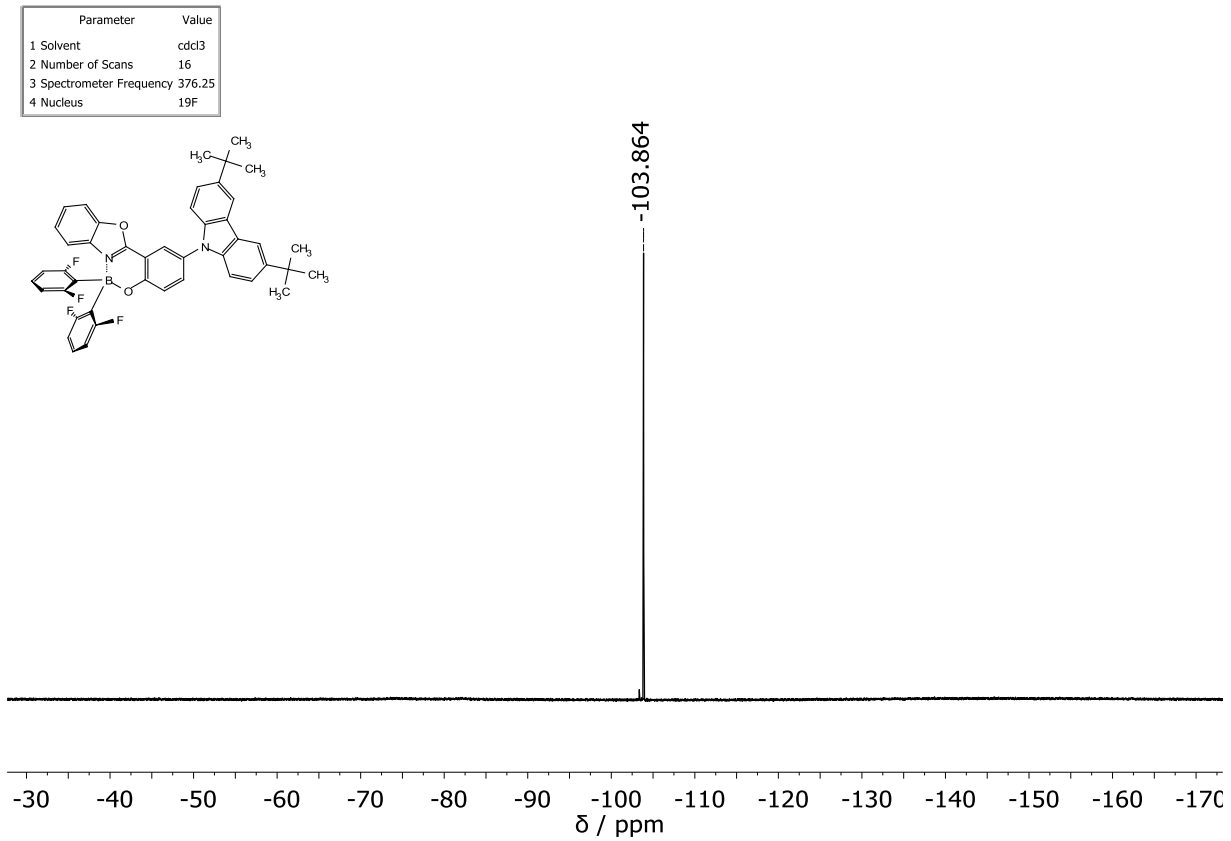

Figure S9.43. $^{19}F\{^{1}H\}$ NMR spectrum (376 MHz, $CDCl_3$) of **10**.

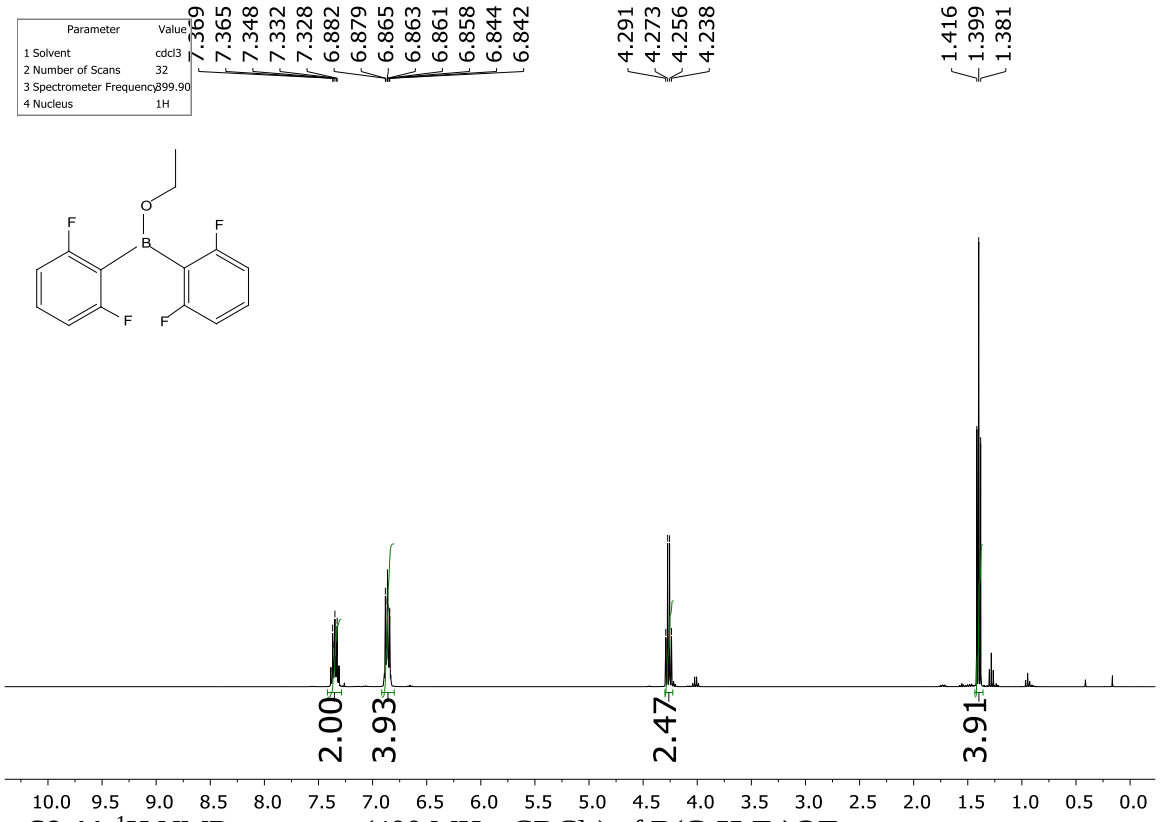

Figure S9.44. ^{1}H NMR spectrum (400 MHz, $CDCl_3$) of **B($C_6H_3F_2$)OEt**.

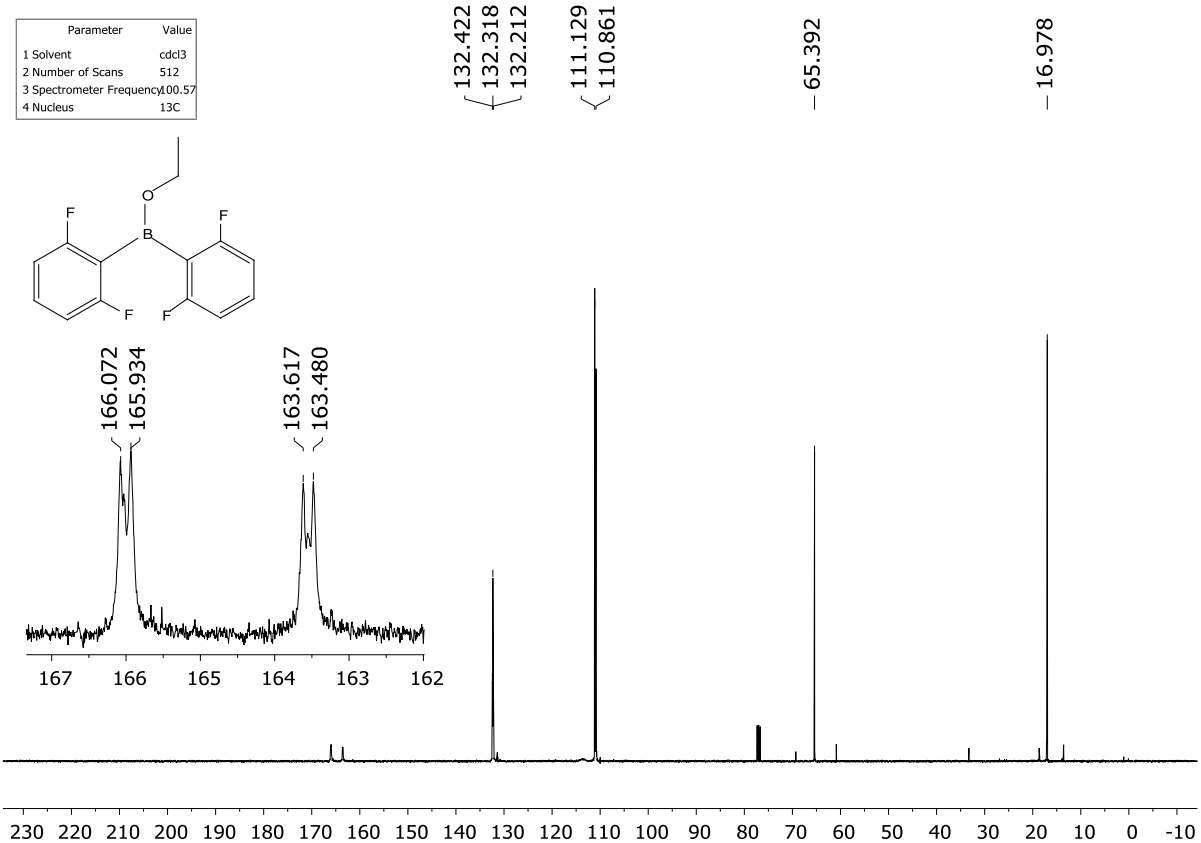

Figure S9.45. $^{13}C\{^{1}H\}$ NMR spectrum (101 MHz, $CDCl_3$) of **B($C_6H_3F_2$)OEt**.

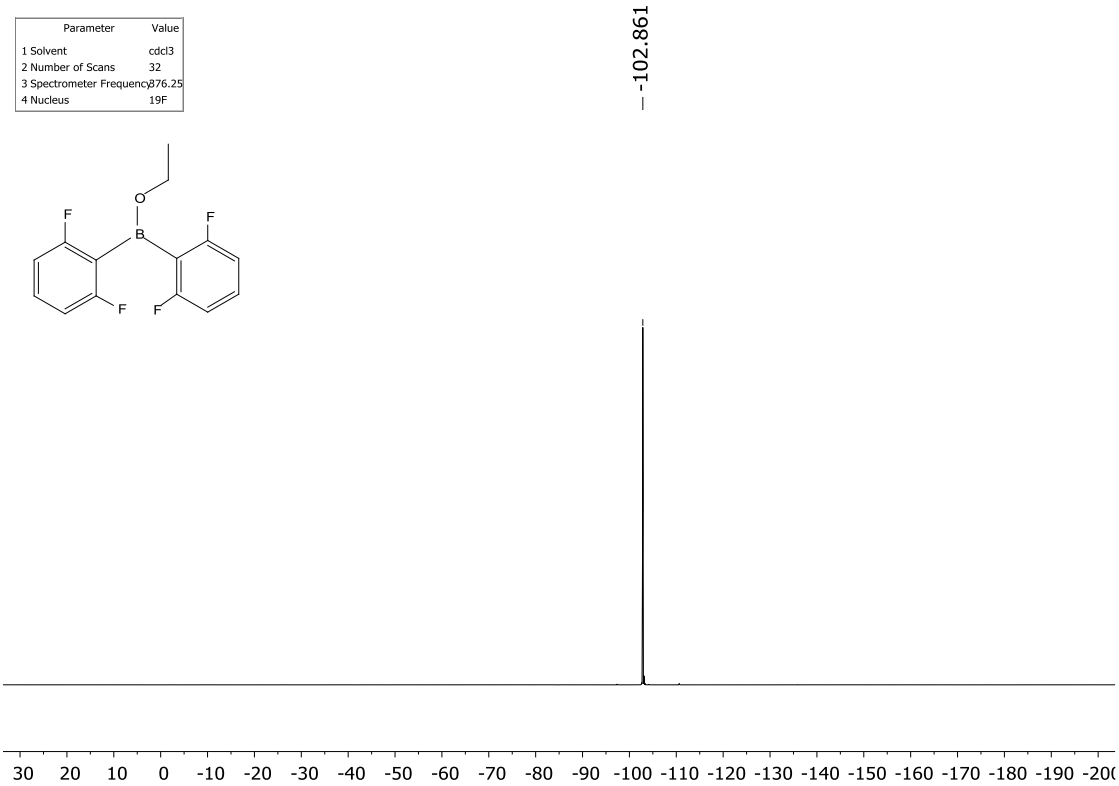

Figure S9.46. $^{19}F\{^{1}H\}$ NMR spectrum (376 MHz, $CDCl_3$) of **B($C_6H_3F_2$)OEt**.

10. HRMS spectra

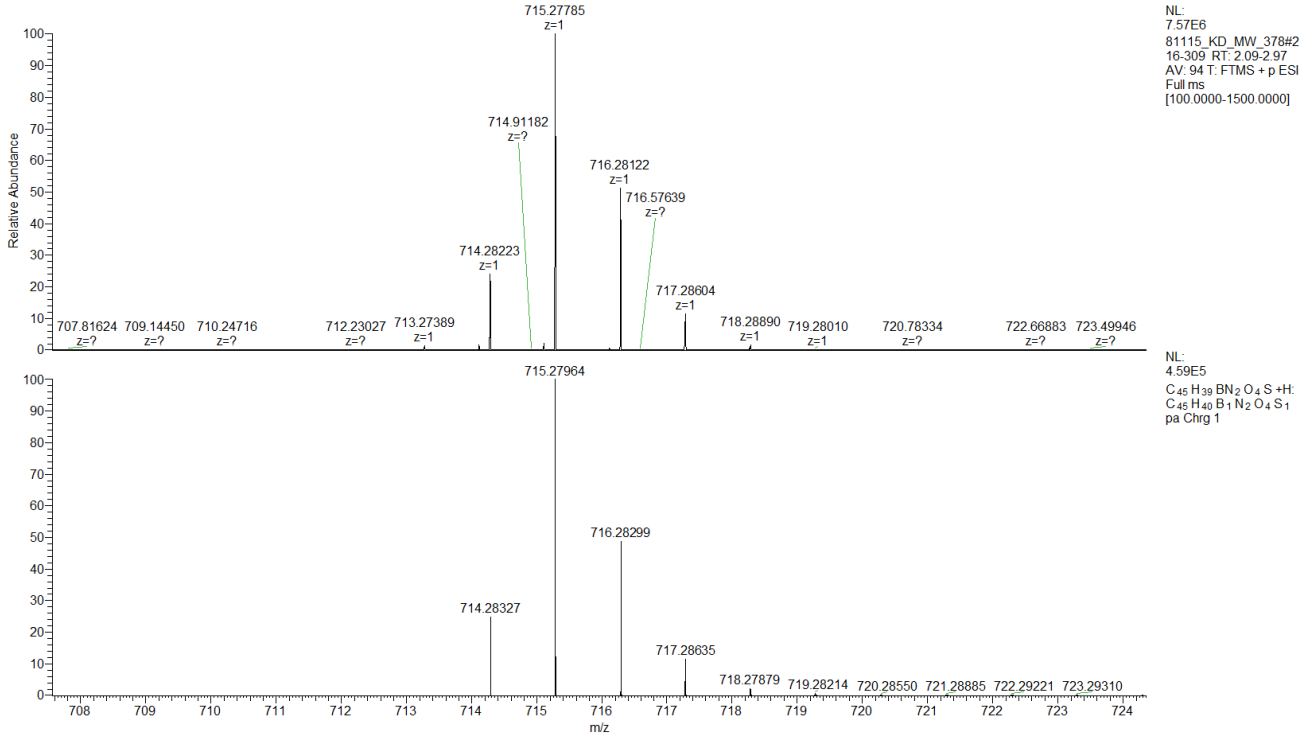

Figure S10.1. HRMS spectrum (ESI, positive ion mode) of **7a**. The calculated spectrum of the formula $C_{45}H_{40}BN_2O_4S^+$ [MH^+] is shown at the bottom.

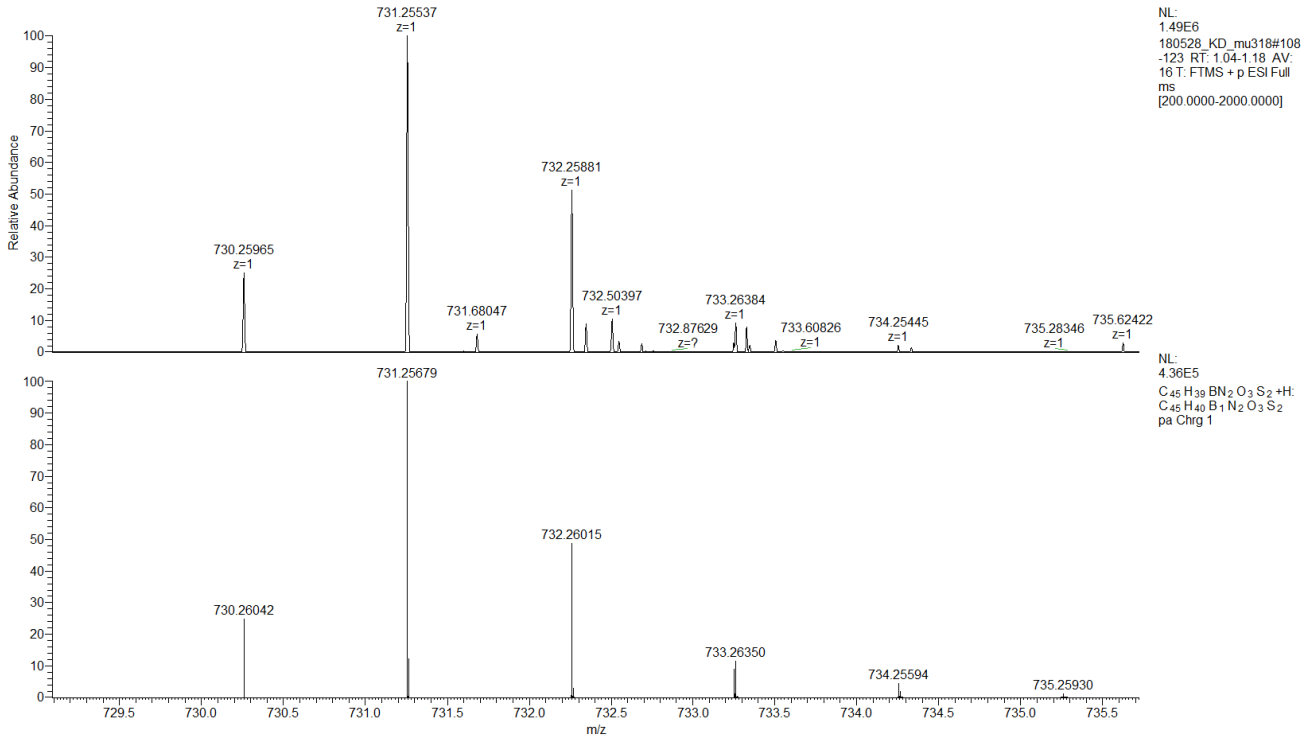

Figure S10.2. HRMS spectrum (ESI, positive ion mode) of **7b**. The calculated spectrum of the formula $C_{45}H_{40}BN_2O_3S_2^+$ [MH^+] is shown at the bottom.

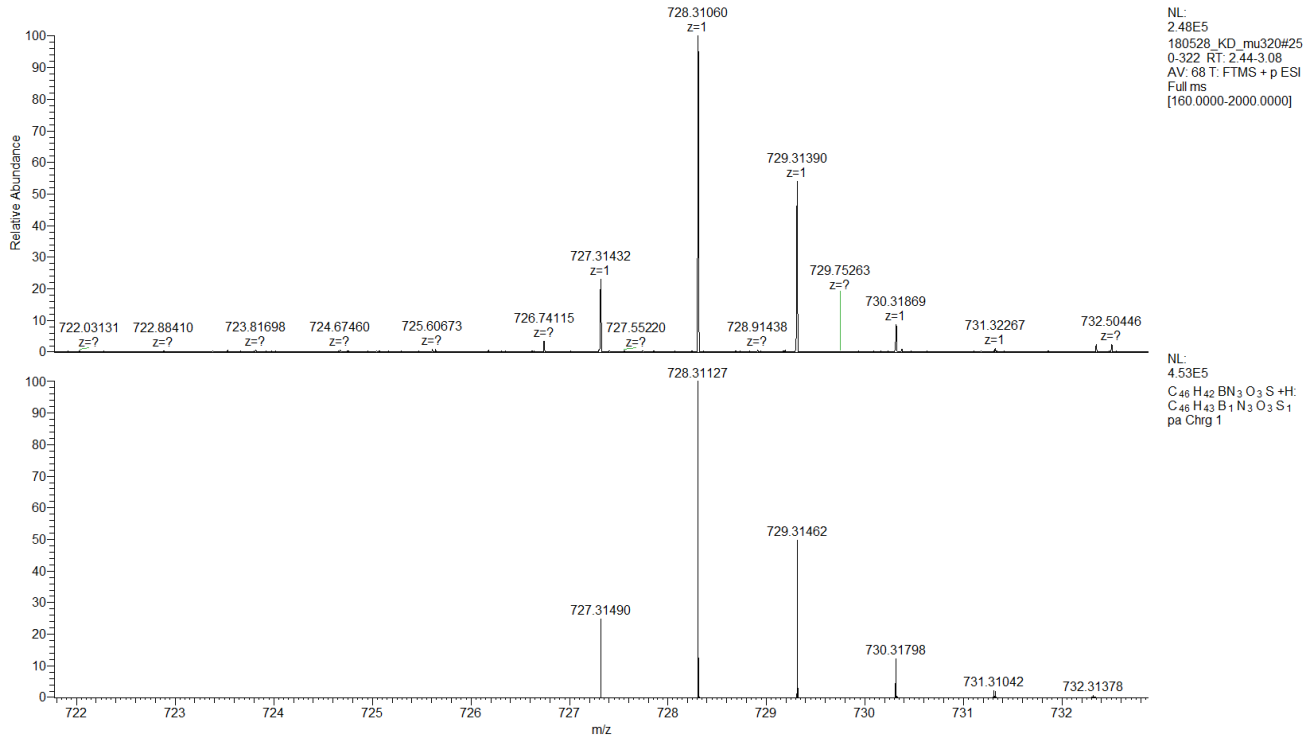

Figure S10.3. HRMS spectrum (ESI, positive ion mode) of **7c**. The calculated spectrum of the formula $C_{46}H_{43}BN_3O_3S^+$ [MH^+] is shown at the bottom.

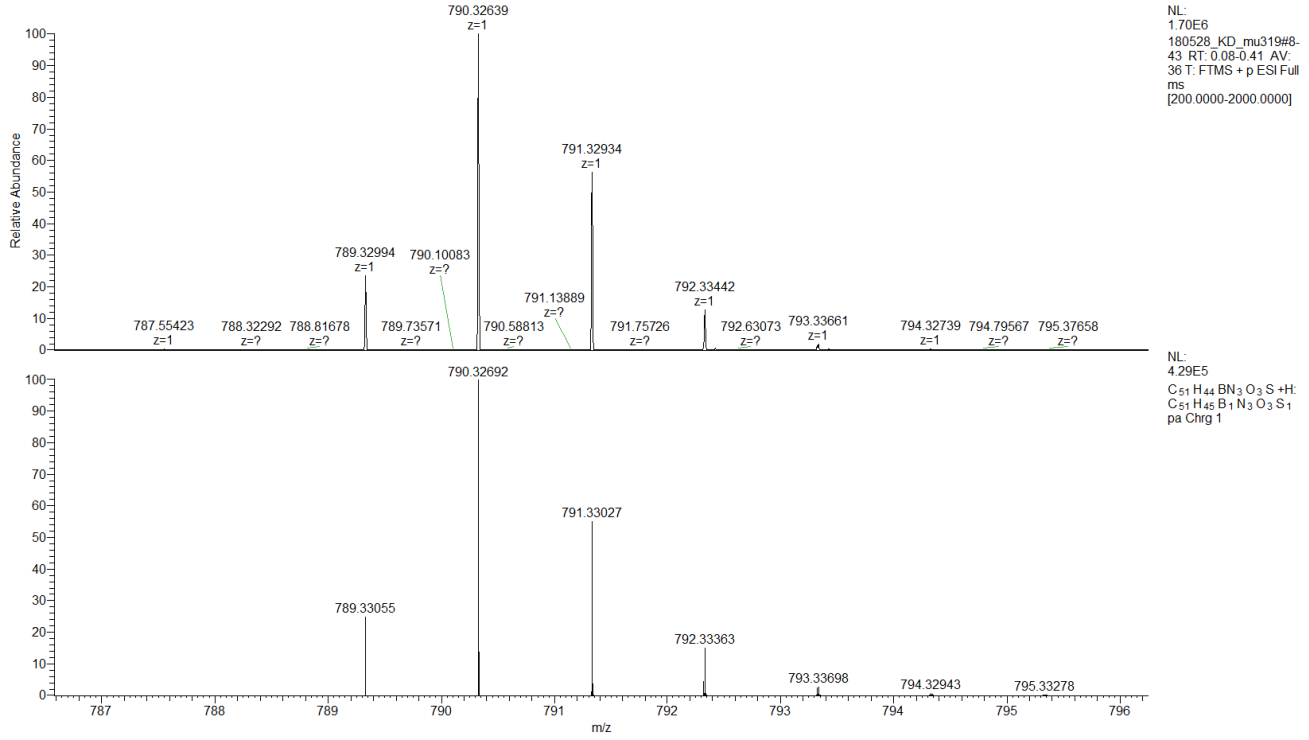

Figure S10.4. HRMS spectrum (ESI, positive ion mode) of **7d**. The calculated spectrum of the formula $C_{51}H_{45}BN_3O_3S^+$ [MH^+] is shown at the bottom.

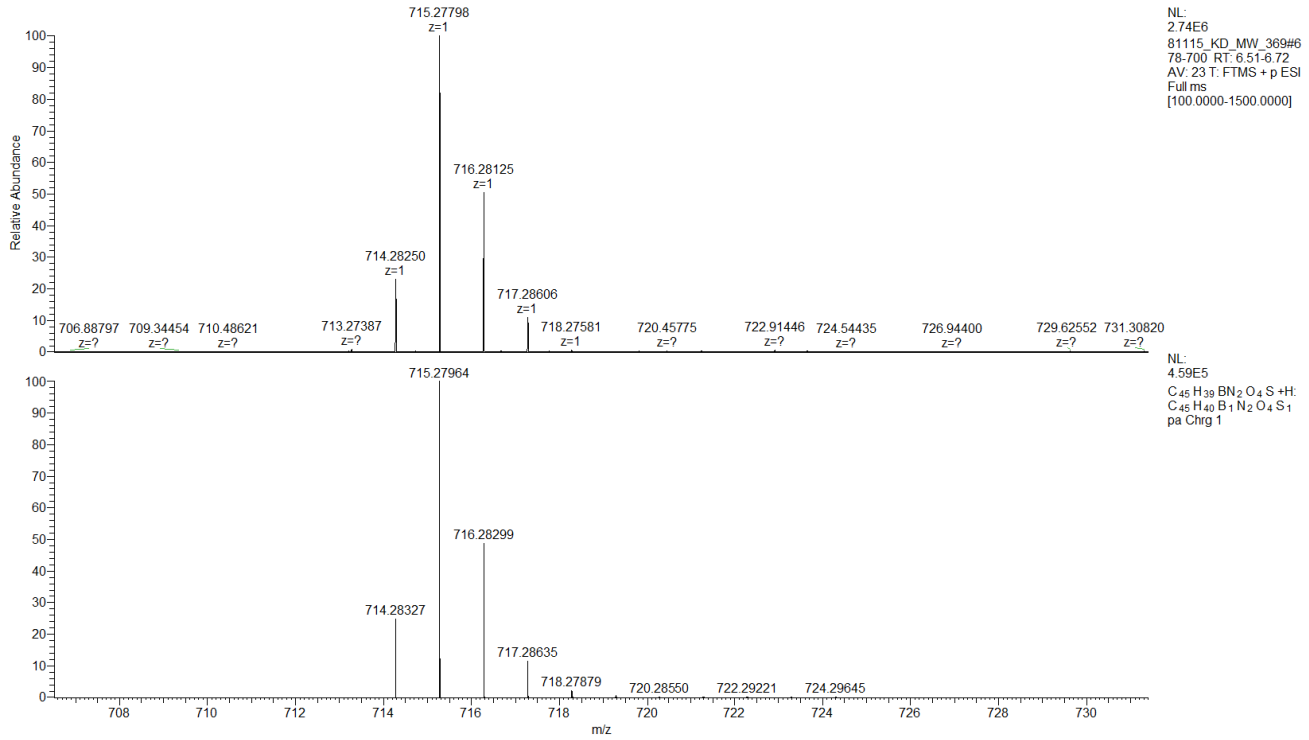

Figure S10.5. HRMS spectrum (ESI, positive ion mode) of **8a**. The calculated spectrum of the formula $C_{45}H_{40}BN_2O_4S^+$ [MH^+] is shown at the bottom.

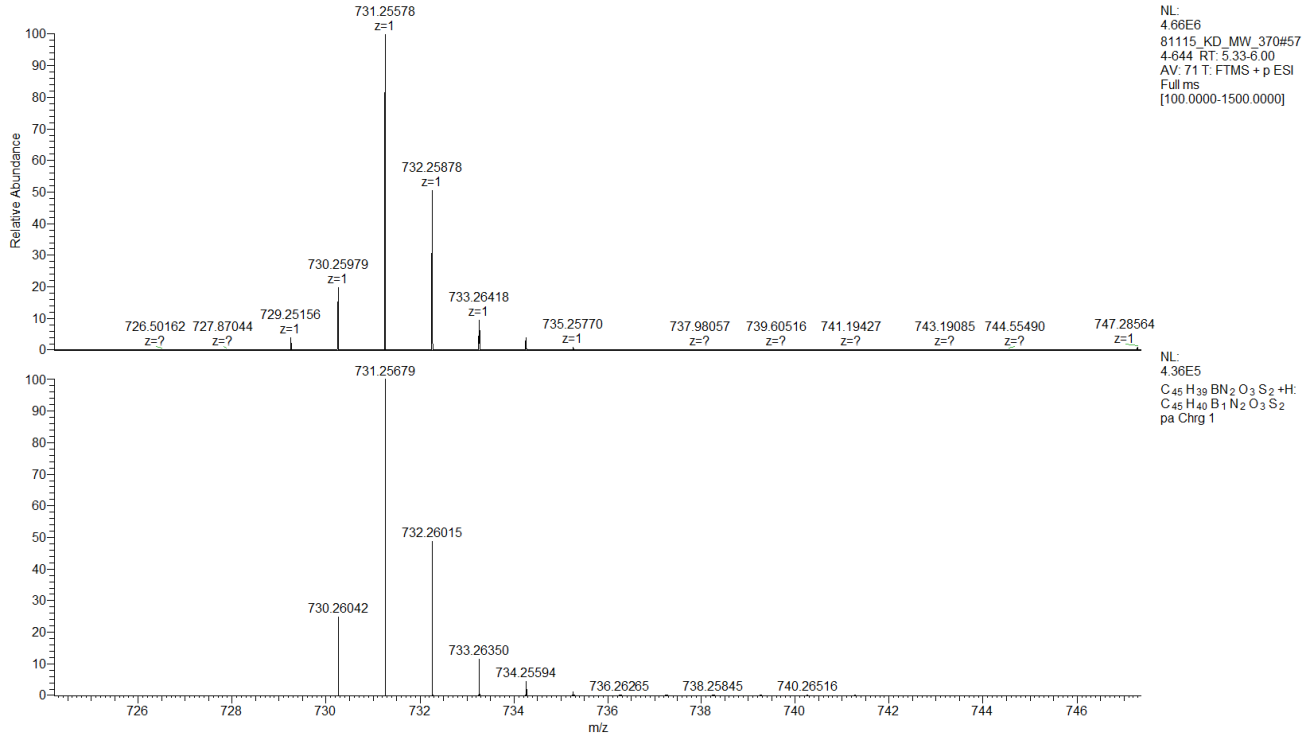

Figure S10.6. HRMS spectrum (ESI, positive ion mode) of **8b**. The calculated spectrum of the formula $C_{45}H_{40}BN_2O_3S_2^+$ [MH^+] is shown at the bottom.

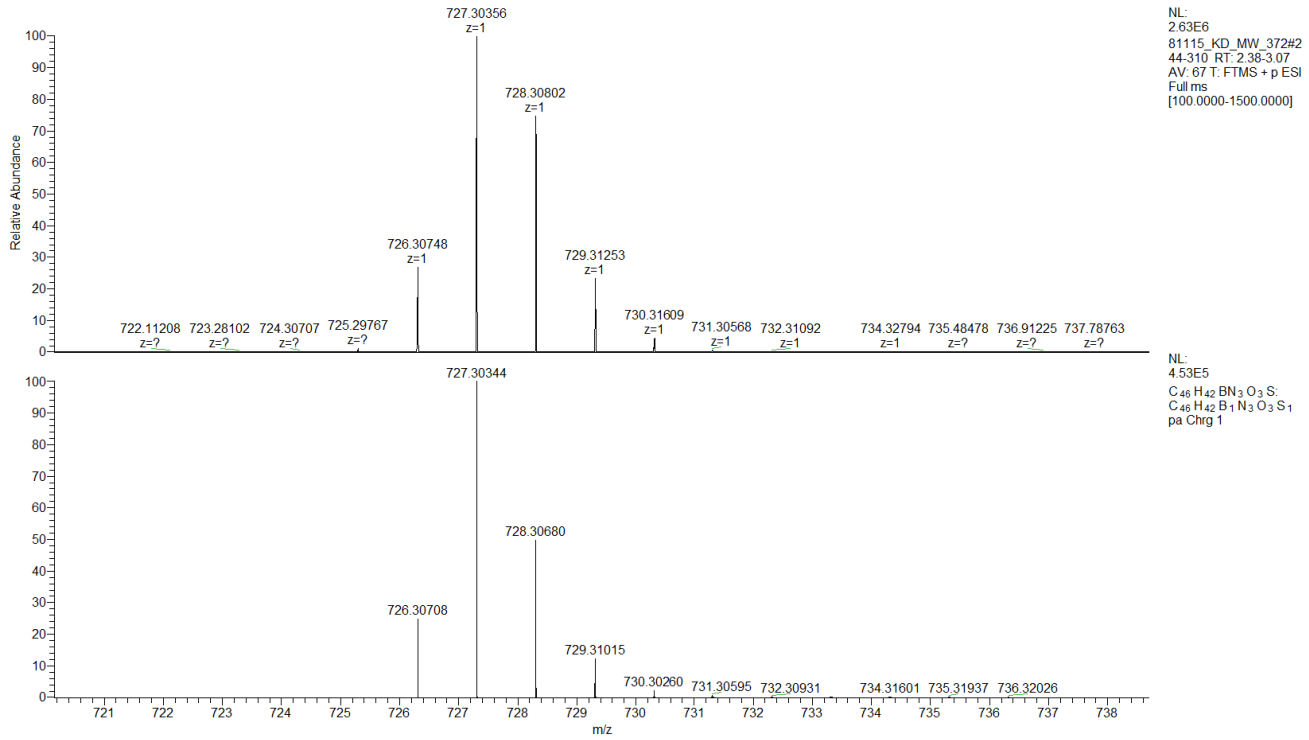

Figure S10.7. HRMS spectrum (ESI, positive ion mode) of **8c**. The calculated spectrum of the formula $C_{46}H_{43}BN_3O_3S^+$ [MH^+] is shown at the bottom.

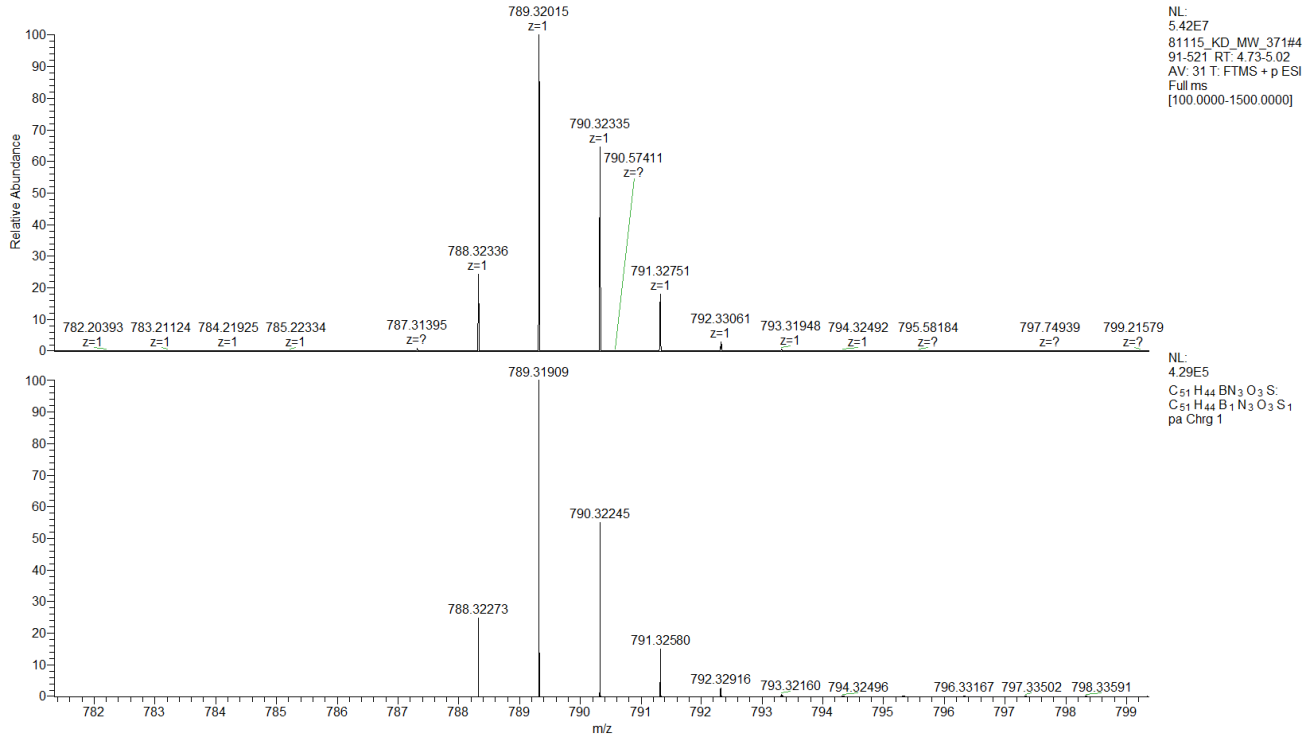

Figure S10.8. HRMS spectrum (ESI, positive ion mode) of **8d**. The calculated spectrum of the formula $C_{51}H_{45}BN_3O_3S^+$ [MH^+] is shown at the bottom.

11. References for Supporting Information

1. S. J. Strickler and R. A. Berg, *J. Chem. Phys.*, 1962, **37**, 814–822.
2. M. Urban, P. H. Marek-Urban, K. Durka, S. Luliński, P. Pander and A. P. Monkman, *Angew. Chem. Int. Ed.*, 2023, **62**, e202217530.
3. S. Montanaro, P. Pander, J.-R. Mistry, M. R. J. Elsegood, S. J. Teat, A. D. Bond, I. A. Wright, D. G. Congrave and M. K. Etherington, *J. Mater. Chem. C*, 2022, **10**, 6306–6313.
4. J. Sun, J. Sun, W. Mi, P. Xue, J. Zhao, L. Zhai and R. Lu, *Dyes Pigm.*, 2017, **136**, 633–640.
5. G. Wesela-Bauman, M. Urban, S. Luliński, J. Serwatowski and K. Woźniak, *Org. Biomol. Chem.*, 2015, **13**, 3268–3279.